FLUORESCENCE STUDIES ON ANTHRAX PROTECTIVE ANTIGEN PORE FORMATION AND IN THE PRESENCE OF THE HOST RECEPTOR, CMG2

A Dissertation by

Kiran Kumar Andra

M.Sc, Andhra University, India 2005

B. Sc, Andhra University, India 2003

Submitted to the Department of Chemistry
and the Faculty of the Graduate School of
Wichita State University
in partial fulfillment of the requirements of the degree of
Doctor of Philosophy

July 2013

FLUORESCENCE STUDIES ON ANTHRAX PROTECTIVE ANTIGEN PORE FORMATION AND IN THE PRESENCE OF THE HOST RECEPTOR, CMG2

The following faculty members have examined the final copy of this dissertation for form and content, and recommend that it be accepted in partial fulfillment of the requirement for the degree of Doctor of Philosophy with a major in Chemistry.

James G. Bann, Committee Chair

Douglas S. English, Committee Member

William C. Groutas, Committee Member

Moriah R. Beck, Committee Member

George R. Bousfield, Committee Member

Accepted for the college of Liberal Arts and Sciences

Ron Matson, Interim Dean

Accepted for the Graduate School

Abu Masud, Interim Dean

To my Loving Parents,

And my Dear Wife Priyanka for their encouragement and support

ACKNOWLEDGMENTS

I would like to express my sincere gratitude to Dr. James G. Bann, as my research advisor. I thank him for giving me a chance to work and support through my doctoral work.

I wish to express my warm and sincere thanks to committee members Dr. William C. Groutas, Dr. Douglas S. English, Dr. Moriah R. Beck and Dr. George R. Bousfield for their advice and support.

I would also thank the Chair of the department, Dr. David M. Eichhorn and Dr. Kandatega Wimalasena for their guidance and suggestions, also late Dr. Erach R. Talaty, for his valuable suggestion in organic synthesis.

I would extend my appreciation to past and present colleagues, Dr. Shyamali Wimalasena, Dr. Maheshinie Rajapaksha, Dr. Sara Hubbard, Alex Williams, Sireesha Mamillapalli, Fatemah Chadegani and Vishnu Chakradhari for their help and support.

I sincerely thank to all faculty, staff and colleagues of the Wichita State Chemistry Department for assisting me in numerous ways. Finally, recognition goes out to my dear parents and my wife, Priyanka who inspired me and provided constant encouragement in my most difficult times.

ABSTRACT

The anthrax toxin secreted by *Bacillus anthracis* is the major virulence factor of anthrax disease. The protective antigen (PA) component of the toxin binds to the von-Willebrand factor A (vWA) domain of capillary morphogenesis protein 2 (CMG2), followed by proteolytic cleavage into two fragments of 20 and 63 kDa. The 63 kDa fragment oligomerizes into heptameric or octameric structures collectively termed "pre-pore", these are endocytosis, and within an acidified endosome undergo a large conformational change to form a membrane spanning pore, resulting in the entry of edema factor (EF) or lethal factor (LF) into the host cell. Although the general pathway of anthrax toxin entry has been elucidated, many details still remain unknown. The key problem is how the heptameric PA-receptor complex initiates formation of the pore and what happens to the receptor after pore formation; is it still bound or dissociated? Understanding the process of anthrax toxin pore formation and the role of the receptor could provide more clues in the investigation of the mechanism of anthrax toxin action and suggest new strategies for inhibiting toxin action.

In my research work, we studied the pH dependent pore formation in presence of receptor, using fluorescence. We show that during the process of pore formation at low pH, a specific tryptophan residue, W346 (located in domain II), comes closer to domain IV, and then receptor dissociates from PA_{63}. Our results show that, even in case of D425A PA_{63} (as a control, not forming a pore), receptor dissociates at the same pH required for pore formation. This mechanism suggests that movement of domain IV away from domain II must occur quickly, followed by a collapse in which the two domains coalesce, and receptor dissociation is induced by low pH.

TABLE OF CONTENTS

Chapter Page

TABLE OF CONTENTS (continued)

Chapter Page

TABLE OF CONTENTS (continued)

Chapter Page

TABLE OF CONTENTS (continued)

Chapter Page

LIST OF FIGURES

Figure Page

LIST OF FIGURES (continued)

Figure Page

LIST OF FIGURES (continued)

Figure Page

LIST OF FIGURES (continued)

Figure Page

LIST OF TABLES

Table Page

COMMON ABBREVATIONS USED

2-FHis	2-Fluoro-L-Histidine
4-FTrp	4-Fluoro- DL-Tryptophan
AcOH	Acetic acid
AF 350	Alexa Fluor 350 maleimide
AF 488	Alexa Fluor 488 maleimide
Asp	(D)-Aspartic acid
ATP	Adenosine triphosphate
ATR	Anthrax toxin receptor
Bis-Tris	2-[bis (2-hydroxyethyl) amino]- 2-(hydroxymethyl) propane-1, 3-diol
cAMP	Cyclic adenosine monophosphate
CHAPS	3-[(3-cholamidopropyl) dimethylammonio]-1-propanesulfonate
CMG2	Capillary morphogenesis protein 2
Cryo-EM	Cryo electron microscopy
Cys (C)	Cysteine
DDM	n-dodecyl-β-D Maltopyranoside
DL	Degree of labeling
DTT	Dithiothreitol
EF	Edema factor
EF_N	N-terminal fragment of EF
Em	Emission
ETx	Edema toxin
Ex	Excitation

FOS-14	N-tetradecylphosphocholine
FRET	Förster resonance energy transfer
Glu (E)	Glutamic acid
GST	Glutathione–S-transferase
HEPES	N-(2-hydroxyethyl)piperazine-N'-3-propanesulfonic acid
His (H)	Histidine
HPLC	High performance liquid chromatography
Ile (I)	Isoleucine
IPTG	Isopropyl β-D-thiogalactopyranoside
LB	Lauria–Bertani
LC/MS	liquid chromatography/mass spectrometry
LF	Lethal factor
LF_N	N-terminal fragment of LF
LTx	Lethal toxin
MAPKK	Mitogen-activated protein kinase kinase
MES	2-(N-morpholino)ethanesulfonic acid
MIDAS	Metal ion dependent adhesion site
MW	Molecular weight
NEM	N-ethyl maleimide
NMR	Nuclear magnetic resonance
PA	Protective antigen
PA_{20}	20-kDa N-terminal fragment of PA
PA_{63}	63-kDa C-terminal fragment of PA

PAGE	Polyacrylamide gel electrophoresis
PBS	Phosphate buffered saline
Phe (F)	Phenylalanine
ppm	Parts per million
QS	Quinine sulfate
QY	quantum yield
RPM	Revolutions per minute
RT	Room temperature
SDS	Sodium dodecyl sulfate
SMRC	Strongest methyl resonance of ^{13}carbon
TCEP	(*tris*(2-carboxyethyl)phosphine)
TEM8	Tumor endothelial marker 8
Tris	Tris Hydroxymethyl aminoethane
Tyr (Y)	Tyrosine
UV	Ultraviolet
vWA	Von Willebrand factor A
WT	Wild type

CHAPTER 1

INTRODUCTION

1.1 Overview

Anthrax disease is an acute infection caused by *Bacillus anthracis*, a rod shaped gram positive bacteria with a width of 1-1.2 µm and length of 3-5 µm (2) (Figure 1B). *B. anthracis* is an endospore forming bacterium, that allows the bacterium to survive rather harsh conditions such a drought for many years, even decades (3, 4). Spores (Figure 1A) become vegetative under physiological conditions (1) or on infecting a host cell.

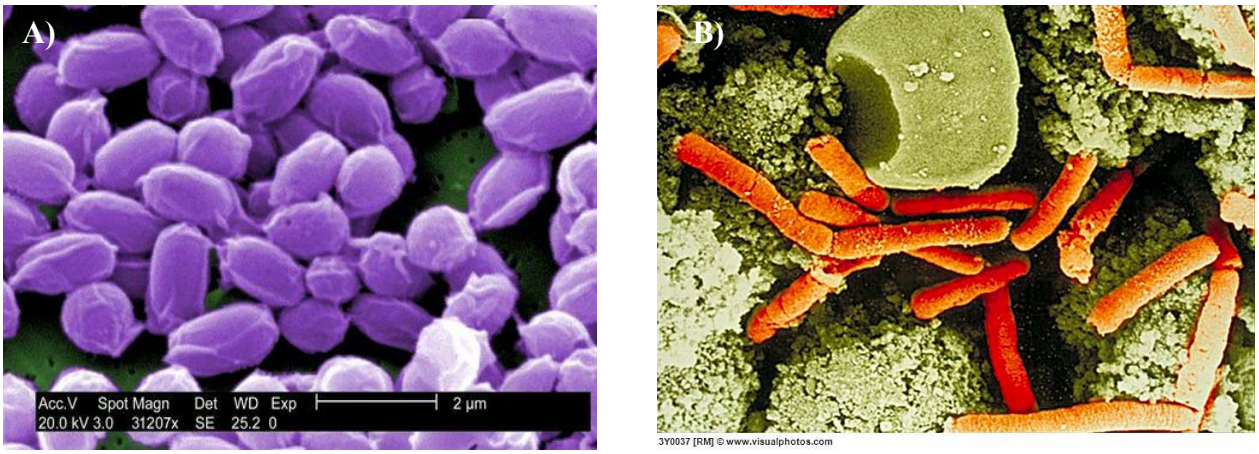

Figure 1. Scanning electron micrograph (SEM) pictures of anthrax spores. A) Spores from Sterne strain of *Bacillus anthracis* and B) Spleen tissue of monkey, rod shaped bacilli (orange color). Pictures were taken from Janice Carr (bcm.edu) (A) and Image library of Biodefense and Emerging Infectious Diseases (B).

The genome of *Bacillus anthracis* contains a single circular chromosome along with two circular extra chromosomal, double stranded DNA plasmids termed pXO1 and pXO2. Full virulence of the bacterium comes from both plasmids. Anthrax toxin components, Protective antigen (PA), Edema factor (EF) and Lethal factor (LF) are in pXO1 plasmid, and the genetic operon which synthesizes the anti-phagocytic capsule, composed of poly-D-glutamic acid, is within pXO2 plasmid (6).

1.2 Types of Anthrax

Three major forms of disease are identified based on the route infection; cutaneous, inhalation and the rarest one, gastrointestinal anthrax.

Cutaneous anthrax is observed when *B. anthracis,* enters the body through a wound or a cut in the skin. This form is prevalent in people handling contaminated wool, skin, hides and hair products of infected animals (7). Symptoms are visualized initially as a raised itchy bump, which turns into a blister in one or two days (8). The blister eventually develops into a painless black ulcer medically termed as eschar. Inflammation surrounding the lymph glands is observed. This type of infection may be cured by administering antibiotics. Infection leading to death in the case of cutaneous anthrax is very rare.

Infection of inhalational anthrax occurs through the inhalation of *B. anthracis* spores. This infection is usually observed 2-3 days after exposure (9). It is difficult to diagnose inhalational anthrax as its symptoms in the initial stages are quite similar to the Flu. They include fever, nausea, vomiting, and fatigue. These symptoms progress to a more serious symptoms that include difficulty breathing and anaphylactic shock leading to death. Early diagnosis is absolutely essential, and typically requires a 60-day antibiotic prophylaxis (or longer) to cure the disease.

Gastrointestinal anthrax is the rarest form of infection, and is acquired through consumption of infected meat. Symptoms include stomach pain, loss of appetite, fever, nausea, bloody diarrhea and blood vomiting. This is considered the deadliest form of infection (10).

1.3 Anthrax as a Biological Weapon

Because of the dormant nature of spores and the fact that the infection is considered not contagious, has led to the development of *B. anthracis* as a biological weapon. First use of *B. anthracis* as a tool of bio-terrorism has been reported during the period between World Wars, I and II (11).

Anthrax was used in the deaths of 2000 prisoners (1940-1942), including civilians were recorded in China (11). Near Scotland anthrax spores were tested for the release by the British government (12, 13). This made the island a biological hazard for several following decades. It was sterilized by treatment with several tons of sea water and formaldehyde in 1986.

In 1979 there was an outbreak at a military base near Sverdlovsk, USSR (8, 14). Initially it was reported to be an outbreak in cattle, which lead to the infection military personnel. Later it was a revealed to be due to the accidental release of weaponized anthrax spores - 96 people were infected and 64 died.

Anthrax has been also been developed as a bioweapon in the United States, and weaponized anthrax spores were used in the attacks that occurred shortly after 9/11. The first inhalational infection case was reported on October 4th 2001 and the last one on October 31st 2001 – 22 confirmed cases resulting in 5 deaths A biological weapon plant established in Vigo, Indiana had the capacity to produce 100 tons of anthrax spores per month (15). More recently, in 2002, a laboratory worker processing environmental samples of *Bacillus anthracis* was diagnosed with cutaneous anthrax (16). The main causative agent of death in cases of anthrax is due to the secretion of the anthrax toxin.

1.4 Anthrax Toxin

Intoxication by *Bacillus anthracis* is mainly due to two factors. One of them is due to the poly-D-glutamic acid capsule (anti-phagocytic) and the other is due to a tripartite AB-toxin that is comprised of three separate proteins – PA –cell binding protein, EF and LF (enzymatic components) (17). Each of these three components are individually nontoxic, however, they become toxic when assembled to form a holotoxin on the host cell. Combination of PA with EF is called Edema toxin, PA with LF is called lethal toxin (17). PA allows cell entry of EF and LF.

Anthrax toxin belongs to a class of components that conform to the toxin A/B paradigm in which the A component is enzymatically active and the B component acts as a cell binding component. This toxin in A_3B_7 or A_3B_8 form where EF and LF constitute the A component and

PA is the oligomeric (heptamer or octamer) B component. Thus, PA mediates the entry of EF and LF through the plasma membrane into the host cell cytosol.

1.5 Anthrax Toxin Assembly and its Translocation

Infection is initiated by binding of the 83 kDa PA to one of two known cellular receptors on the host cell; Capillary Morphogenesis Protein 2 called as CMG2 or Tumor Endothelial Marker 8 called as TEM8 (18). Proteolytic cleavage by a furin like protease cleaves a 20 kDa fragment often called PA_{20}, leaving the PA_{63} fragment. The receptor bound PA_{63} assembles together forming a heptameric (19) or octameric (20) structure termed as 'pre-pore'. The pre-pore undergoes conformational changes and it becomes a β-barrel translocase 'pore' (a channel). The surface of the pre-pore oligomer has an affinity for the enzymatic components EF and LF, thereby facilitating their transport into the cytosol for further action (Figure 2). The heptamer complexes (with EF or LF) are taken into the cell by receptor-mediated endocytosis and trafficked to an acidic compartment. Acidic pH induces a conformational change of the pre-pore to form a membrane spanning pore. Translocation of EF and LF across the membrane into the cytosol is mediated by pore formation.

EF is a calcium/calmodulin adenylate cyclase, increases cAMP levels leading to edema, while LF is a zinc metalloproteinase that cleaves mitogen activated protein kinase kinases. The latter enzymatic component is the major cause of death in anthrax infection.

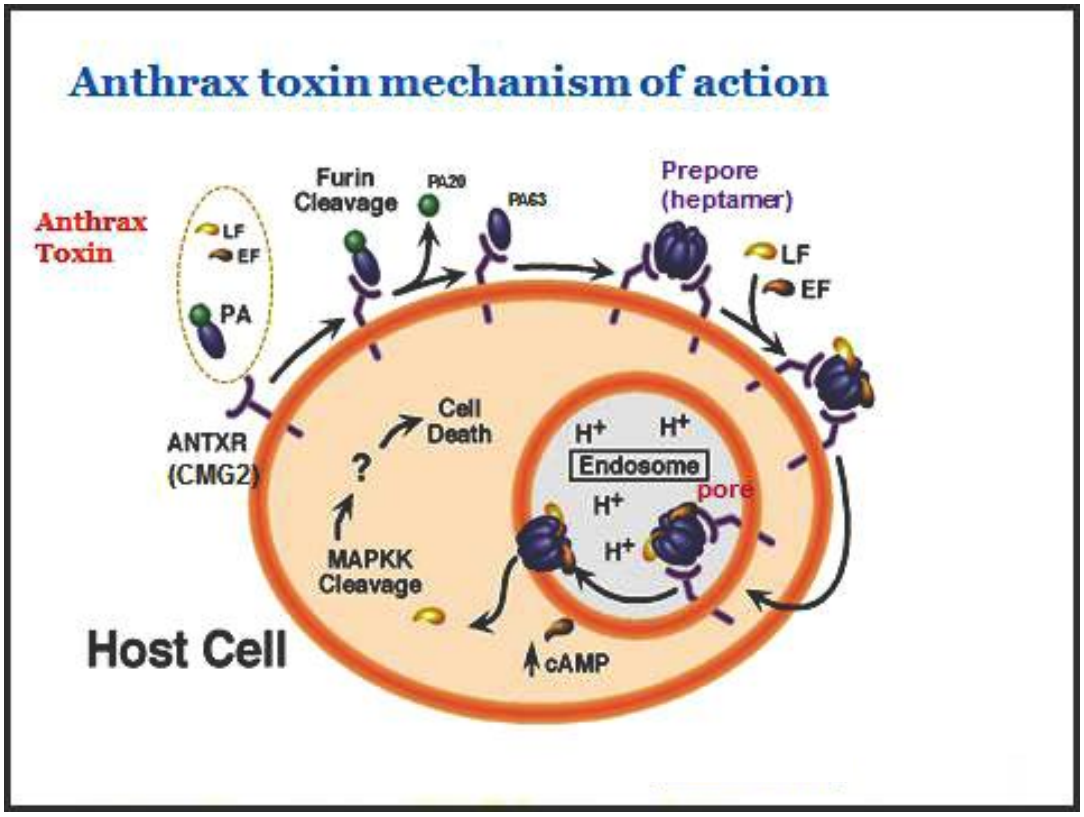

Figure 2. *B. anthracis* pathogenesis. Infection starts with the binding of PA to a host cell receptor. The PA molecule is then cleaved and the receptor-bound fragments oligomerized. Next EF or LF bind forming a complex, these complexes are then internalized into the cell. At low pH, PA undergoes conformational changes forming a transmembrane pore, which allows EF or LF to enter into the cytosol, resulting in cell death. Picture was adapted from http://ysm.research.yale.edu/article.jsp?articleID=415

1.6 Structure

1.6.1 Protective Antigen

Protective antigen (PA) is a monomeric 83 kDa protein which constitutes the B component (cell binding component) of anthrax toxin. Protective antigen triggers the cell binding and mediates the uptake of the enzymatic components EF and LF. PA is called protective antigen based on its use as vaccine in treating anthrax. The crystal structure reported by Petosa *et. al*. (21).

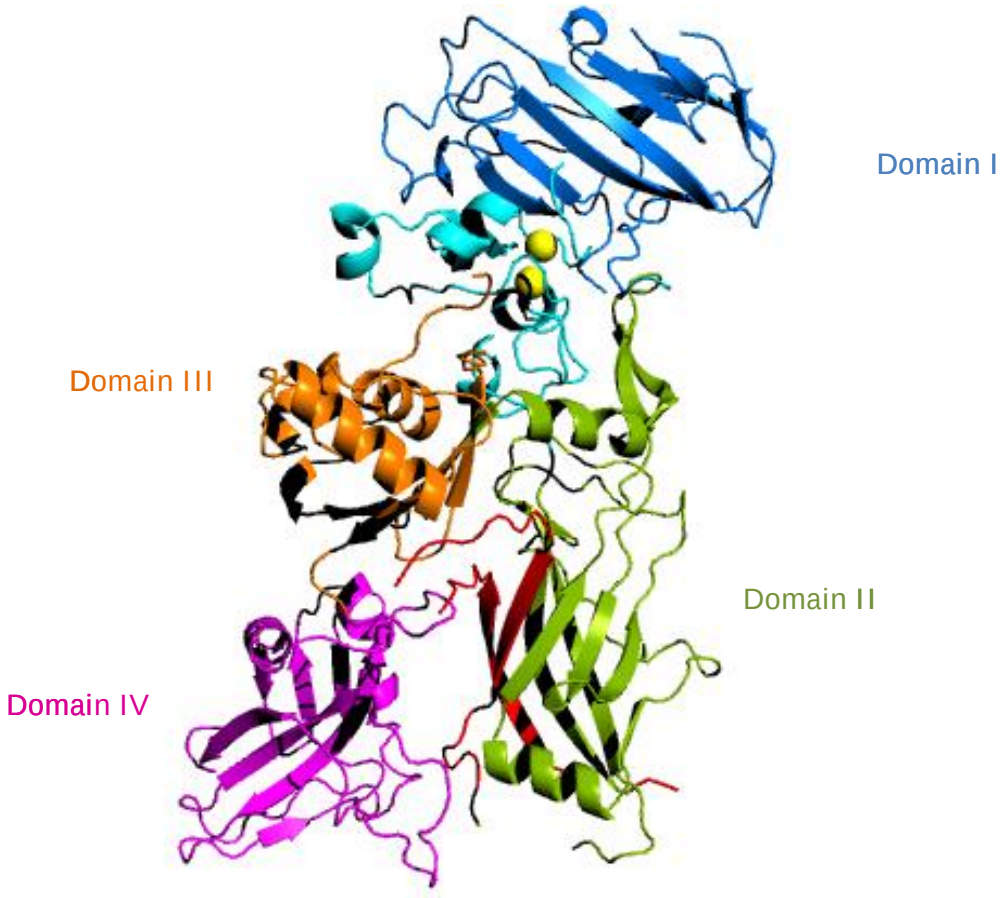

Figure 3. Crystal structure of Anthrax toxin protective antigen PA_{83} (PDB 1ACC) color identified domains. Domain I (Blue), domain II (green, with $2\beta_2$-$2\beta_3$ loop, red) domain III (golden brown) and domain IV (magenta). Figure was generated using PyMol v.99

and coworkers reveals PA as a long flat molecule, consisting mostly of β- sheet structure (21, 22).

1.6.2 Domain I

Domain I constitutes the residues from 1-258, and also contains a site for furin cleavage which activates the binding of enzymatic components to PA. This proteolytic cleavage of PA occurs between residues 164-167 and is necessary for toxin action. This cleavage results in the removal of residues from 1-167 as a 20 kDa protein called as PA_{20} (22, 23). PA_{20} is believed to prevent premature oligomerization of PA. Loss of PA_{20} triggers the pre-pore formation which is soluble in water and inserts itself into the host membrane. The remaining residues in domain I are known to be responsible for internalization of LF and EF (21, 24, 25). It contains two bound calcium ions on its surface that help PA in self-assembly and compete with ligand binding (21, 22) (Figure 3 and 4)

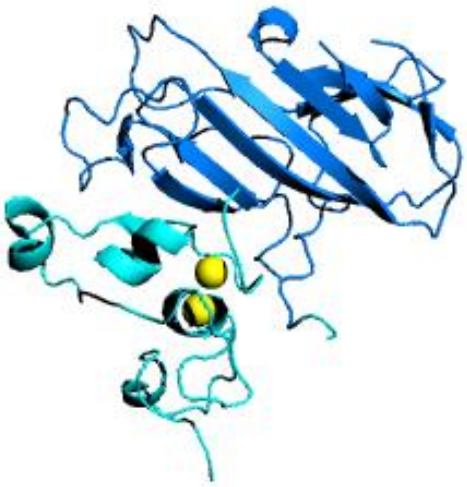

Figure 4. Crystal structure of domain- I; PA_{20} (PDB ID 1ACC) in blue and rest of the domain I in cyan with two calcium ions (yellow spheres). Figure was generated by using PyMol v.99.

1.6.3 Domain II

Domain II, residues from 259-487, forms the central core lining the lumen of the heptamer. The presence of an amphipathic disordered loop comprising residues 302-323 in $2\beta_2$-$2\beta_3$ strands shown in the crystal structure is believed to take part in the membrane insertion as a hairpin loop that combines to form a 14-stranded β-barrel pore. This loop cannot reach and span the membrane pore unless the $2\beta_2$-$2\beta_3$ peel away from domain II together with $2\beta_1$, $2\beta_4$ enabling the formation of an extended β-barrel region involving residues 285-340 (21, 26, 27). Evidence from channel conductance experiments have shown that the $2\beta_2$-$2\beta_3$ loops of the seven monomers of the heptamer are involved in the formation a β-barrel channel, which share homology with that observed in *Staphylococcus aureus* α-hemolysin (21, 28). Laterally projected loops of the crystallographic heptamer mid-section move towards the base and coalesce to form the β-barrel along the heptamer axis. This is made possible when the Greek-key motif constituting the first four β-strands including contiguous $2\beta_2$-$2\beta_3$ strands peel away from domain II (21)(Figure 5). Mutations in solvent exposed residues of domain II block pore formation, suggesting that they participate in the conformational rearrangements of heptamer (29). Cysteine-scanning studies reveal an effective way to block pore formation involves

Figure 5. Crystal structure of domain II (PDB ID 1ACC), with $2\beta_2$-$2\beta_3$ strands in red. Figure was generated by using PyMol v.99.

residues mostly in domain II clustered in the lumen of the pre-pore (30).

1.6.4 Domain III

Residues from 488-595 together called as domain III of PA which accounts mainly for the periphery of the heptamer. This domain displays a fold similar to that of the ferridoxin class of proteins (Figure 6). Recent mutagenesis studies reported that a single point mutation, D512A in domain III blocked formation of the heptameric pre-pore (31). Thus domain III is identified to play a key role in the oligomerization and stabilization of the pre-pore (23).

Figure 6. Crystal structure of domain III (PDB 1ACC). Figure was generated by using PyMol v.99.

1.6.5 Domain IV

Domain IV comprises residues from 596-735 and it has limited contacts with rest of PA. These amino acid residues are grouped into two receptor binding sites; the large loop consisting of residues 704-723 and the small loop from 679-693, at the C-terminal end aids receptor binding

(32). Mutational analysis and monoclonal antibody studies have demonstrated that antibodies 3B6 and 14B7 bind the region within amino acids 671-721 and reduce the toxicity in a way, inhibiting the receptor binding to PA (32-34).

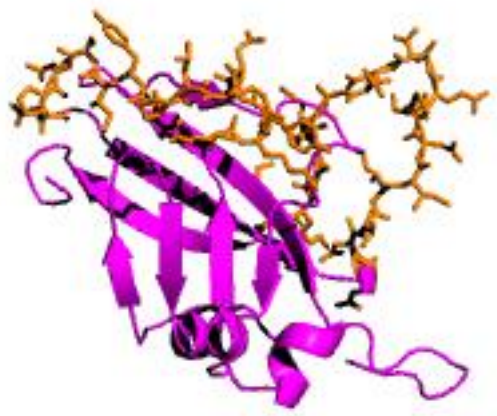

Figure 7. Crystal structure of domain IV (PDB ID 1ACC), with binding loop regions, 704-723 and 679-693 in orange. Figure was generated by using PyMol v.99.

1.7 Lethal Factor

Lethal factor is a 90 kDa, Zn^{2+} metalloprotease, consisting of four domains (Figure 8). Lethal factor (LF) along with protective antigen are often called lethal toxin. LF displays its toxic effect by destroying the signaling cascade involving mitogen-activated protein kinase kinases (MAPKK's). The effect of LF on kinases is cleavage of the proline abundant N-terminal kinase domain causing interference with protein-protein interaction sites, thus destroying the assembly of signaling complexes in the cascade. Immune cells, which constitute the defense mechanism of the body, are inhibited in various ways by the lethal toxin. Pro-inflammatory cytokine production

plays a key role in producing the inflammatory response is inhibited by LF (35, 36). The neutrophil chemotaxis ability is observed as a result of block in Hsp 27 phosphorylation (37, 38). Activities of importance such as proliferation, activation, cytokine expression in T-cells are blocked by lethal toxin (39-41). Deactivation of MAPKs indirectly inhibits B-cell proliferation and production of antibodies (42). Thus both innate and acquired immune responses are altered by lethal toxin in the body.

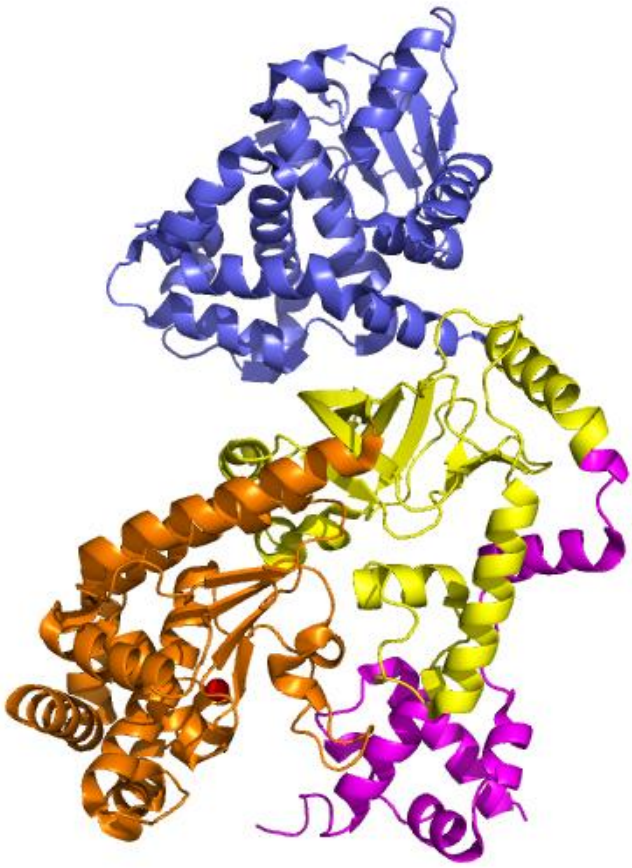

Figure 8. Crystal structure of Lethal factor (PDB ID 1J7N) with colored domains. Domain I (Blue), domain II (magenta), domain III (yellow) and domain IV (orange). Figure was generated using PyMol v.99

Domain I enables the binding of LF to the membrane-translocation component PA. The actual substrates for LF activity are bound by domains II and III, followed by cleavage at the N-terminus of domain IV. Domain III shares homology with domain II and domain IV, contains the active center having Zn^{2+} ion coordinated in a tetrahedral geometry by one water molecule and three protein side chains.

1.8 Edema Factor

Edema factor (EF) is a calcium-calmodulin-dependent adenylate cyclase, and it is require for binding of calmodulin (a eukaryotic calcium binding protein) for activity (43). EF adenylate cyclase is different from the mammalian enzyme to a large extent but shares a unique common feature of having two metal ion catalytic mechanisms (43). The binding interface of EF with PA involves seven amino acid residues. Mutations in these amino acids prevent the interactions of PA and EF (44).

The EF-calmodulin complex displays catalytic activity in the conversion of cytosolic ATP to cyclic AMP (cAMP) (45). This abrupt increase in the cAMP levels raise the water levels in the body, but there is also evidence that anthrax toxin receptor expression on cells is increased, creating more sites for PA binding and toxin internalization (46).

Three globular domains constitute the active site of EF. The catalytic core is located at the interference between the two domains (47) (Figure 9). A short peptide linker joins the third domain with the first one (Figure 9). EF contributes to most of cutaneous and systemic anthrax.

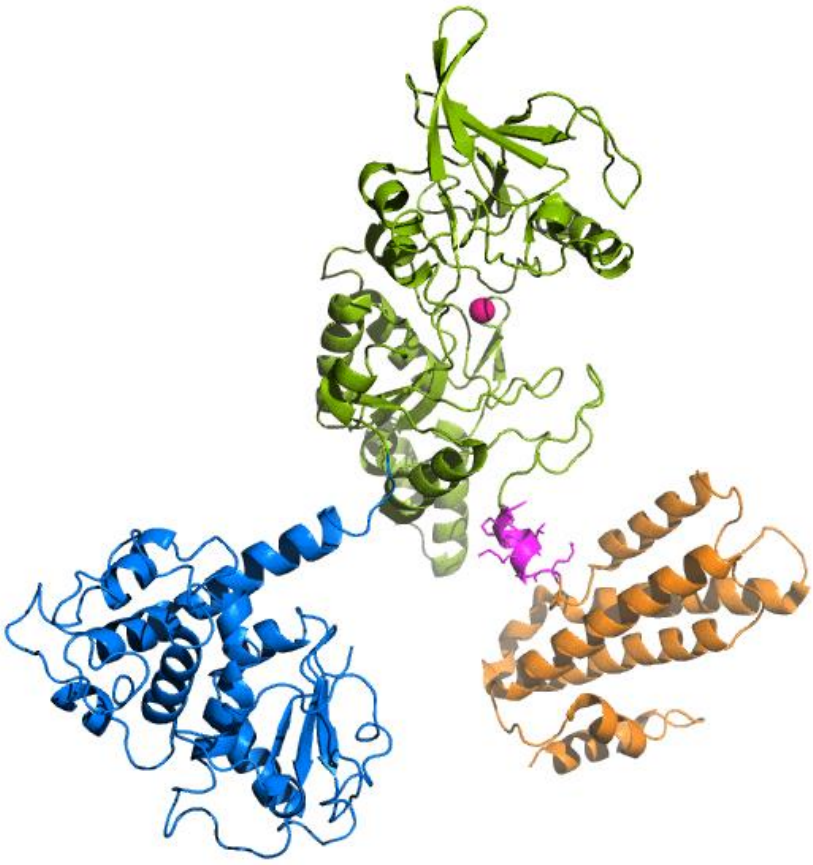

Figure 9. Crystal Structure of Anthrax Edema factor (PDB 1XFU) with colored domains. Domain I (Blue), domain II (green), domain III (orange), and linker region (magenta). Figure was generated using PyMol v.99

1.9 Anthrax Toxin Receptors

1.9.1 Capillary Morphogenesis Receptor (CMG2)

Intoxication of PA is initialized and aided by a specific cellular receptor. There are two such receptors. Tumor endothelial marker 8 (TEM8) and capillary morphogenesis protein 2 (CMG2) are also called anthrax toxin receptors 1 and 2 respective Both are similar in possessing a single peptide, a single extracellular von Willebrand domain A (vWA), a single trans-membrane domain and a cytosolic tail. TEM8 and CMG2 share 60% homology in the vWA domain and are believed to exist as multiple isoforms because of alternative splicing (33, 48). Endothelial cells have higher expression of CMG2 than TEM8 due to capillary morphogenesis in three dimensional collagen matrices (49). Effects due to alteration in CMG2 are juvenile hyaline fibromatosis (JHF), infantile systemic hyalinosis (ISH) (50, 51) and allelic disorders.

The active site within CMG2 for PA interactions is termed the Von Willebrand factor (vWA) domain. They function as sites for protein-protein interactions in almost all cell adhesion proteins (52). vWA domains include a highly conserved metal ion dependent adhesion site, (MIDAS) that is involved in ligand binding (52, 53). These vWA domain interactions closely resemble vWA domain interactions in α-integrin proteins (54). β1-integrin domains are believed to exist in two possible conformations: open and closed conformations which differ in positioning the coordinating residues at the MIDAS site. The atomic resolution structures of the CMG2-vWA domain, with and without the naturally occurring disulphide bond have been determined (Figure 10). The structures share similarity with high affinity open conformations of αM-integrin 1 domain (53). This ability might create a framework for high affinity binding of CMG2 for PA and the importance of receptor in toxin pathogenicity.

The active core of six-stranded β-sheets together with the surrounding six α-helices constitute the vWA domain structure. Hydrogen bonding of Asp 50 and Asp148 with water molecules also coordinates the Mg^{2+} ion (Figure 10) (55). None of the structures show that CMG2 is capable of adopting a closed conformation, attributing to the fact that residues involving a structural change are mostly conserved in CMG2.

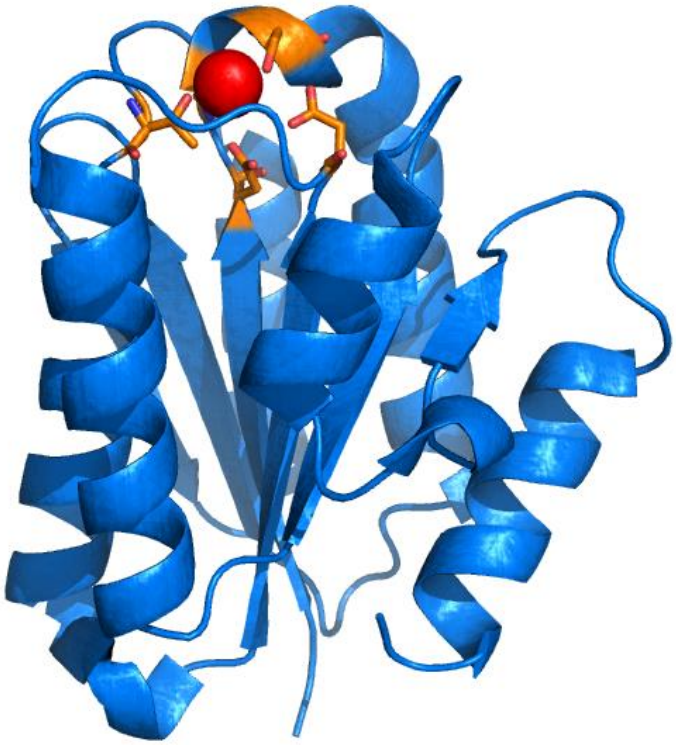

Figure 10. Crystal structure of vWA domain of CMG2 (PDB ID 1SHT) with amino acids (orange) coordinating metal ion (Mg^{2+}, red) in the MIDAS site. Figure was generated using PyMol v.99

1.9.2 Tumor Endothelial Marker 8 (TEM8)

Overall structure of TEM 8 is analogous to CMG2 (Figure 12). TEM8 is rarely detected in adult tissues such as lung, brain, kidney and muscles where CMG2 is abundant. Tumor

endothelial cells and the vasculature of developing embryos mark the presence of TEM8 to a higher extent (33, 56, 57). This may be the reason for CMG2 being preferred over TEM8 for anthrax toxin translocation. TEM8 has three domains: N-terminal domain, extra-cellular Von Willebrand factor type A domain (a single trans-membrane spanning domain) and a C-terminal cytosolic domain (33, 48).

The Crystal structure of TEM8 extra-cellular domain was resolved to 1.7Å (58). The dinucleotide binding fold which is otherwise called α/β open sheet fold is seen in the structure. Five parallel β strands and one antiparallel β strand make up the β core starting from β1, residues 42–50,77–85, 73–79, 173–179 and 196–199) and short antiparallel β strand form (89–96) (Figure 11). Amphipathic α-helices six in number surround the hydrophobic groove that is formed by residues in β sheet. The α-helices numbered as (53–72, 99–110, 120–135, 141–149, 155–170 and 200–217 residues) (58). Differences were observed in the quaternary structures of CMG2 and TEM8. The α3-β4 loop differs in a way that it is shifted 10Å apart when compared to CMG2. Extension of the conserved helices in different directions in the N-terminal region of α6 makes a significant difference (58).

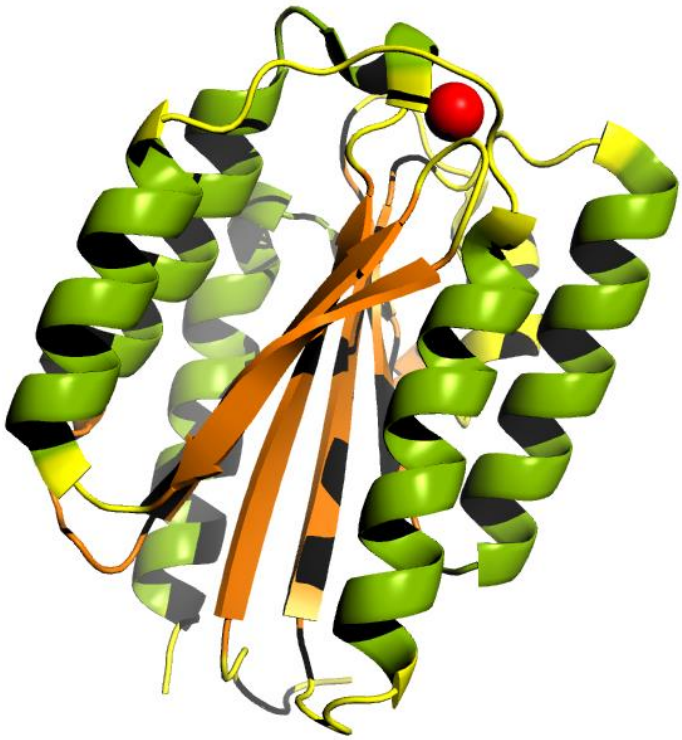

Figure 11. Crystal structure of vWA domain of TEM8 (PDB 3N2N) with 5 parallel β-sheets and 1 anti-parallel (orange) and Mg^{2+} ion in red. Figure was generated using PyMol v.99

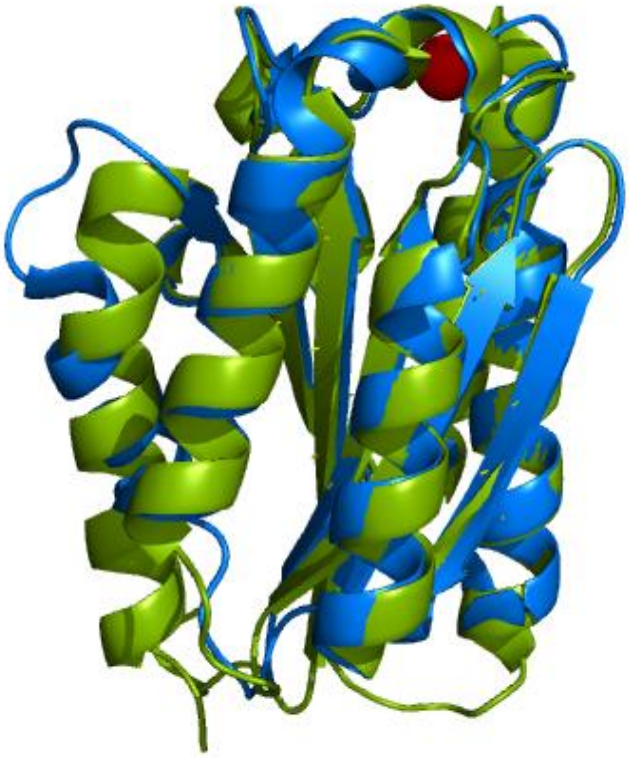

Figure 12. Overlay of Crystal structures of vWA domains, TEM8 and CMG2 (PDB ID 3N2N, 1SHT) TEM8 is green color, CMG2 in blue and Mg^{2+} ion in red. Figure was generated using PyMol v.99

1.10 PA–Binding Interaction with Receptors

The cell binding component of anthrax toxin is found to be the one that interacts with the cell surface receptor and promotes the internalization of the toxin (59). TEM8 and CMG2 are the two identified cell surface receptors for the toxin to bind. TEM8 was first identified as a receptor (48, 60). Binding studies revealed that PA has a higher affinity for CMG2 than TEM8 (33). Integrin β1 heterodimeric complexes also bind PA and promote endocytosis.

Although two receptors were identified that bind PA, striking differences in function made CMG2 more likely to mediate anthrax toxic effects. CMG2 has 1000 fold greater affinity towards PA than TEM8 (61, 62). The pH optimum is one unit lower compared to TEM8 for the formation of the pore (63-65). The increased surface area in PA-CMG2 complex (2000Å) in comparison with the α-integrin ligand (1300 Å) enables PA to have higher affinity for CMG2 (63, 66). Earlier biochemical studies on full length PA and receptor complex revealed that domain IV of PA is the primary site for attachment of both the receptors (67, 68). D683 is the residue of domain IV which competes with the MIDAS site on PA for binding (Figure 13). Mutations in this area were shown to prevent pore formation (69). Domain IV alone contributes approximately 1300 Å buried surface area (48, 66, 70). The additional $2\beta_3$-$2\beta_4$ loop added another 600 Å of surface area to the binding interface (71). This increased surface area in the binding interface corresponds to the high affinity of CMG2 towards PA than TEM8 (61, 69).

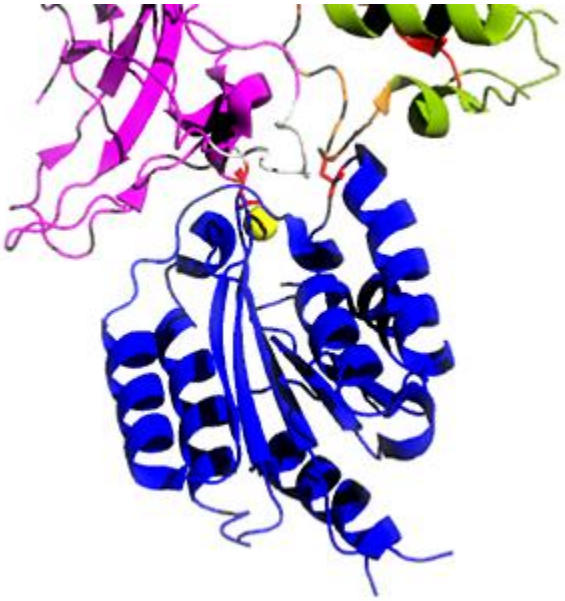

Figure 13. Crystal structures of PA_{63} bound to vWA domain of CMG2 (PDB ID 1TZN) PA63 domain II and domain IV, domain II is on top right (green) and domain IV is on top left (purple) CMG2 in blue. The metal ion in the MIDAS SITE is yellow and Asp 683 in domain IV and Arg 40 in CMG2 are in red sticks, essential for binding interactions.

1.11 PA- Oligomerization

PA binding to the cell surface receptor is followed by proteolytic processing by furin like proteases resulting in the cleavage of first 167 residues in domain I as a 20 kDa protein commonly termed as PA_{20} (72). This happens to be similar in bacterial toxins such as *Pseudomonas* exotoxin (PE) and Diphtheria toxin (DT) (73, 74), with the only marked difference is PA is cleaved at the sequence RKKR-167 whereas PE and DT are cleaved at RQPR-279 and RVRR-193 sequences, respectively (75).

Removal of PA_{20} from domain I is followed by self oligomerization of seven or eight monomers of cleaved PA_{20} to form either a donut shaped heptameric (Figure14) (63) or octameric structure (20). The heptamer formed is commonly referred to as the pre-pore, soluble in water at high pH and is capable of forming ion-selective channels at low pH. The crystal structure of the soluble heptamer was resolved to 4.5 Å by Petosa *et al*. The crystal structure reported that the binding interface of monomers in heptamer involves the contacts between domain I and domain IV (21, 63). The heptamer's diameter measures about 160 Å and the height is 85 Å.

The donut shaped structure results in the presence of a lumen that has a surface area of about 35Å. Domain I and II are found packed inside the heptamer whereas domain III and IV are found lining the periphery of the structure. The hydrophobic cleft left over after the cleavage of PA_{20} creates a binding site for anthrax toxin enzymatic components EF and LF. Single point mutations in domain III were shown to block the pre-pore formation by Mogridge and co-workers (31). The mutation of D512A interferes with the intramolecular hydrogen bond necessary for the stabilization of the pre-pore. A specific combination of techniques like electrophysiology, crystallography and mass spectrometry by Kintzer *et al*. showed the presence of octamers both in solution as well as at the cell surface (20). The octamer was shown to be more stable at physiological temperature, and is likely the form that is more prevalent during infection.

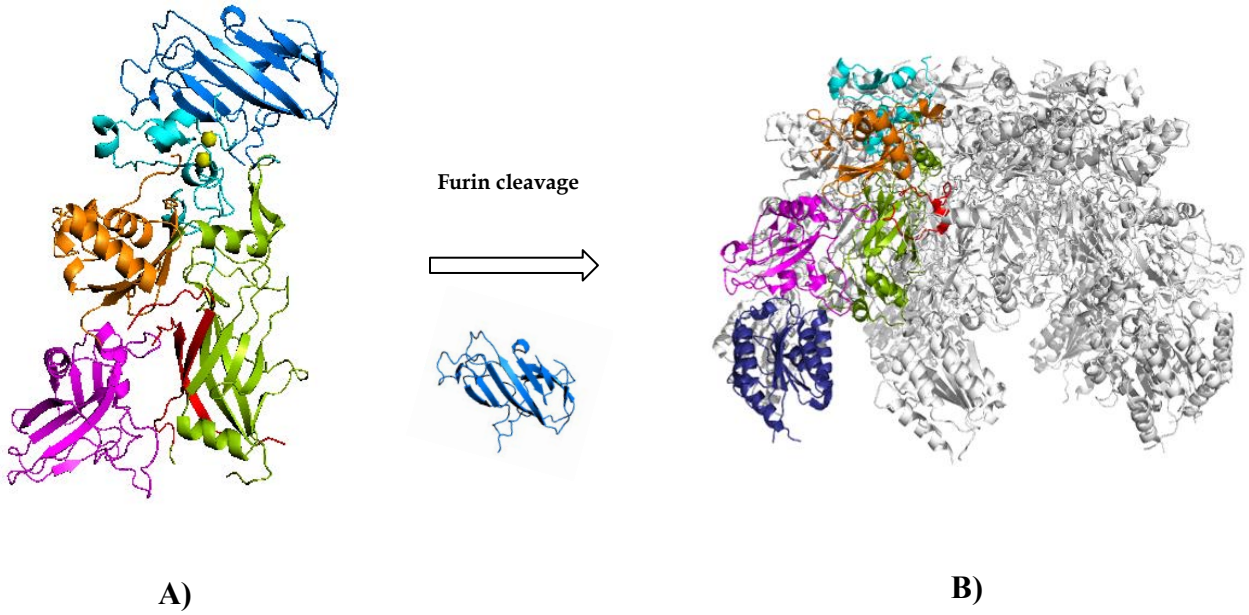

Figure 14. Crystal structures of PA_{83} (PDB ID 1ACC) and PA_{63} bound to vWA domain of CMG2 (PDB ID 1TZN) (1). Illustration of the conversion of PA_{83} to heptamer (pre-pore). A) PA_{20} region of domain I in blue, left over domain I shown in cyan, and calcium ions shown as yellow spheres; domain II is green, and the region which comprises the β-barrel portion of the pore (residues 275-352) is shown in red; domain III is shown in orange, and domain IV is shown in magenta; B) Crystal structure of pre-pore bound to CMG2 (blue)

1.12 Endocytosis

The heptameric receptor bound holotoxin is taken up into the cell by receptor-mediated endocytosis. Lipid rafts are the specialized regions of the plasma membrane rich in cholesterol and spingomyelin (76-78) through which internalization of the pre-pore occurs. Clathrin mediated endocytosis was also shown to occur which shares similarity with the uptake of other cellular proteins, including the low density lipoprotein (LDL) through LDL receptor (79). The major difference between the two processes: LDL is naturally present within lipid rafts while the anthrax receptor is recruited to the lipid rafts after PA binding (74, 76, 77).

Recent studies by Wei *et al*. reported that lipoprotein-receptor related protein1 (LRP6) is required for manifestation of toxin effects in mammalian cells (80). Later controversy of these results was shown by Young *et al.* (81). They revealed that there is no significant role of LRP6 in PA-mediated endocytosis of anthrax toxin (81). EF and LF are taken up along with the heptamer in to the cell. The conversion of endosome to a membrane spanning pore takes place only under acidic conditions.

1.13 Formation of a Membrane Spanning Pore

Pore formation is the pivotal event required for the translocation of the enzymatic components of the toxin EF and LF. Pore formation occurs as a consequence of low pH, and is characterized by an extended 14 stranded β-barrel similar to that produced in case of *Staphylococcus aureus* α-hemolysin (82) Cysteine scanning mutagenesis and labeling the membrane with an impermeable probe, MTS-ET, by Benson and Nassi showed that the residues 275-352 constitute the stem of the pore. $2\beta_2$-$2\beta_3$ and $2\beta_3$-$2\beta_4$ loops include the transmembrane region (residues 303-324) (26, 27). F427 residue located in the lumen of the pore is predicted to

play a significant role in the formation of a key structure called phi (ϕ) clamp. This residue enables the translocation of the EF and LF into the cell *via* formation of a leak free seal around the polypeptide chain (83, 84). Formation of pore involves the $2\beta_2$-$2\beta_3$ and $2\beta_3$-$2\beta_4$ peeling away from domain II. Santelli *et. al.* and coworkers reported that many steric factors hinder this process. Domain IV prevents the movement of the $2\beta_3$-$2\beta_4$ in turn restricting the movement of the $2\beta_2$-$2\beta_3$ which is critical for the formation of the pore. This suggests that domain IV should partially move away from domain II for this process to occur (66, 85). Pre-pore to pore conversion occurs, in the absence of the receptor, within a pH range of ~7-7.5. Earlier it was stated that this might be due to the presence of histidine residues as histidine has the pK_a close to physiological pH (~6-6.5), there are five histidines within domain II, four within the $2\beta_2$-$2\beta_3$ strands, and protonation of these residues may cause the conformational change in the pre-pore to a pore (25). Later studies using the labeled PA with 2-fluorohistidine showed that there is no effective change in the pH values for the formation of the pore between the WT and 2-fluorohistidine labeled proteins (86).

Pore formation is immediately followed by the translocation of EF and LF through the channel. (83, 87).Attempts made to determine the crystal structure of the pore were not successful, owing in large part to aggregation (88). Using electron microscopy (EM), the structure of the pore bound to the chaperone GroEL bound pore was reported in 2008 by Fisher and coworkers (89) diameter of the mushroom shaped structure was 125 Å and length of the stem measuring about 100 Å. EM pictures of PA inserted into lipid vesicles and nanodiscs were published by the same group (90). Studies directed at translocation of EF and LF have shown that this process is critically dependent on the formation of the ϕ-clamp, comprised of seven F427 residues from each monomer contributing to the heptamer (65). Translocation could be

reduced by mutating F427 to smaller amino acid residues that were less hydrophobic, suggesting that hydrophobicity played a role in translocation (84). Mutation of F427 into Gly or a charged amino acid has also been shown to prevent pore formation as reported by Sun (91). Certain other mutations such as to histidine, serine or threonine had no effect on pore formation but could selectively inhibit translocation of enzymatic components.

CHAPTER 2

RESEARCH BACKGROUND AND GOAL

2.1 Background

Bacillus anthracis produces three monomeric proteins, Protective antigen (PA), Edema factor (EF) and lethal factor (LF) (Figure 15). As a first step, protective antigen (PA) binds to one of the two possible receptors, CMG2 or TEM8 to form a toxin (anthrax toxin). Receptor-bound PA_{83} is cleaved by a furin like protease, which generates a 20-kDa PA20 subunit and a 63-kDa subunit (PA_{63}). CMG2 bound PA_{63} subunits assembles into either heptameric or octameric

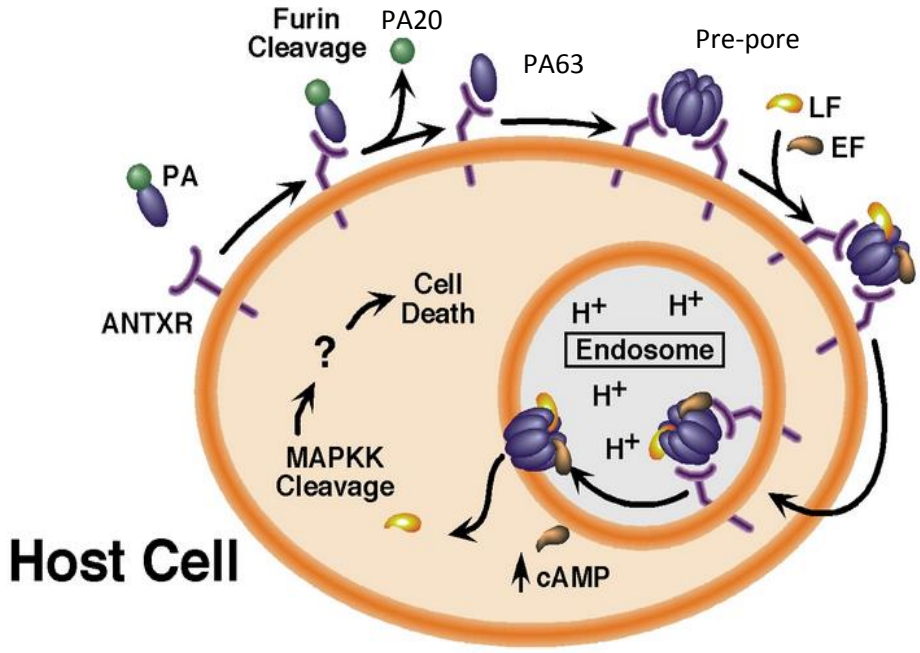

Figure 15. Detailed illusion of Anthrax toxin assembly on host cell surface followed by internalization and release of enzyme moieties (EF or LF). Picture was adapted from http://ysm.research.yale.edu/article.jsp?articleID=415

pre-pore in lipid rafts (20, 21, 76, 92) and these assemblies create a binding pocket for EF or LF. After forming a complex with EF or LF, the toxin–receptor complexes are delivered to an acidic compartment by either clathrin-dependent endocytosis and or other endocytic mechanisms (76, 93). Low pH triggers the formation of a pore within an endosomal membrane through which EF or LF are translocated and enter into the cytosol (65, 76, 77).

X-ray structural analysis of monomeric and heptameric PA-ANTXR2 vWA-domain complexes consisting of the toxin binding, integrin-like I domain of CMG2 revealed that CMG2

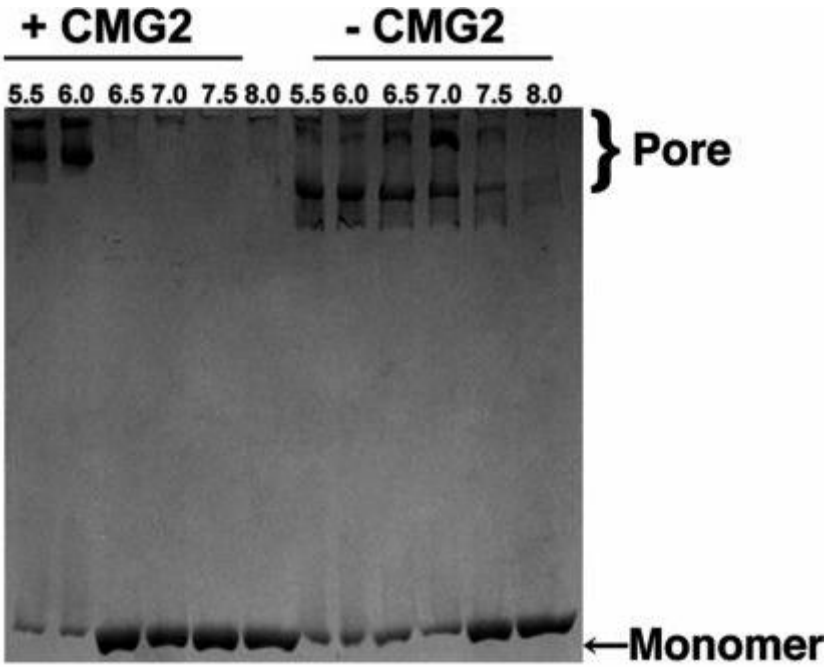

Figure 16. The pH-dependent conversion of PA_{63} pre-pore to pore. Data taken from reference (63) and reproduced here to show the formation of an SDS-resistant state.

binds to PA domains II and IV (63, 66). Based on these findings, it has been proposed that acidic pH causes the release of receptor from domain II to allow conformational changes required for pore formation (63, 66). This model is consistent with binding of CMG2 to heptameric pre-pore which shifts the pH requisite for pore formation, from a pH of 7.5 (absence of CMG2) to a pH of

~6 (63) (Figure 16). Later it was proposed that the receptor might remain bound, likely to domain IV of PA, a structural support for the newly formed pore (66, 94). Recent studies using the 2-FHis-labeled PA had shown that pore formation was completely blocked in presence of CMG2, even though it was able to form a pore in the absence of receptor. It has been shown (by using NMR) that the receptor does not release at low pH, suggesting that the pore formation was related to the release of receptor (95).

Receptor dissociation has also been shown by co-immunoprecipitation experiments, (Figure 17). PA_{63} was bound to EGFP-tagged versions of $CMG2^{488}$ (dGAB-treated cells). The cells were then incubated in buffers at pH 7.3, 6, and 5.2, and lysed. PA-associated receptors were detected by immunoprecipitation with an anti-PA antibody followed by immunobloting with an EGFP-specific antibody. Results show that in the absence of pore formation, PA was associated with $CMG2^{488}$-EGFP (pH 7.3 and pH 6) but not at pH 5.2, when pore formation was observed (Figure 17A) (64). Evidence of receptor release as a consequence of pore formation has come from NMR studies, using the SMRC method. ^{13}C-2-FHis-CMG2 (two fold excess to PA) was used to monitor binding and dissociation with respect to pH. Binding of CMG2 to PA was observed from pH 8 to 6, but there was a significant increase (~30%) of Strong Methyl Resonance of ^{13}C, SMRC intensity at pH 5, suggesting receptor dissociation (95, 96) (Figure 17B).

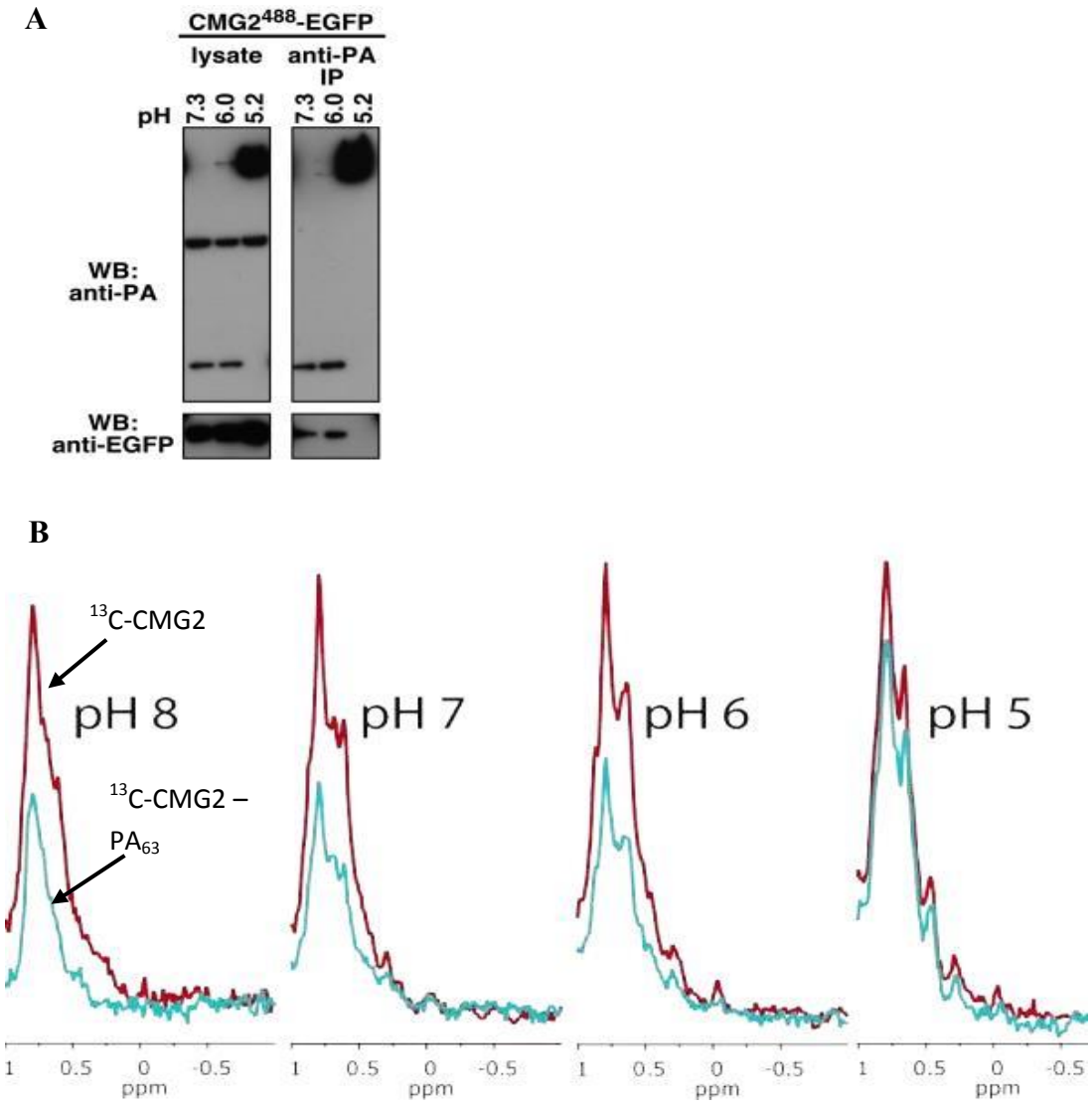

Figure 17. Receptor dissociates (CMG2) from PA_{63} upon pore formation. A) Data from reference (64) showing the results of immunoprecipitation of PA with TEM8 or CMG2 as a function of pH. B) Data from reference (96) showing that the receptor dissociates partially at low pH.

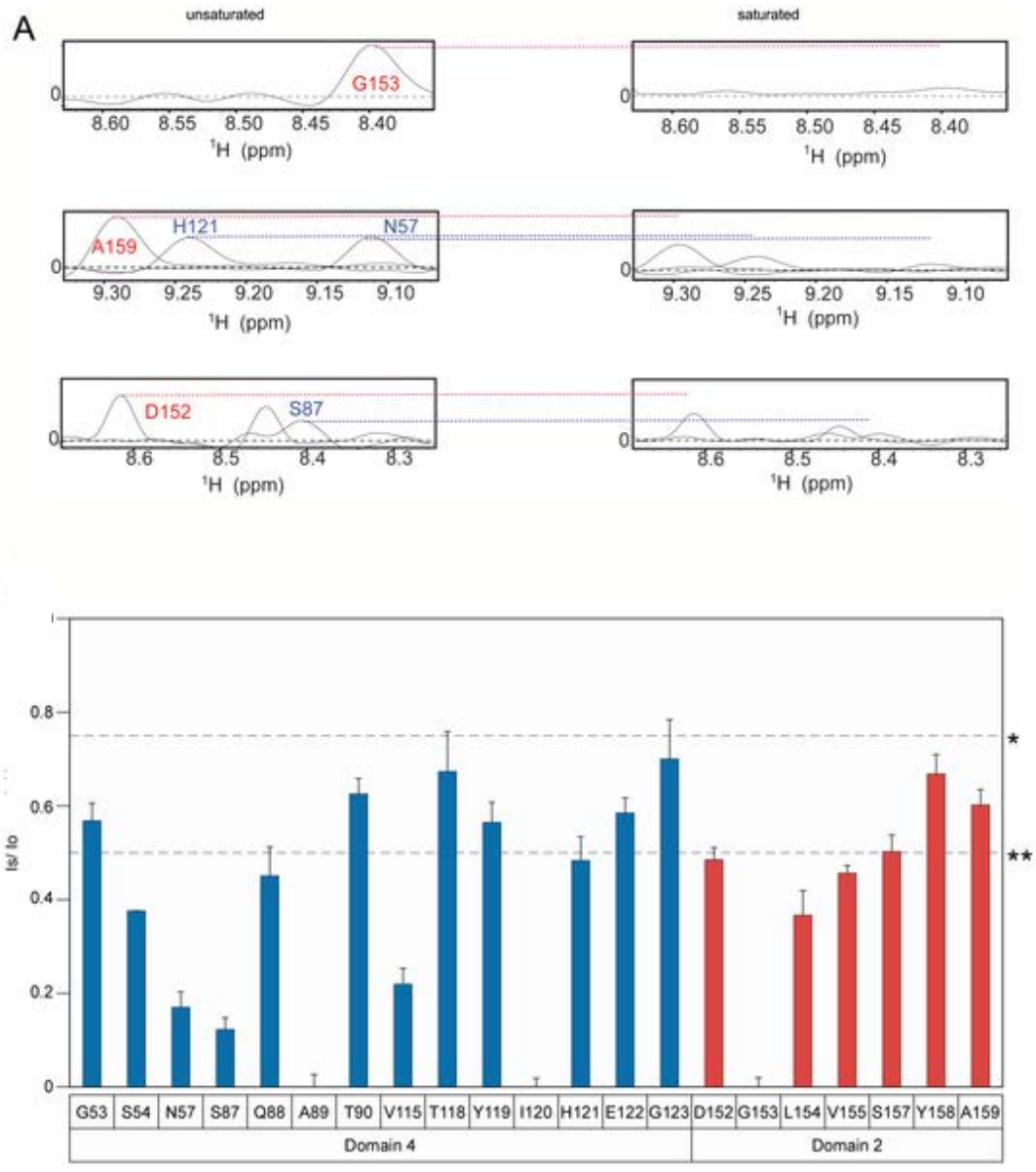
A
unsaturated
saturated
G153
H121
N57
A159
D152
S87
^{1}H (ppm)
Is/ Io
*
**
G53 S54 N57 S87 Q88 A89 T90 V115 T118 Y119 I120 H121 E122 G123 D152 G153 L154 V155 S157 Y158 A159
Domain 4
Domain 2

B

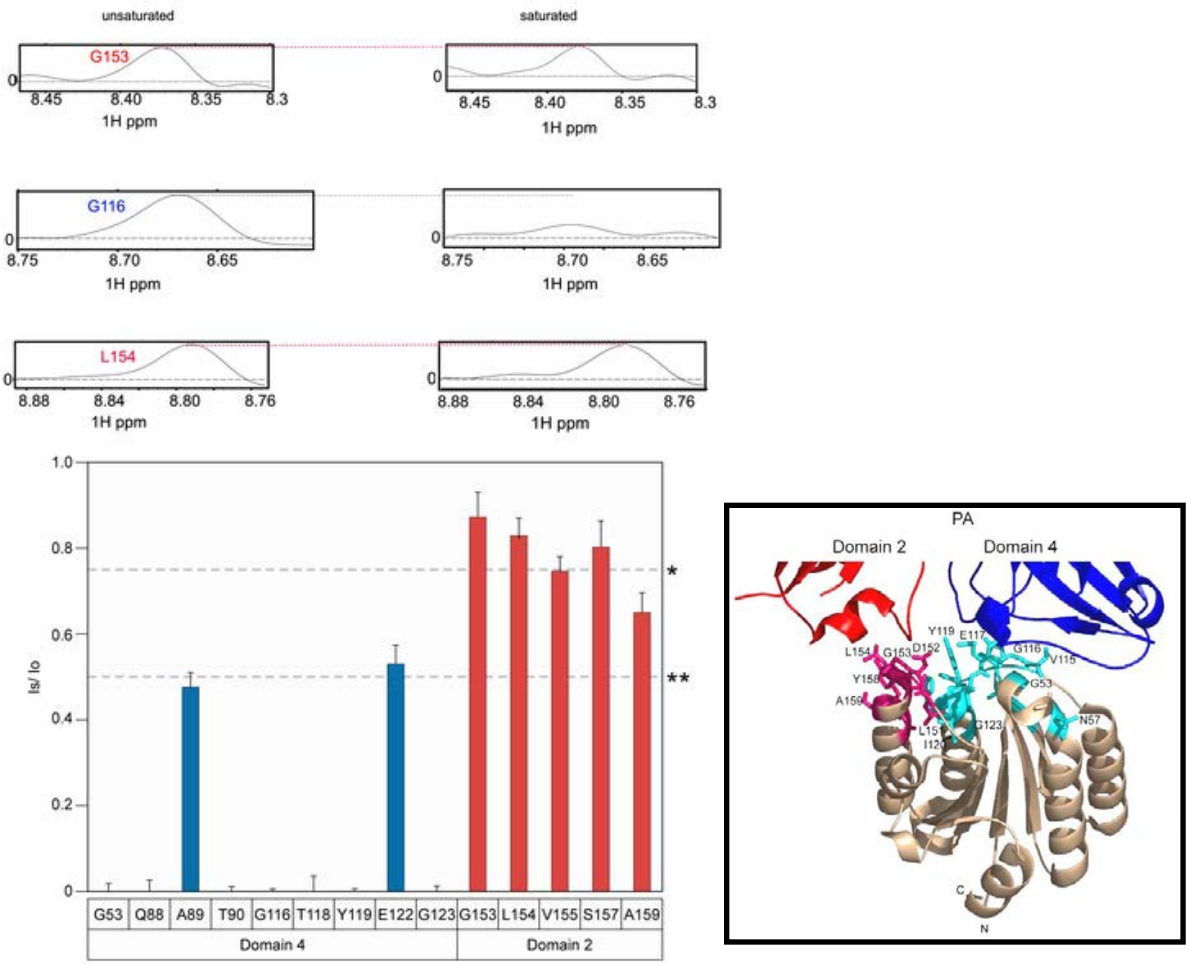

Figure 18. CMG2 contact residues with PA domain II and IV that are saturated at pH 8.0 and pH 5.1. A) Data taken from reference (97) using TROSY NMR that PA remains associated at low pH. B) Same as in A at pH 5.1. The inset show CMG2 contact residues – please see reference (97).

Alternatively, recent NMR studies (97) with 10 fold excess of CMG2 bound to PA_{63} have shown that receptor is still bound to domain IV at low pH even though it dissociates from domain II of PA (Figure 18A and 18B) and it is in agreement with domain IV of PA binding studies from NMR (70). Above NMR studies showed that receptor remains bound to PA even at low pH (66, 98). A key question that remains to be resolved is the mechanism of the conformational change to a pore, and identifying the individual steps in that process. To that end, we have carried a series of fluorescence studies to study the mechanism of pore formation when bound to the receptor CMG2. These studies provide a potential basis for future studies aimed at identifying the mechanism of pore formation.

There has been speculation that low pH could destabilize LF which undergo unfolding and this results in translocation through the newly formed PA_{63} pore (79, 87, 99, 100). EF and LF (N-terminal, PA binding regions) are partially unfolding at lower pH 5-6 range, generating molten globule states, which translocate through PA_{63} pores that are formed on cell surfaces which requires pH values of 5.5 or less (100); however, this mechanism is poorly understood. Recently Smith *et.al*., proposed an electrostatic ratchet (model) of the pore, comprised of opposing rings of charged residues, which interacts with charged cassettes in the substrate to drive unfolding by generating sufficient force (101).While the molecular basis of the ratchet is still unclear; in Chapter 3, we develop a method to understand the unfolding mechanism of LFn using fluorescence.

CHAPTER 3

TOWARDS MONITORING THE CELLULAR REFOLDING OF ANTHRAX LETHAL FACTOR

3.1 Introduction to Anthrax Lethal Factor

Anthrax toxin released by the bacterium, *Bacillus anthracis* is a major cause of death in animals infected with anthrax. Pathogenesis relies on receptor mediated endocytosis of protective antigen (PA_{63}), which forms a pore under acidic conditions, and subsequently allows translocation of EF or LF through this pore(65). EF or LF is transported into cells when the pre-pore form of PA_{63} undergoes a pH-dependent conformational change to a membrane spanning pore. In order to translocate through the pore, EF and LF must unfold due to the narrowness of the β-barrel channel, and then refold once inside the cell. However, the mechanism of refolding that takes place after the translocation is not well understood.

LF (91kDa) is a protease that cleaves mitogen activated protein kinase kinases. Three molecules of LF bind to a heptamer of PA_{63} and four molecules of LF bind to an octamer (20, 92, 102, 103). LF is composed of four domains (Figure 19): domain I is the PA binding domain. Domains II, III and IV together form a deep long groove that holds the N-terminal tail of MAPKK; domain IV carries the zinc catalytic center. Recently the Krantz group reported that the first α-helix and β strand of each LF_N (N-terminal of Lethal factor, residues 1-263, that specifically binds to PA)(104), unfold and dock into an amphipathic cleft on the surface of PA (102). To study the translocation mechanism, we modified the LF_N by introducing 4 cysteine molecules (Figure 20) which allows the binding of fluorescent dye AsCy3. My role in this project was the synthesis of the AsCy3 dye, which is described below.

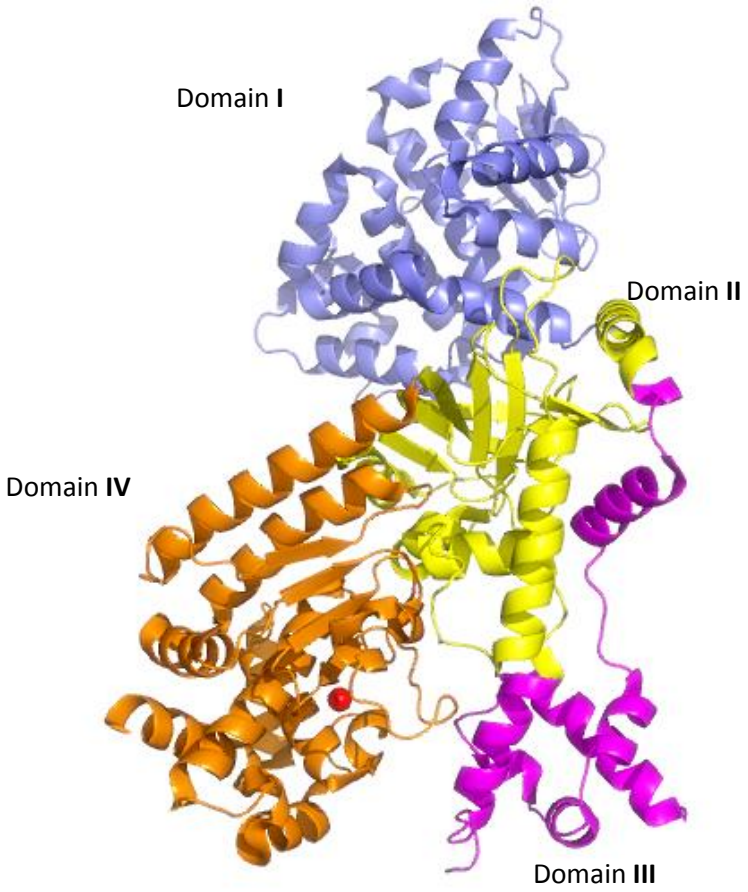

Figure 19. Crystal structure (PDB: 1J7N) of anthrax toxin lethal factor, cartoon representation colored by domain. Domain I (blue), domain II (yellow), domain III (magenta), domain (orange) and Zn in red sphere. Figure was generated by using PyMol v.99

AsCy3 is a biarsenical fluorescent probe that has high binding affinity with a tetra cysteine motif (CCKAEAACC). AsCy3 is a fluorescent probe that, when bound exhibits a large increase in quantum yield (105) (Figure 21). Among all arsenic fluorescent probes AsCy3 has better photostability and minimal environmental sensitivity (106-108).

As a step towards understanding the kinetics and potential factors required for refolding toxins within the cell, we describe here the biochemical properties of LF_NC4, which is labeled with the reversible fluorescent dye AsCy3. The synthesis and photophysical properties of this dye have been described recently(106).

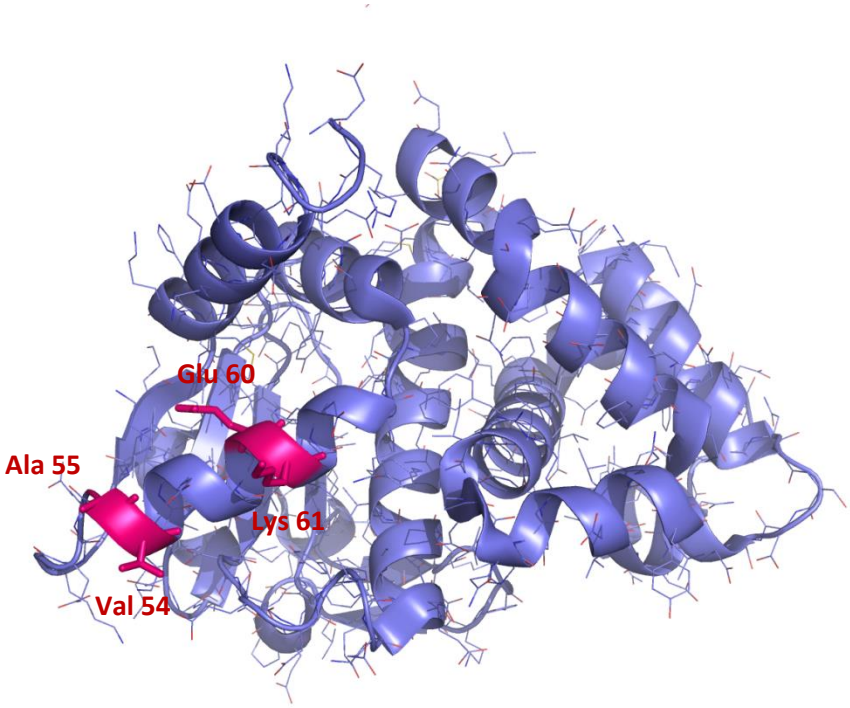

Figure 20. Structure of LF_N residues 54, 55, 60 and 61 (red), which have been mutated to Cys. Figure was generated by using PyMol v.99

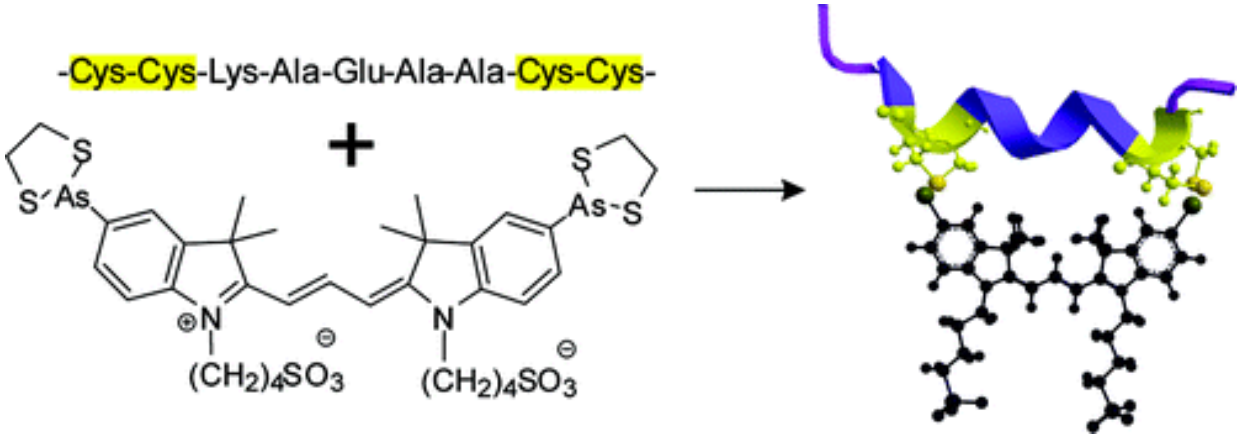

Figure 21. Reaction of AsCy3 with tetracysteine peptide binding motif, Cy3 tag (CCKAEAACC)(106)

3.2 Synthesis of AsCy3 (Figure 23)

3.2.1 Experimental Procedures

Compound (1). 1, 2-dichlorobenzene (14 mL) was refluxed with 2, 3, 3-trimethyl-indole (1.60g) and 1, 4-butanesulfone (4.5g) at 120°C for 16 hours under Argon atmosphere. Cooled the reaction mixture to RT and precipitated with 200 mL acetone, filtered and washed with acetone. (2.3 g). ^{1}H NMR (DMSO-d_6): δ 1.5 (s, 6H), 1.74 (m, 2H), 1.95 (m,2H), 2.49 (m, 2H), 2.84 (s, 3H), 4.48 (t, 2H), 7.61 (m, 2H), 7.82 (m, 1H), 8.03 (m, 1H).

Compound (2). In acetic anhydride/ acetic acid mixture (14 mL AcOH, 9 mL acetic anhydride and 0.6g sodium acetate) Compound **1** (1.0 g) and triethyl orthoformate (1.0g) were heated O/N at 120°C. Evapoured the solvent and purified the crude product by HPLC (0.2g. ^{1}H NMR (DMSO-d_6): δ 1.7 (s, 12H), 1.84 (m, 8H), 2.62 (m, 4H), 4.09 (t, 4H), 6.6 (d, 2H), 7.3 (t, 2H), 7.5 (d, 2H), 7.6 (d, 2H), 8.34 (t, 1H). ESI MS: [MH]+ 600.

Compound (3 and 4). Mercuric oxide (110mg) and compound (**2**) (100mg) were stirred in trifluoroacetic acid (3.0mL) O/N at 25° C. Evaporated the solvent and washed with water, compound, (**3**) (170mg). Dried the crude compound (3) with phosphorous pentoxide (P_2O_5) overnight, (80mg) and then resuspended in anhydrous *N*-methyl pyrrolidinone (NMP, 1 mL) with arsenic trichloride (100µL), diisopropyl ethyl amine (60µL) and palladium acetate (5mg). Stirred for 10 h at room temperature. Reaction mixture was dissolved in phosphate buffer (7 mL) and 1, 2-ethanedithiol (200 mL) and extracted with chloroform. Purified the crude product by preparative TLC.

^{1}H NMR (DMSO-d_6): δ 1.7 (m, 20H), 3.0 (m, 4H), 4.0 (m, 4H), 6.6 (d, 2H), 7.49 (d, 2H), 7.74 (d, 2H), 7.9 (s, 2H), 8.29(t, 1H). ESI MS: 933.2.

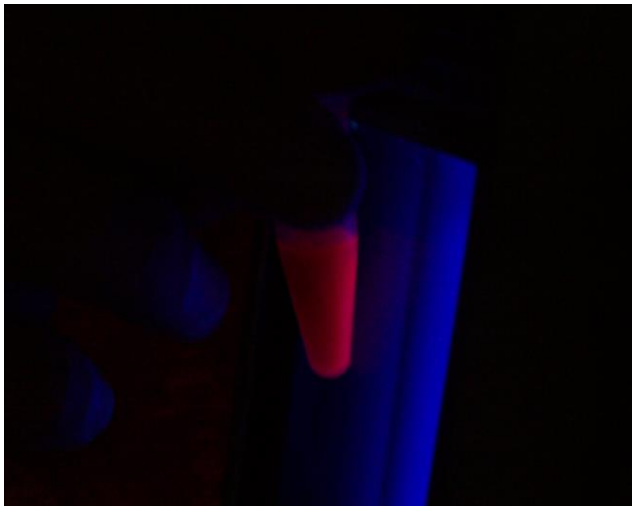

Figure 22: Fluorescence induced by exposure to ultraviolet light in vial containing AsCy3.

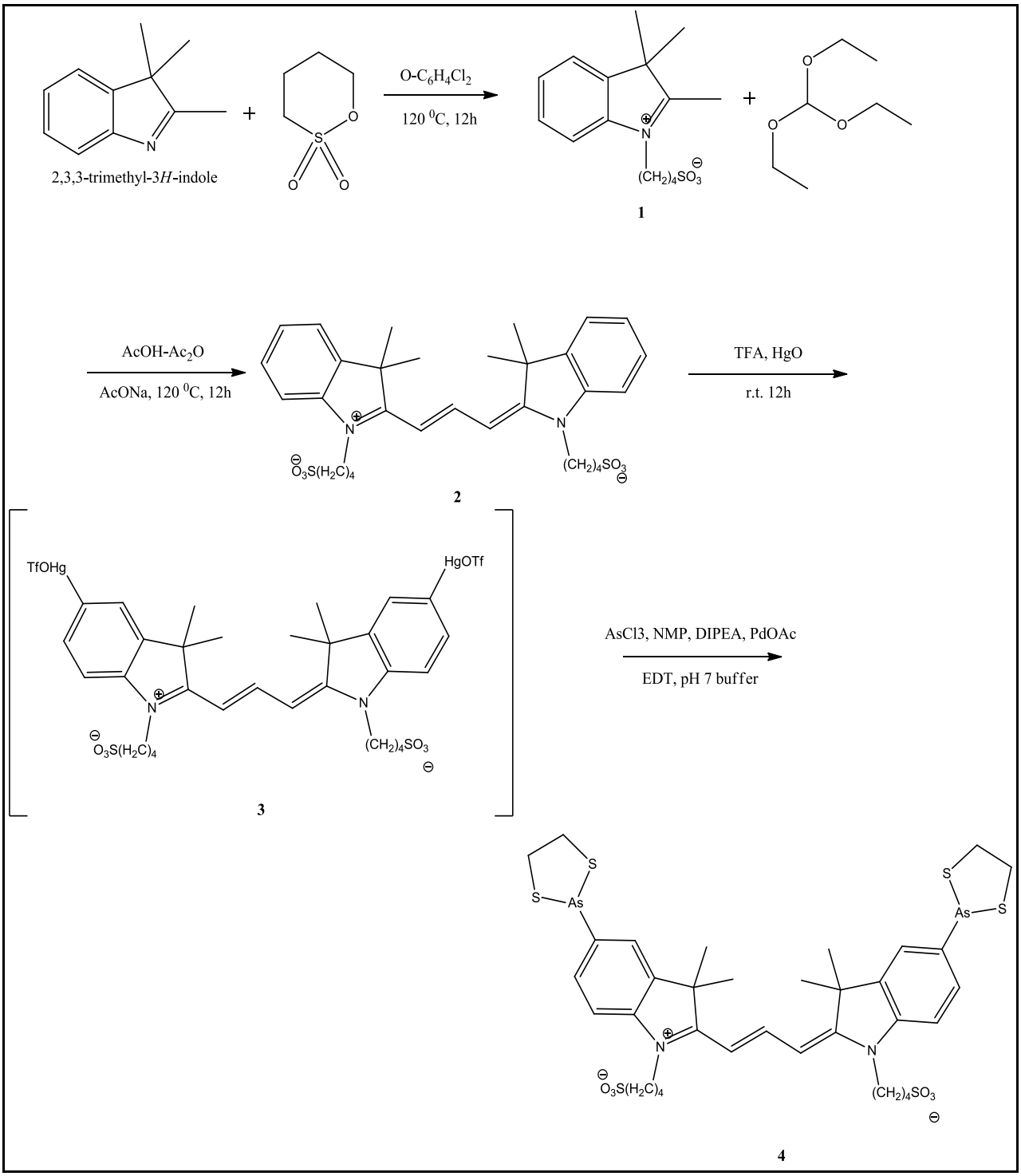

Figure 23. Synthetic scheme of AsCy3 (106)

3.3 Materials and Methods:

Reagents and buffers

AsCy3 has been was synthesized as described earlier.

TCEP.HCl from Thermo scientific

Buffer A: 20 mM sodium phosphate pH 7.4, 0.5 M NaCl, 5mM Imidazole

Buffer B: 20 mM Sodium Phosphate pH 7.4, 0.5 M NaCl, 5M Imidazole

Buffer C: 20 mM HEPES, 100 mM NaCl pH 8.0

Buffer D: 50mM Tris, 0.1mM TCEP pH 8.0

LF_N expression and purification are summarized in Appendix B.4.5

3.3.1 Labeling of AsCy3

To 2-3 mg of LF_NC_4 protein (in buffer C) was added 10 fold excess of TCEP to reduce disulfide bonds. The mixture was then incubated with 10 fold excess of AsCy3 overnight at overnight at 4^0C. After completion of the reaction, we added 10 fold excess of β-mercapto ethanol to eliminate excess reactive dye during the purification step. Labeled protein was purified by passing through a Sephadex the S-200 gel filtration column equilibrated with buffer C, to remove the unreacted dye.

3.3.2 Absorption and Emission Spectra of labeled proteins

Emission and absorption spectra of labeled proteins were measured in buffer C at 20 ^{0}C. Fluorescence emission maxima of AsCy3 were shifted greatly towards higher wavelength (red-

shift) upon binding to LF_N from 568 nm (AsCy3 alone) to 580 nm (LF_NC4-AsCy3). But however there was no change in absorption spectra with respect to LF_NC_4 binding.

3.3.3 Circular dichroism (CD) analysis of LF_N

CD spectra were acquired on a Jasco-J-810 spectropolarimeter equipped with a temperature-controlled water bath. Samples of WT LF_N and LF_NC_4 (1.8 mg/mL) in buffer D were placed in a 0.1mm CD cell. Spectra (five scans) average was an average of spectral scans was collected from 260 to 180 nm at 20^oC with a 20 nm/min scan rate and a response time of 2 S. Data were normalized to the mean residue ellipticity based on the value for 262 peptide bonds.

3.3.4 Urea denaturation studies:

Urea denaturation curves were obtained from the fluorescence intensity measurements at 308 nm upon excitation at 280 nm. All solutions for denaturation experiments were prepared in 30 mM HEPES buffer, pH 7.45 with 0.1 mM TCEP. To 2 μM $WTLF_N$ and LF_NC_4, stock denaturant solutions (10 M urea) were added to get the desired final concentration of 5 M urea. The final resulting mixture was incubated for 16 h at room temperature before measurements were made. Blank solutions that contained the appropriate concentrations of denaturants were also used.

3.3.5 Equilibrium binding titration

We performed AsCy3 binding titrations under equilibrium conditions to study the stoichiometric ratio of LF_NC_4 to AsCy3. AsCy3 was diluted to 0.1 μM in 30 mM HEPES pH 7.5. sub stoichiometric quantities of LF_NC_4 were added to increase the concentration from 0.1 to 1. Samples were incubated overnight at 4^0C. Fluorescence emission spectra were recorded for each

aliquot in a Cary-Eclipse spectrofluorometer at 20 ^{o}C. The AsCy3 fluorophore was excited at 553 nm and the emission at 580 nm were recorded.

3.4 Results and Discussion:

PA undergoes self-assembly and forms an oligomer that binds LF and EF. These holotoxin complexes are endocytosed and transported to an acidic compartment in the cell. At low pH, PA oligomer converts into a membrane-spanning pore, translocates channel, LF and EF must pass through the pore which is so narrow that, presumably LF and EF must unfold to translocate (87).

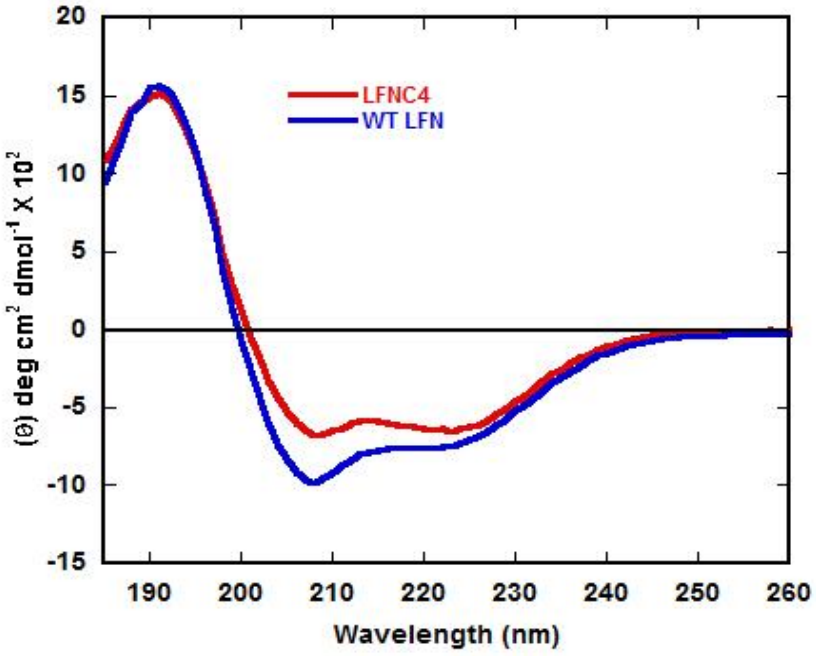

Figure 24. Far-UV circular dichroism analyses. Residual molar ellipticity (Θ) was measured from 180 to 260 nm at 25°C of LF_NC_4 and WT LF_N (1.8 mg/mL) in 50mM Tris with 0.1 mM TCEP.

Recent crystal structure studies revealed that unfolding of LF α1 and β1 is pre-requisite for proper binding to PA oligomers (102). To investigate refolding of LFN within the cell, we introduced four cysteine residues at positions 54, 55, 60, and 61 in helix 2 and labeled the mutant fragment with AsCy3. Structural characterization of WT LF_N and LF_NC_4 was carried out by CD spectroscopy for comparison. Far UV-CD spectra show quite similar structures at 20 ^{0}C, the spectrum contains a minimum at ~208 and a shoulder 222 nm characteristic of proteins containing predominantly α-helix and small percentage of β-sheets (Figure 24).

To characterize the stability properties of the LF_NC_4, we studied the urea denaturation of the protein by fluorescence spectroscopy at pH 7.45 and 20° C. While increasing the concentration of urea, the fluorescence intensity decreased at peak maxima of ~308 nm, thereby indicating the denaturation of LF_NC_4. Thermal denaturation studies by CD also showed a similar T_m (~55° C) indicating both WT LF_N and LF_NC_4 have possess similar stabilities (Figure 25 A) (Figure and 25 B).

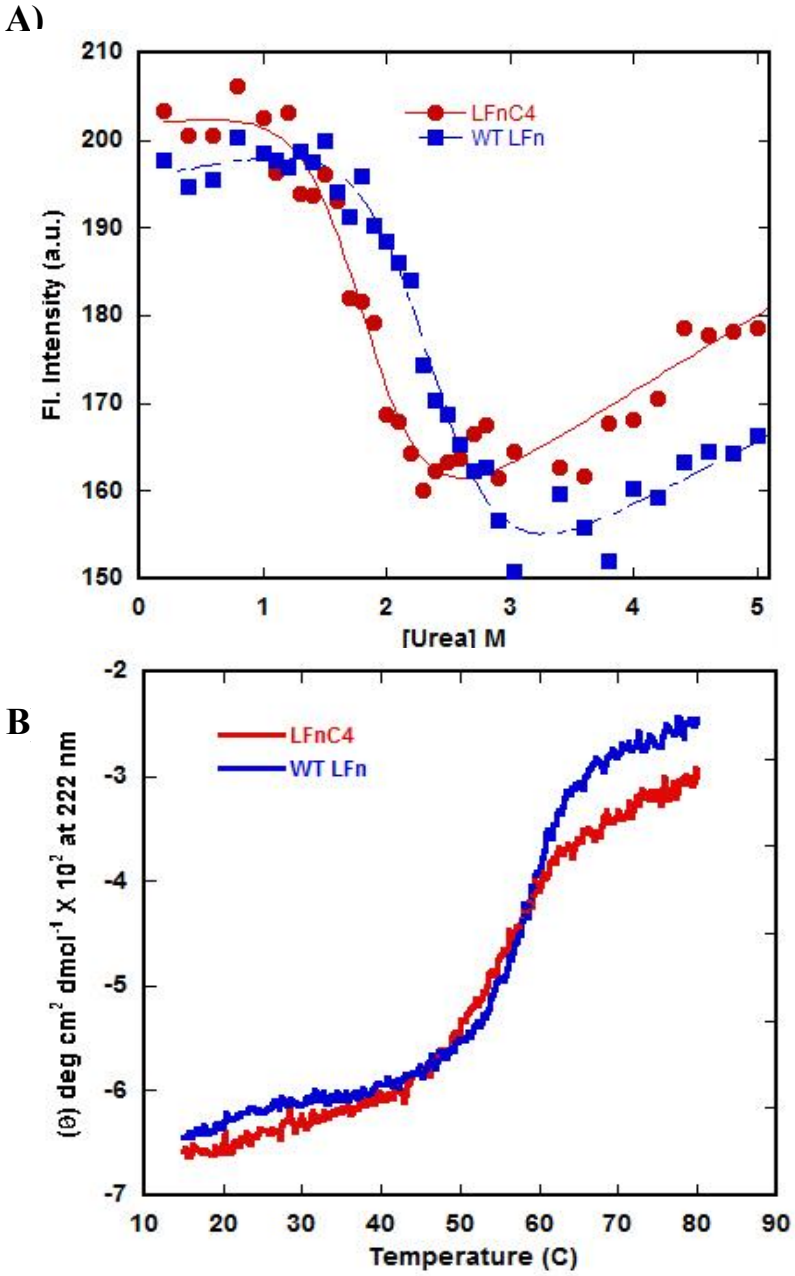

Figure 25. Stability of WT LF_N and LF_NC_4 to urea. **A)** Urea denaturation of WT LF_N (■) and LF_NC_4 (●) were measured using fluorescence and represent the normalized emission intensity at 308 nm (excitation 280 nm). All spectra were recorded at 20 °C, in 30 mM HEPES buffer, pH 7.45 with 0.1 mM TCEP, and represent the average of 3 scans. B) CD thermal denaturation at 222 nm of WT LF_N (■) and LFNC4 (●)

To determine the binding efficiency of AsCy3 to LF_NC_4, we carried out fluorescence binding titration by increasing the concentration of LF_NC_4 (from 0 to 4 μM) with constant amount of AsCy3 (0.1 μM). Our results from binding titration illustrated in Figure 26 reveals that AsCy3 binds to LF_NC_4 with 1:1 binding stoichiometry by increasing the fluorescent intensity, along with red shift of fluorescent spectrum (emission peak maxima from 572 to 580 nm) Figure 27. The observed binding association of AsCy3 to LF_NC_4 was comparable with AsCy3 to Cy3TAG; it is evident that AsCy3 was binding to LF_NC_4.

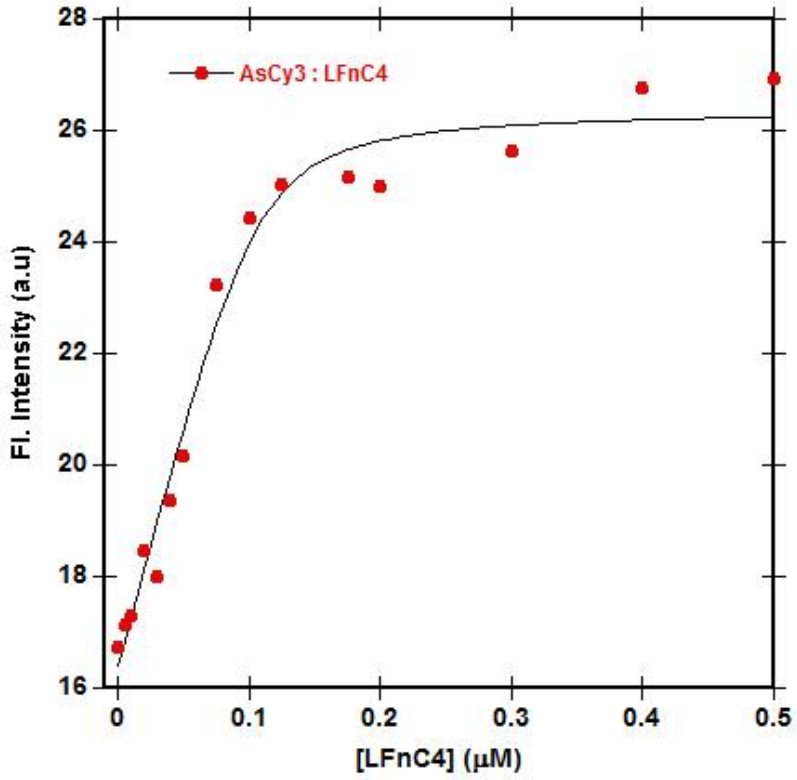

Figure 26. Binding of 0.1 μM AsCy3 to LFnC4 as concentration of LFnC4 was increased from 0 μM to 4 μM, shown by fluorescence emission spectra and intensities which were measured using an excitation wavelength of 553 nm and slit width set to 5 on a Cary Eclipse spectrofluorometer. Emission peak maxima ranged from 572 nm to 580 nm.

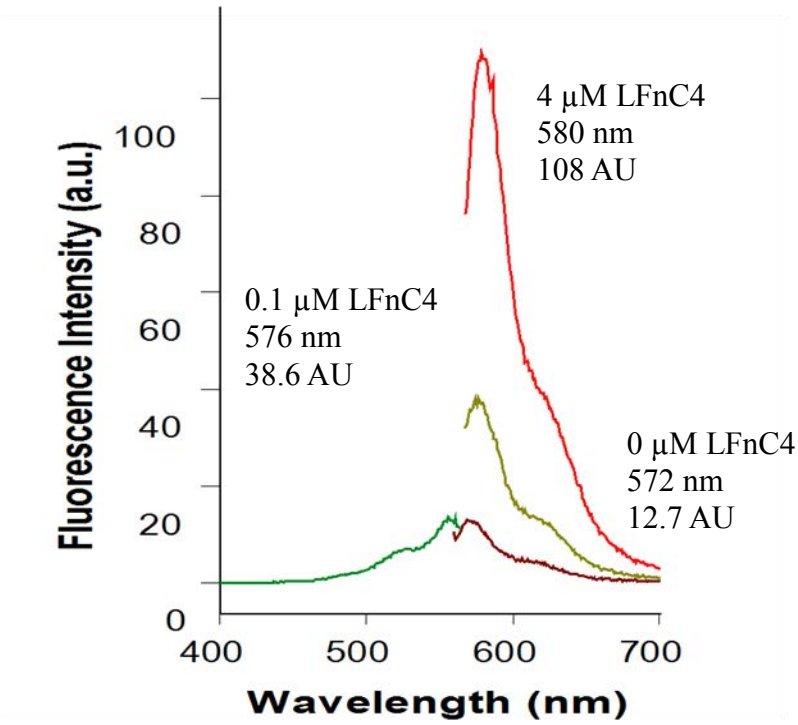

Figure 27. Fluorescence excitation and emission spectra showing the binding of 0.1 µM AsCy3 to LF_NC_4 as [LF_NC_4] was increased from 0 (Maroon), to 0.1 µM (green) to 4 µM (red). Spectra shows a 8.5-fold increase in intensity from 0 to 4 µM LF_NC_4 as well as 8 nm red-shift of emission peak maximum.

3.5. Conclusions

In this study, we synthesized a biarsenical fluorescent probe, AsCy3, which successfully bound to LF_NC_4 at helix 2. By introducing AsCy3 into $LF_{N,}$ we can use fluorescence to the timeframe of refolding of LFN within the cell. Our circular dichroism studies showed that LF_NC_4 and WT have basically similar structures and stability. As measured by urea denaturation, the stability of LF_NC_4 to urea was shown by fluorescence to be very similar to WT LF_N (~ 2M urea). Binding of AsCy3 to LF_NC_4 was successfully demonstrated via an increase in fluorescence intensity and red-shift in the peak maximum for AsCy3.

Since AsCy3 shows fluorescence enhancement when it is bound versus when it is unbound, it may be a useful probe for monitoring the timeframe of translocation of lethal factor into the cell cytoplasm and for determining the parameters required for cellular refolding.

CHAPTER 4

CRYSTAL STRUCTURE OF 2-FLUORO-L-HISTIDINE

4.1 Introduction:

Histidine is an important biological amino acid, through its ability to undergo protonation and de-protonation at physiological pH. Fluorinated amino acids have been shown to be valuable biochemical and pharmacological tools (109). Recently fluorine-containing analogues of histidine, proline and tryptophan, have been synthesized and have gained a lot of attention because of their advantageous biophysical, chemical and biological properties (86, 110-112). We are particularly interested in 2-fluorohistidine because the fluorine substitution has a very small impact on its structure and steric consequences (109). Histidine is one of most important amino acids in terms of protein function and catalytic action of enzymes (113). It is challenging to study the role of histidine in biological processes because of its size, shape and tendency to form hydrogen bonds and salt bridges at local pH environments (114). In histidine, the imidazole ring is mostly protonated and stabilized by resonance (Figure 28). Because of the pK_a of the

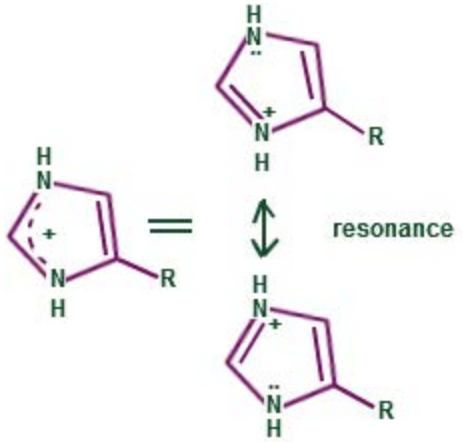

Figure 28. Resonance structure of histidine side chain. R stands for $–CH_2$-CH (NH_2) (COOH)

imidazole ring of histidine, protonation and de-protonation can occur within physiological pH range.

Since the fluorine atom has high electronegativity and is slightly larger than the hydrogen atom, it is expected to have little effect on native protein structure (115) (Figure 31). This is advantageous for protein folding studies because of the high sensitivity of the fluorine nucleus to its local environment. However, 2-Fluoro-L-histidine (2-FHis) is unable to protonate at physiological pH, due to a greatly reduced side chain pK_a (~1), in contrast to the normal histidine pK_a (~6) (Figure 29).

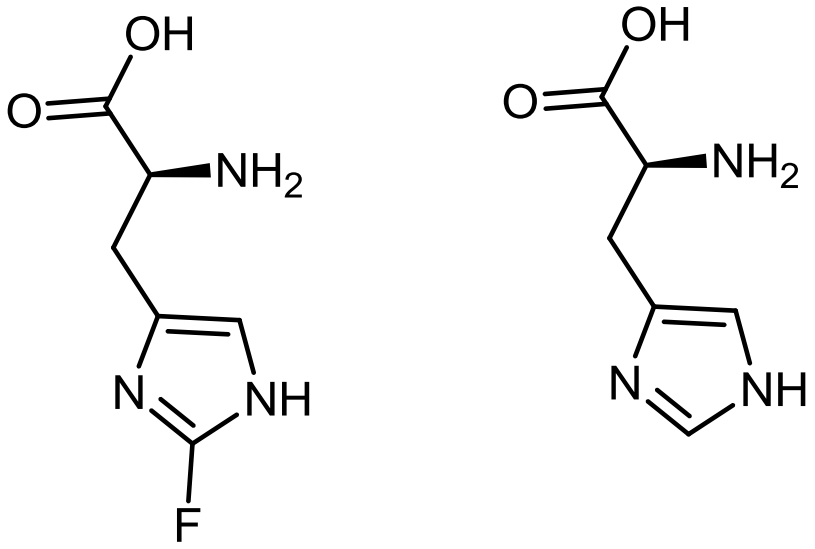

(A) **(B)**

Figure 29: Structure of 2-fluoro-L-histidine and Histidine.

Usually, histidine gets protonated at low pH (Figure 28) and loses its function by chemical modification. This makes 2-fluoro-L-histidine a unique analog to probe the role of histidine in protein structure and function (86, 116). We have investigated 2-fluoro-L-histidine by X-ray crystallography to determine its structure.

4.2 Experimental and Structure Solution:

A large number of colorless needles were obtained by slow evaporation of an aqueous solution of 2-Fluoro-L-histidine and then dried over calcium chloride. A colorless crystal with the dimensions 0.16x0.14x0.13 mm was affixed to nylon cryo-loop using oil (paratone-n, Exxon) and mounted in the cold stream of a Bruker Kappa-Apex-II area-detector diffractometer. The temperature at the crystal was maintained at 150 K using a cryostream 700 Ex cooler. The unit cell was determined from the setting angles of 87 reflections collected in 36 frames of data.

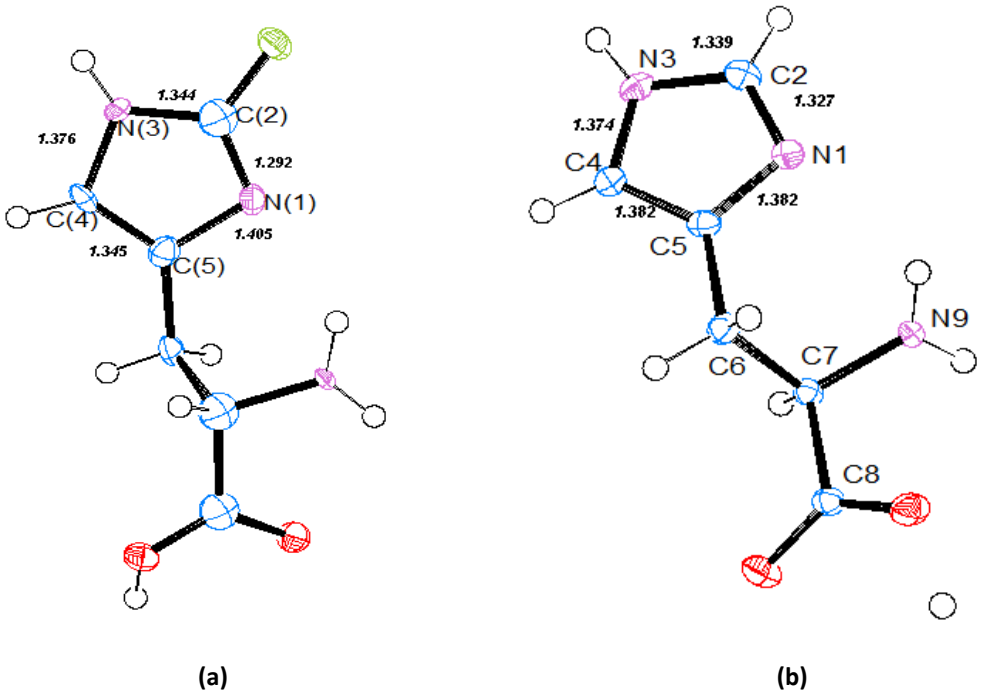

(a) (b)

Figure 30. The conformation structures of (a) 2-Fluoro-L-histidine and (b) L-histidine crystals.

Data were measured with a redundancy of 3.88 using a CCD detector at a distance of 50 mm from the crystal with a combination of phi and omega scans. A scan width of 0.5 degrees

and time of 60 seconds was employed along with graphite mono-chromated Molybdenum Kα radiation (λ= 0.71073 Å) that was collimated to a 0.6mm diameter. Data collection, reduction, structure solution, and refinement were performed using the Bruker Apex2 suite (v2.0-2). All available reflections to $2\theta_{max} = 52°$ were harvested (3663 reflections, 1352 unique) and corrected for Lorentz and polarization factors with Bruker SAINT (v6.45). Reflections were then corrected for absorption (numerical correction, μ=0.14 mm^{-1}), interframe scaling, and other systematic errors with SADABS 2004/1 (combined transmission and other correction factors min. /max. = 0.9852/0.9906. The structure was solved (direct methods) and refined (full-matrix least-squares against F^2) with the Bruker SHELXTL package (v6.14-1). All non-hydrogen atoms were refined using anisotropic thermal parameters. All hydrogen atoms were included at idealized positions; hydrogen atoms were not refined. Pertinent crystal, data collection, and refinement parameters are given in Table 1, atomic parameters and equivalent isotropic thermal parameters are given in Table 2, and anisotropic thermal parameters are given in Table 3.

4.3 Crystal data

Table 1:

Empirical formula	$C_6 H_8 F N_3 O_2$
Formula weight	173.15
Temperature	150 K
Wavelength	0.71073 Å
Crystal system	Orthorhombic
Space group	P2(1)2(1)2(1)
Unit cell dimensions	a = 5.1880(3) Å
	b = 7.3480(5) Å
	c = 18.7169 (12) Å
	α = 90°
	β = 90°
	γ = 90°
Volume	713.51(8) $Å^3$
Z	4
Density (calculated)	1.612 Mg/m^3

Table 1 (continued)

Absorption coefficient	0.140 mm^{-1}
F(000)	360
Crystal size	0.16 x 0.14 x 0.13 mm
Crystal habit	Plate
Crystal color	Colorless
θ range for data collection	2.98 to 25.99°
Limiting indices	-6<=h<=6
	-9<=k<=9
	-22<=l<=17
Reflections collected/unique	3663/1352[R(int) = 0.0222]
Completeness to θ = 25.99°	98.0 %
Refinement method	Full-matrix least-squares on F2
Data / restraints / parameters	1352 / 0 / 109
Refinement threshold	I>2sigma(I)]
Data>threshold	1257
Goodness-of-fit on F2	1.055

Table 1 (continued)

Final R indices [I>2sigma (I)]	R1 = 0.0433, wR2 = 0.1216
R indices (all data)	R1 = 0.0473, wR2 = 0.1251
Largest diff. peak and hole	0.442 and -0.417 e.Å^{-3}

The compound sits in a general position in the orthorhombic space group *P2 (1)2(1)2(1)*. There is one molecule in the asymmetric unit. The molecule contains an intramolecular hydrogen bonding interaction between one of the imidazole N and the N of the amine with a N···N distance of 2.86 Å. The molecule contains an intermolecular hydrogen bonding interaction between the carboxylic acid O and the imidazole N of a symmetry related (3/2-x, 1-y,-1/2+z) molecule with a O···N distance of 2.75 Å. The molecule contains an intermolecular hydrogen bonding interaction between the carboxylic acid O and the amine N of a symmetry related (2-x,-1/2+y, 1/2-z) molecule with a O···N distance of 2.89 Å. The molecule contains an intermolecular hydrogen bonding interaction between the carboxylic acid O and the amine N of a symmetry related (1-x,-1/2+y, 1/2-z) molecule with a O···N distance of 2.69 Å. Inter atomic bond distances and angles are provided in Tables 4 and 5. Two ORTEP (ORTEP3 for Windows - Farrugia, L. J. (1997) J. Appl. Cryst. 30, 565) figures are provided with thermal ellipsoids drawn at the 50% probability level.

Table 2: Atomic coordinates (x 104) and equivalent isotropic displacement parameters (Å2x 103) for KA0003. U(eq) is defined as one third of the trace of the orthogonalized Uij tensor.

	x	y	z	U(eq)	
N(1)	4443(4)	5346(3)	4471(1)	18(1)	
C(2)	4353(5)	5534(4)	5157(1)	18(1)	
N(3)	6359(4)	4835(3)	5519(1)	18(1)	
C(4)	7962(5)	4134(4)	5002(1)	17(1)	
C(5)	6798(5)	4441(3)	4366(1)	16(1)	
C(6)	7728(6)	4010(4)	3630(1)	17(1)	
C(7)	8280(5)	5747(3)	3191(1)	14(1)	
C(8)	9310(5)	5230(3)	2449(1)	14(1)	
N(9)	5862(4)	6829(3)	3114(1)	14(1)	
F (1)	2479(3)	6321(2)	5517(1)	31(1)	
O (1)	11696(3)	4958(3)	2408(1)	18(1)	
O (2)	7692(4)	5062(3)	1960(1)	21(1)	

Table 3: Anisotropic displacement parameters ($Å^2 x\ 10^3$). The anisotropic displacement factor exponent takes the form: $-2\pi^2 [h^2 a^{*2} U^{11} + ... + 2\ h\ k\ a^*\ b^*\ U^{12}]$

	U^{11}	U^{22}	U^{33}	U^{23}	U^{13}	U^{12}
N(1)	19(1)	19(1)	16(1)	1(1)	1(1)	3(1)
C(2)	19(1)	19(1)	15(1)	0(1)	6(1)	-1(1)
N(3)	22(1)	21(1)	11(1)	0(1)	-1(1)	-3(1)
C(4)	17(1)	16(1)	18(1)	3(1)	2(1)	-2(1)
C(5)	18(1)	15(1)	15(1)	3(1)	3(1)	0(1)
C(6)	23(1)	16(1)	13(1)	2(1)	3(1)	5(1)
C(7)	13(1)	14(1)	14(1)	-1(1)	0(1)	0(1)
C(8)	17(1)	12(1)	14(1)	0(1)	4(1)	-1(1)
N(9)	16(1)	18(1)	8(1)	0(1)	0(1)	4(1)
F(1)	31(1)	36(1)	27(1)	-5(1)	6(1)	6(1)
O(1)	17(1)	23(1)	16(1)	-6(1)	3(1)	0(1)
O(2)	18(1)	35(1)	10(1)	-3(1)	-1(1)	-3(1)

4.4 Results and Discussion

The most interesting result of this investigation is the evidence found for the basicity and nucleophilicity of imidazole ring nitrogens. The present crystal structure is similar to L-histidine, shown in Figure. 31. The fluorine atom is substituted on C (2) which pulls the shared electrons towards the central carbon from both ring nitrogen atoms, resulting in the changes in bond angles and bond lengths shown in Tables 4 and 5. In comparison to L-Histidine, the bond angles of 2-Fluoro-L-Histidine closely resemble the protonated form of L-Histidine. N (1)-C (2)-N (3) is 115.7^0 for 2-Fluoro-L-histidine and 112.2^0 for L-histidine un-protonated. This is consistent with an increase in the sp^2 character of the bond hybridization at the ring carbon. In addition, the angles at N (1) and N (3) are squeezed to 102.7^0 and 104.9^0 respectively.

This molecule contains three inter-molecular as well as intra molecular hydrogen bonds. The intra molecular hydrogen bond between the amine nitrogen and the ring nitrogen is N (9)… N (1) =2.86 Å, (0.08Å) longer than the L-histidine shown in Table 6. Inter molecular hydrogen bonds define the packing of the carboxyl and amino groups, and link the head of one molecule N (3) to the tail of the next O (2) as is shown in Figure 32. The bond length of C (2)-N (1) is significantly reduced and the hydrogen bond distance is increased (N (9)--N (1)) 2.86 Å due to the presence of fluorine (inductively electron withdrawing) at C (2). The basicity is further confirmed by the fact that the N (1)- C (2) bond in 2-fluoro-L-hisitidine is considerably shortened (1.292 Å) compared to histidine (1.327 Å).

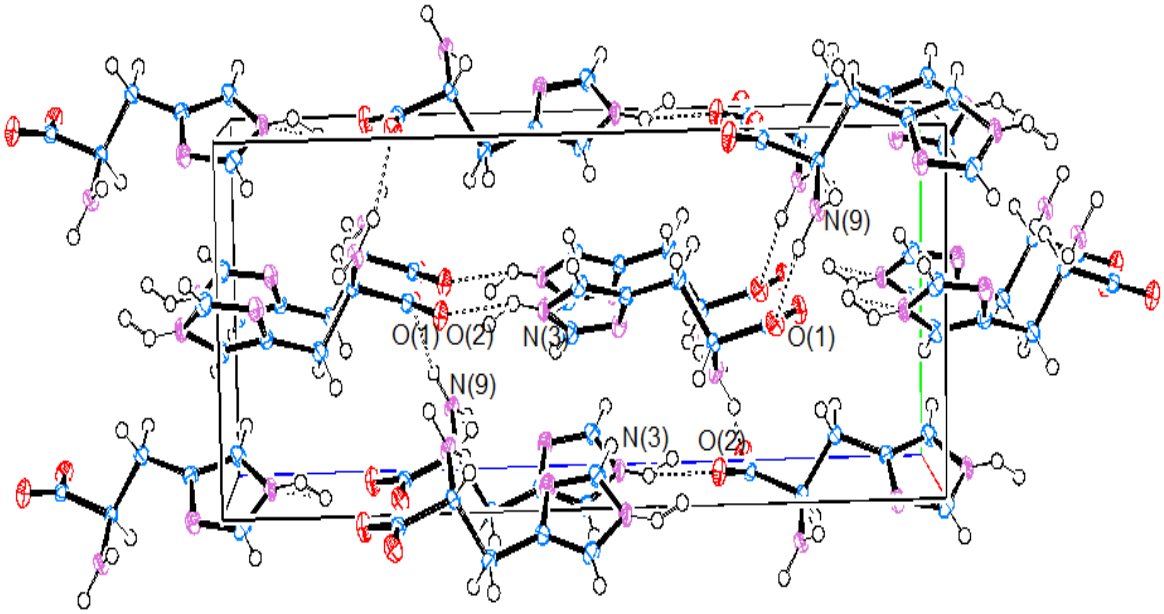

Figure 31. An ORTEP plot of the unit cell, 2-Fluoro-L-histidine. The dotted lines represent hydrogen bond found in this structure.

Table 4:

4.5 Comparison of the bond lengths in orthorhombic 2-fluoro-L-histidine and L-histidine

	2-Fluoro-L-histidine	L-histidine
C(5)-N(1)	1.405(3)	1.382(2)
C(2)-N(1)	1.292(3)	1.327(3)
C(2)-N(3)	1.344(4)	1.339(3)
C(4)-N(3)	1.376(3)	1.374(3)
C(5)-C(4)	1.354(4)	1.361(3)
C(6)-C(5)	1.493(4)	1.505(3)

Table 4 (continued)

	2-Fluoro-L-histidine	L-histidine
C(7)-C(6)	1.545(4)	1.536(3)
C(7)-N(9)	1.492(3)	1.493(2)
C(8)-C(7)	1.536(4)	1.545(2)
C(8)-O(2)	1.248(3)	1.247(2)
C(8)-O(1)	1.256(3)	1.250(2)
C(2)-F(1)	1.317(3	----------
C(7)-H(7A)	1.0000	1.000(2)
C(6)-H(6A)	0.9900	0.97(3)
C(6)-H(6B)	0.9900	0.97(2)
C(4)-H(4)	0.9500	0.98(3)
N(9)-H(9A)	0.8800	0.89 (2)
N(9)-H(9B)	0.8800	0.91(3)
N(3)-H(3B)	0.8800	0.96(3)
O(1)-H(1)	0.8400	

Table 5:

4.6 Comparison of bond angles in 2-fluoro-L-histidine with L-histidine

	2-Fluoro-L-histidine	L-histidine
N(1)-C(2)-N(3)	115.7(2)	112.2(2)
C(2)-N(3)-C(4)	104.9(2)	106.9(2)
C(2)-N(1)-C(5)	102.7(2)	104.9(2)
C(4)-C(5)-N(1)	110.1(2)	109.6(2)
N(1)-C(5)-C(6)	120.7(2)	120.5(2)
C(5)-C(4)-N(3)	106.6(2)	106.4(2)
C(4)-C(5)-C(6)	129.2(2)	129.9(2)
C(5)-C(6)-C(7)	112.1(2)	112.7(2)
C(8)-C(7)-C(6)	110.0(2)	110.6(1)
N(9)-C(7)-C(8)	109.7(2)	109.5(1)
N(9)-C(7)-C(6)	109.6(2)	109.8(1)
O(2)-C(8)-O(1)	127.0(2)	126.7(2)
O(2)-C(8)-C(7)	117.0(2)	117.1(2)
O(1)-C(8)-C(7)	116.0(2)	116.3(2)

Table 5 (continued)

	2-Fluoro-L-histidine	L-histidine
N(9)-C(7)-H(7A)	109.2	
C(8)-C(7)-H(7A)	109.2	
C(6)-C(7)-H(7A)	109.2	
C(5)-C(6)-H(6A)	109.2	
C(7)-C(6)-H(6A)	109.2	
C(5)-C(6)-H(6B)	109.2	
C(7)-C(6)-H(6B)	109.2	
H(6A)-C(6)-H(6B)	107.9	
C(5)-C(4)-H(4)	126.7	
N(3)-C(4)-H(4)	126.7	
N(1)-C(2)-F(1)	125.6(2)	
F(1)-C(2)-N(3)	118.7(2)	
C(7)-N(9)-H(9A)	120.0	
C(7)-N(9)-H(9B)	120.0	
H(9A)-N(9)-H(9B)	120.0	

Table 6:

4.7 Comparison of the Hydrogen –bond lengths (Å) found here with L-histidine

	2-Fluoro-L-histidine	L-histidine
N (9) ------N (1)	2.86 Å	2.78
N (3) ------O (2)	2.75 Å	2.78
N (9) ------O (2)	2.89 Å	2-85
N (9) ------O (1)	2.69 Å	2.77

This crystalline data suggests that proton transfer from N (1) to N (9) or proton addition at N (1) is un-favorable. Lower the bond angle at N (1), shorter the bond length of N (1)-C (2) decreases the sp^2 character of bond hybridization at N (1). In this respect, the fluorinated imidazole moiety of histidine would appear to be well suited for physiological studies.

4.8 Pore formation studies of Anthrax protective antigen using 2-Fluoro histidine

Anthrax toxin protective antigen (PA) forms heptameric or octameric pores, which allows entering the enzymatic moieties (EF or LF) into the cytosol. This whole process is dependent on conformational changes that occur from pre-pore to pore at low pH. Initially, it has been hypothesized that protonation of one or more histidine in PA triggers the pore formation. We used 2-fluoro-L-histidine (2FHis) to study the pore formation. 2FHis PA shows increase in stability to pH and urea studied using fluorescence and CD. Although 2FHis labeled protein increased the stability it still formed the pore at the same the pH with the same rate (86).

Significantly, SDS-PAGE and K+ release assay shows that the pore formation is independent to histidine protonation (86). Nevertheless, translocation studies in planner lipid bilayers showed that 2-FHis PA_{63} could not translocate LF_N through the pores into the cytosol of CHO-K1 cells. These studies indicate that 2FHis pore is biologically inactive, agrees with the conclusion that histidine plays a role in translocation but does not alter the pore formation in the absence of the receptor. Initial SDS-PAGE assay results showed that in the presence of CMG2, 2-FHis PA_{63} does not form a pore at low pH (95).

Recent studies on 2-FHis PA_{63} (structural stability and dynamic properties) by using various biophysical techniques suggests 2-FHis PA can be used as a potential candidate for anthrax vaccine (117). Optical density (OD) data at 350 nm were collected simultaneously during CD measurements. Aggregation of 2-FHis PA_{63} was measured by increase in optical density (OD) values with increasing in temperature and it is compared with rPA (Figures 32 C and D). The temperature dependent OD changes (i.e., protein aggregation) are overall matches with the observations made from the CD and intrinsic fluorescence measurements, with similar trends of temperature and pH. These results suggest that 2-FHis PA_{83} was significantly more stable than rPA at pH 5, Tm of 2FHis PA 39.0^{o}C and rPA 28.5^{o}C (Figure 32A and B).

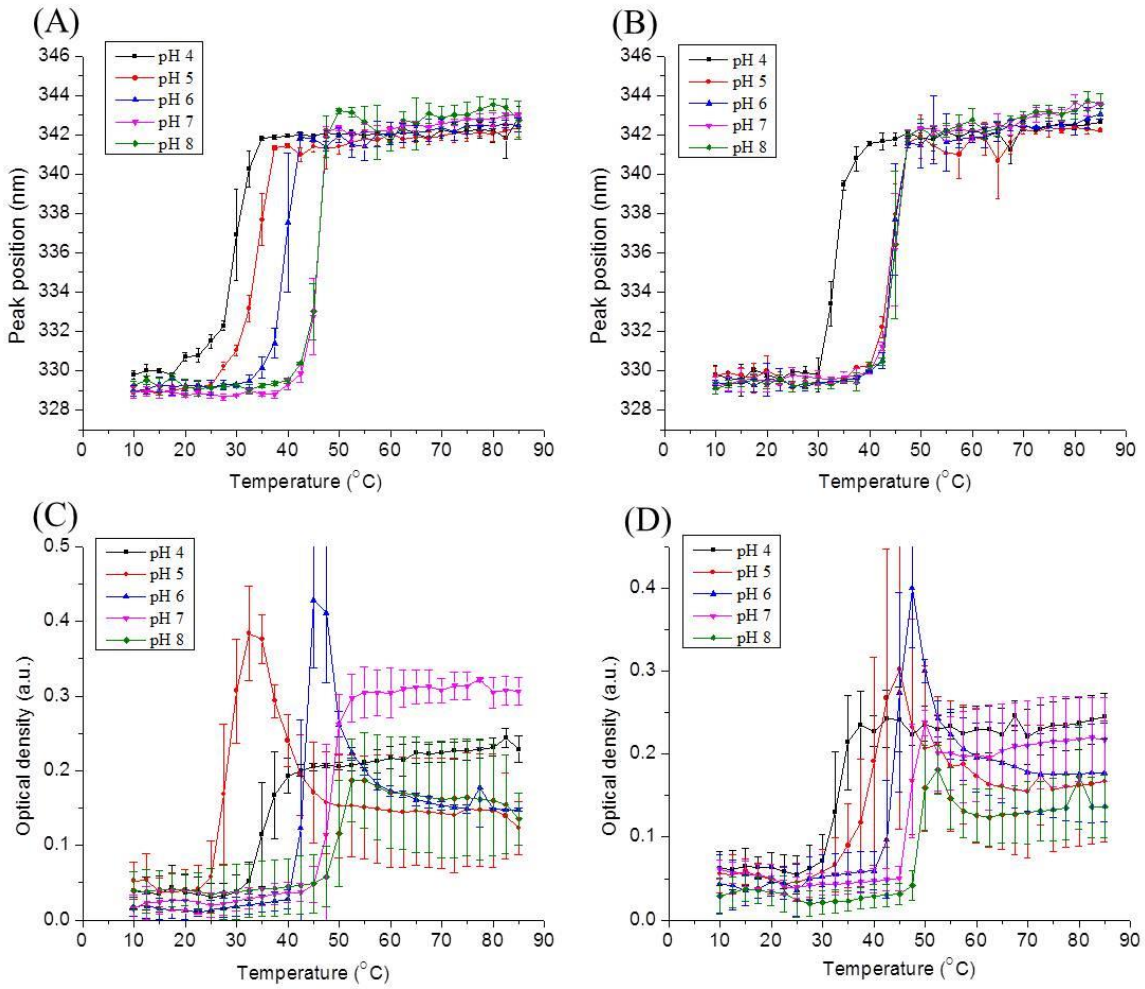

Figure 32. Thermal stability of rPA (Figures A and C) and 2-FHis PA (Figures B and D) as a function of pH: (A) and (B) Intrinsic Tryptophan fluorescence emission maximum (peak position) was monitored; (C) and (D) Optical density at 350 nm was monitored. Data represents the mean of three independent samples, with error bars showing the standard deviation.

These studies provided more insight and very important biophysical information about the effect of 2-FHis on the conformational stability of PA in response to environmental stress factors such as pH and temperature. The results showed that the two proteins have similar stability at pH 7 and 8. 2-FHisPA analogue is more stable at pH 6 and shows dramatically increased stability at pH 4-5 and also more dynamic than PA at pH 5. These data provide useful information to better understand the differences and similarities in physical properties of the two proteins in solution. Presently, PA is a primary component in the licensed anthrax vaccine.

CHAPTER 5

FLUORESCENCE STUDIES ON ANTHRAX PROTECTIVE ANTIGEN PORE FORMATION AND IN THE PRESENCE OF THE HOST RECEPTOR, CMG2

5.1 Introduction.

Infectious *Bacillus anthracis* secretes three proteins, cellular receptor binding protein, protective antigen (PA) and the two enzymatic moieties edema factor (EF) and lethal factor (LF). Individually these proteins are non-toxic but undergo self-assembly on the surface of eukaryotic cell receptors to form toxic complexes. PA (83 kDa) binds to one of two cellular receptors: tumor endothelial marker 8 (TEM8) or capillary morphogenesis protein 2 (CMG2) (33, 48). Recent studies have shown that PA also binds to integrin β1 (118). A furin like protease cleaves PA and separates a 20 kDa protein from domain I and leaves a 63 kDa fragment (PA_{63}) bound to CMG2, which on self-assembly forms a heptamer $(PA_{63})_7$ or octamer $(PA_{63})_8$ pre-pore structure, which in turn creates a binding pocket for EF and LF (Figure 33). Upon binding either EF or LF, the whole complex is internalized by receptor mediated endocytosis into an acidic compartment (93). Under acidic conditions (pH ~5.5), PA undergoes structural changes leading to translocation of EF and LF into the cytosol(17). Low pH induces the domain II β_2-β_3 strands to peel away from the core of domain II and insert into the membrane, forming a 14-stranded β-barrel called the pore (26, 27, 89). The pore allows translocation of EF and LF into the cytosol by a proton gradient, which disrupts cell signaling mechanisms required for host immunity (83, 84, 87).

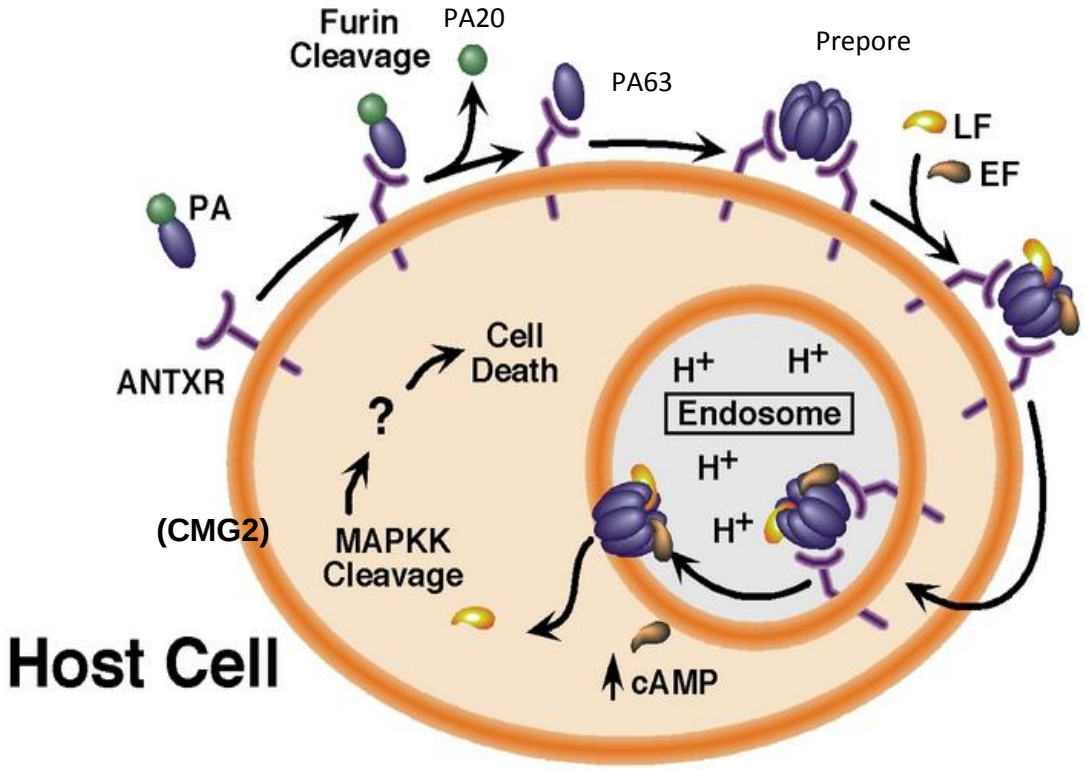

Figure 33. Anthrax toxin assembly, internalization and release of enzymatic moieties (EF or LF). The picture was adapted from http://ysm.research.yale.edu/article.jsp?articleID=415

CMG2 is perhaps the most heavily studied receptor, and crystal structures of PA_{83} and PA_{63} bound to CMG2 have been solved by X-ray crystallography. The binding site for the receptor is located in domain IV, which has an aspartic acid residue (D683) that coordinates a Mg^{2+} ion (Figure 36). The Mg^{2+} ion is bound to CMG2 through a metal ion-dependent adhesion site (MIDAS) (119, 120). Mutation of conserved amino acids in the MIDAS region (D50A and T118A mutations) in CMG2 have been shown to block the interactions between PA and the

receptor (119). In our studies, we used the D50A CMG2 mutant as a negative control to determine the influence of pH on the fluorescence of labeled proteins in the absence of binding.

Receptor binding to PA is essential for its function; the pH dependent conformational change from the pre-pore to pore is greatly influenced by CMG2. X-ray structural analysis reveals that CMG2 binds to PA by interacting with domain IV, but also domain II, where a small loop, the domain II β_3-β_4 loop, binds in a groove on the surface of CMG2 (Figure 36). Interactions with this loop have been shown to dictate the pH requisite for pore formation (121), such that loss of interactions with this loop raise the pH for pore formation.(64, 85). This loop also forms part of the β-barrel pore, and must undergo a conformational change to allow for pore formation. Binding interactions between CMG2 and this loop hinder pore formation, and thus must dissociate in order to facilitate pore formation. Recent studies by NMR suggest that at low pH, contacts to the domain II β_3-β_4 loop are lost, while contacts with domain IV are maintained (97)

In an attempt to understand the steps that are required for pore formation, whether receptor release actually occurs and if so, is prior to, concomitant with or occurs after pore formation, we have studied pore formation using a FRET based assay by labeling R40C CMG2 with an acceptor (AF488) and E712C PA (located in domain IV) with a donor (AF350).

FRET depends on the ability to transfer, in a non-radiative manner, energy from an excited state donor fluorophore to an acceptor molecule, and is a distance-dependent process. If the donor fluorophore is close enough in space to an acceptor to allow for induced-dipole induced-dipole interactions, the fluorescence of the donor will decrease. The acceptor, if it is fluorescent, and the two are close in space (depending on the R_0 value), the fluorescence will

increase due to transfer of energy from the donor. Efficiency of FRET (E_{FRET}) is calculated by $E_{FRET} = 1/[1 + (r/R_0)^6]$, R_0 is the distance at which 50% of energy transfer takes place and r is the distance between the two dyes. The value of R_0 varies for different fluorophores and is dependent on several other parameters, such as the amount of overlap between the excitation and emission spectra of the donor and acceptor (Figure 35), the relative orientation of the donor and acceptor and the quantum yield, or brightness, of the donor (122).

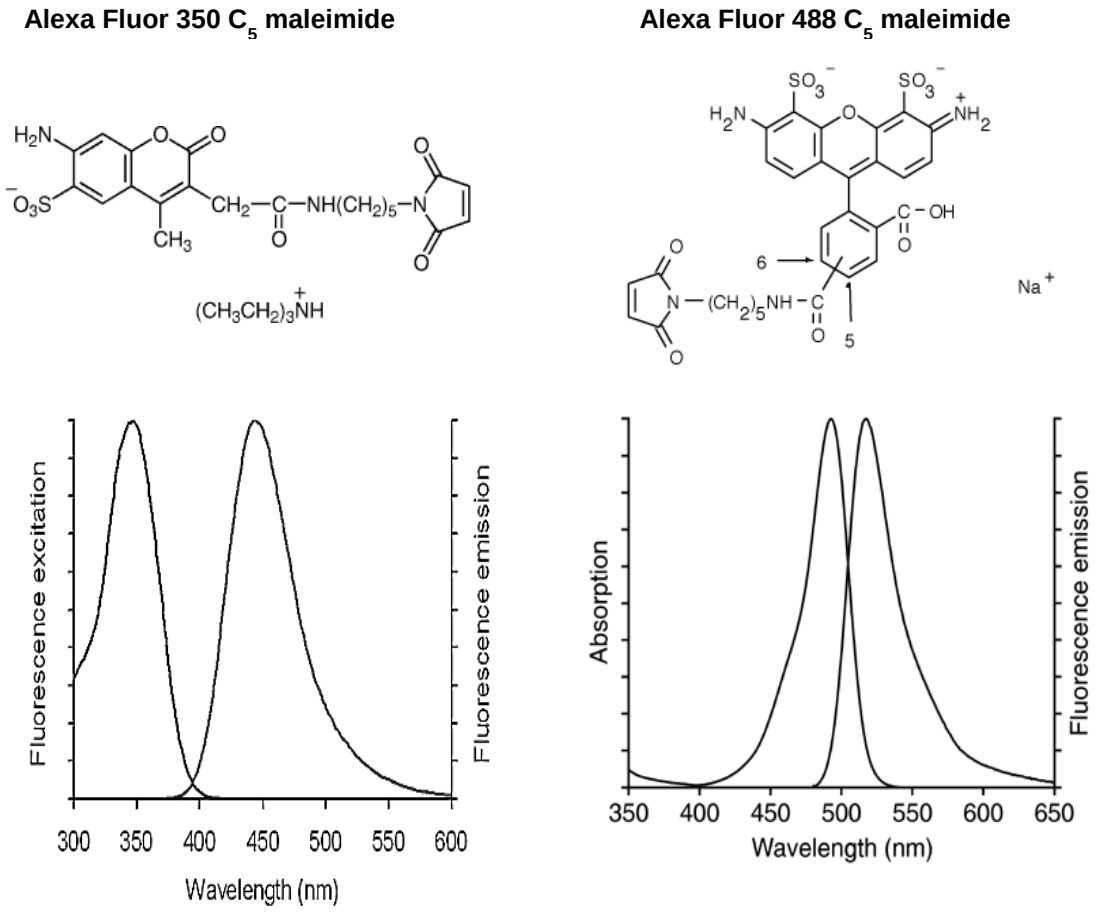

Figure 34. Absorption and Emission spectra of donor Alexa Fluor 350 and acceptor Alexa Fluor 488 fluorescent probes (www.invitrogen.com)

In the current study, we labeled PA with a donor fluorophore Alexa Fluor 350 C5-maleimide (AF350) *via* a unique cysteine E712C and CMG2 was also modified (R40C) and labeled with the acceptor fluorophore Alexa Fluor 488 C5-maleimide (AF488) (Figure 34). We chose the Alexa Fluor dyes because of their stability against photo-bleaching and are relatively insensitive to local environmental changes such as pH and hydrophobicity (123). The fluorescence emission spectrum of PA-CMG2 complex at excitation of 350 nm shows that there is a decrease in fluorescence intensity at 440 nm, and a concomitant increase in the emission of the acceptor at 520 nm, which is due to energy transfer between donor and acceptor (FRET).

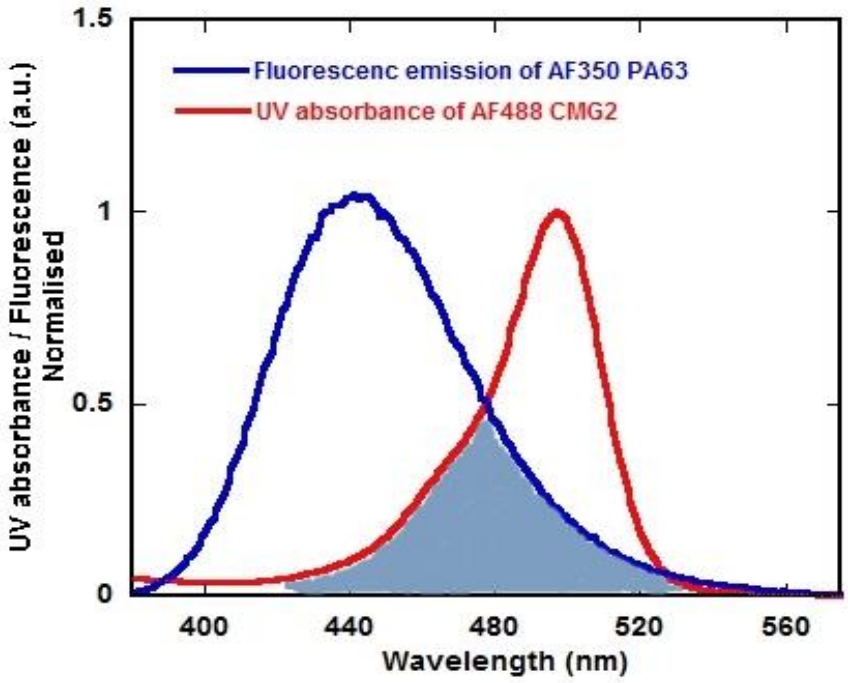

Figure 35. Spectral requirement for FRET. Fluorescence emission of AF350 labeled PA_{63} (blue) and UV absorption spectrum of AF488 labeled CMG2. Overlapped spectral region is shaded

The distance between the two fluorophores, based on the crystal structure, is ~44 Å, certainly within the R_0 that has been determined for this dye pair (~40 Å) (Figure 38).

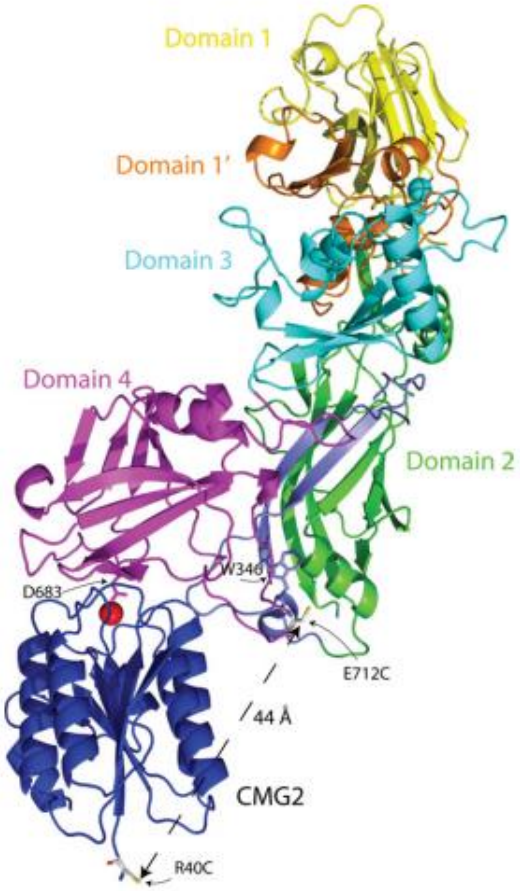

Figure 36. Crystal structure of WT PA bound to CMG2 (PDB ID 1T6B) with side chains of E712C and the R40C (CMG2—blue) in gray sticks. Domain I (1–167, PA_{20}) is colored in yellow and rest of the domain I (168–258) is colored orange; domain II is colored green with the residues that comprise the pore (275–352) in blue; W346 within the domain II $2\beta_3$-$2\beta_4$ loop is shown as a blue stick figure; domain III is colored cyan and domain IV is colored magenta. The manganese ion on the surface of CMG2 is colored red. The distance between E712C in domain IV (magenta) and R40C in CMG2 is shown (44 Å). Figure was taken from (5)

5.2 Materials and Methods

Reagents: The reagents used were purchased either from Sigma (St. Louis MO) or Fisher Scientific with purity ≥99%. Fluorescent dyes, Alexa Fluor-350 C5 maleimide (AF350), Alexa Fluor–488 C5 maleimide (AF488) and monobromobiamine (mBBr) were purchased from Invitrogen. 4-Fluoro-DL-tryptophan (4FTrp) was purchased from Gold Biotechnology (St. Louis MO).

Plasmid construction, mutagenesis of D50A CMG2 and D425A PA, and protein purification is described in detail in Appendix A3.1, A3.3 and B.4.1

5.2.1 Labeling proteins with Fluorophores.

Approximately 10-12 mg of E712C, E712C D425A PA_{83} and E712C W346F PA_{83} were purified to remove excess DTT by passing through an S-200 gel filtration column which was pre-equilibrated with buffer, 20 mM Tris 8.0, 0.15 M NaCl (degassed with N_2). Prior to labeling, a 10 mM stock solution of either AF350 or AF488 C5-maleimide (Invitrogen) was prepared in N_2 degassed water. 10-15 moles of reagent for each mole of protein were added to each protein; where a 10 fold molar excess of TCEP was present. The reaction was allowed to proceed for 2 h at room temperature while rocking, and upon completion of the reaction 10 fold molar excess of β-mercaptoethanol was added to eliminate any excess reactive substances during the purification (5, 86). After labeling, all proteins were purified apart from the free dye by another S-200 gel filtration column in 20 mM Tris 8.0, 0.15M NaCl, in the absence of TCEP (Figure 37 A and B).

Efficiency of labeling was calculated according to manufacturer guidelines (Invitrogen) and was ≥95%. Purity of protein was identified by SDS-PAGE, pooled the pure fractions, concentrated and kept on ice. For N-ethyl maleimide (NEM) labeling of CMG2 and PA, similar

procedure was used. 4FTrp labeled CMG2 was purified as described previously (96), CMG2 labeled with 4FTrp were ≥ 95%, determined by mass spectroscopy.

5.2.2 SDS Resistant Pore Formation Assay.

pH-dependent pore formation assay was carried out by incubating WT and mutant prepore $(PA_{63})_7$, at 2.7 μM with or without 5.4 μM CMG2 in 20 mM Tris, pH 8, 0.4 M NaCl, 1mM $MgCl_2$ and 1mM $CaCl_2$ for 30 min. After incubation, 10 μL of complex was added to 10 μL of appropriate pH buffers (0.5 M Tris, 0.25M MES, 0.25 M AcOH of pH 5.5, 6.0, 7.0 and 8.0) and incubated at room temperature for 1 h. After 1 h, 10% SDS was added to get a final concentration of 1.25% proteins and incubated at room temperature for an additional 20 min. The proteins were then applied to a 4-20% gradient gel which was run for 3.5 h at constant voltage (200 V) at 4^{o}C.

5.2.3 Fluorescence Equilibrium Binding Titration.

Binding titrations were carried out in a manner similar to that described by Wigelsworth and Rajapaksha (5, 61) . $(PA_{63})_7$ proteins were diluted to 50 nM in 2 mL constant ionic strength (CIS) buffer containing 50 mM Tris/25 mM MES/ 25mM AcOH, pH 8.0 supplemented with 0.1mg/mL BSA, 1mM $CaCl_2$ and 1mM $MgCl_2$. CMG2 was added to this solution in 100μL aliquots, with a 100 μL aliquot removed after the addition until the molar ratio of CMG2: PA from 0.1 to 20 (Molar ratio was calculated by [CMG2]/[$(PA_{63})_{7}$]. Each 100 μL aliquot was subsequently incubated overnight at 4 ^{o}C to ensure complete binding. Fluorescence emission spectra were recorded for each aliquot in a Cary-Eclipse spectrofluorometer at 20 ^{o}C. The donor fluorophore was excited at 350nm and the emission at 440nm and 518nm were recorded, with

slits set at 5 nm Ex and 10 nm Em. Ratio of the acceptor (λ= 518 ± 5 nm) to donor (λ=440± 5 nm) fluorescence emission defines the apparent FRET signal.

5.2.4 Gel Filtration Analysis.

For analysis of heptamer formation, samples were applied to an analytical gel filtration (Superdex 200) column equilibrated with 20 mM Tris, pH 8.5 supplemented with 0.4M NaCl and 1mM $CaCl_{2,}$. Approximately 500 µL of sample (5 µM) was loaded onto a Superdex-200, preparatory grade gel filtration column (GE-Healthcare) and eluted at a flow rate of 1 mL/min using an AKTA-Prime system (GEHealthcare), which allowed continuous monitoring of the UV absorbance at 280 nm.

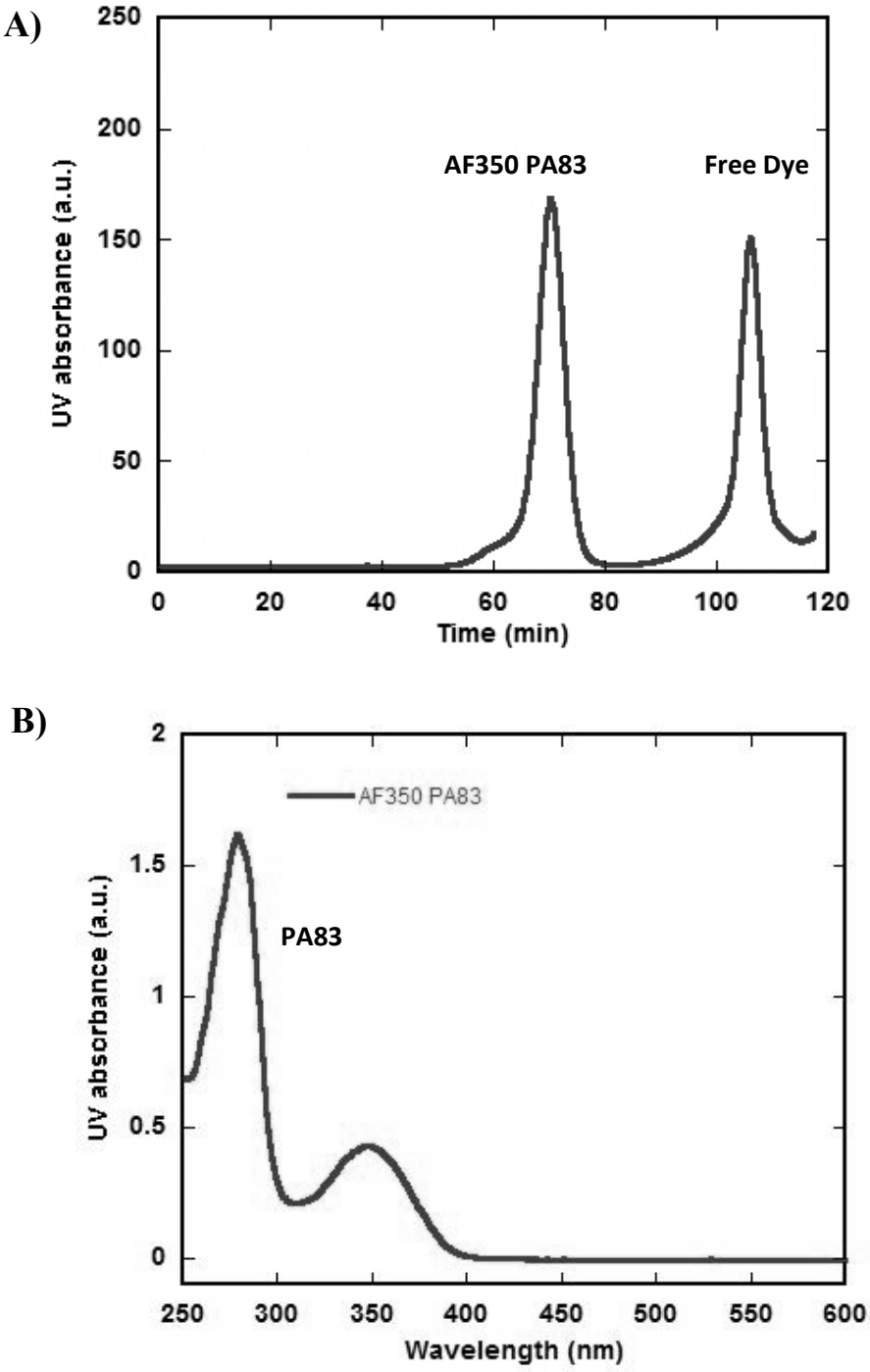

Figure 37. A) Sephadex S-200 gel filtration of PA_{83} AF350. Protein labeled with the fluorescent probe eluted at 70 min whereas the free dye eluted at 110 min. B) UV-Vis spectrum of AF350 PA_{83}. The absorbance values at 280 nm and 350 nm were used to calculate the degree of labeling.

DL= A_{max} (Dye) / ε (dye)*M, where

M= A_{max} (protein) – [A_{max} (dye)* ε (Dye)/1000] / ε (protein)

ε of PA83 was used as 80220 $M^{-1}cm^{-1}$, W346F PA83 as 74720 $M^{-1}cm^{-1}$, CMG2 as 13075 $M^{-1}cm^{-1}$, R40C CMG2 12950 $M^{-1}cm^{-1}$ AF350 as 19000 $M^{-1}cm^{-1}$and AF488 as 73000 $M^{-1}cm^{-1}$

ε = Protein molar extinction coefficient

A_{max} = Absorbance (A) of protein or dye measured at the wavelength maximum (λ max)

M= Protein concentration

5.2.5 pH Equilibrium Titrations (Condition 1).

The complex of PA_{63} and CMG2 complex was made using AF350-PA_{63} AF488-CMG2 or N-ethylmaleimide (NEM) labeled CMG2 in a 1:5 ratio in 20mM Tris pH 8.5, 0.4M NaCl, 1mM $CaCl_2$ incubated at room temperature for 30 min. The protein complex was diluted to 50 nM PA_{63} (250 nM CMG2) in CIS buffer system with variable pH's (50 mM Tris, 25 mM MES and 25 mM AcOH) supplemented with 0.1 mg/mL BSA, 1mM $MgCl_2$ and 1mM $CaCl_2$, incubated overnight at 4°C. Samples were analyzed using a Cary-Eclipse spectrofluorometer at 20°C, exciting at 350 nm and monitoring the emission at 440nm and 520nm (in the case of AF488 CMG2), slits were set a 5 nm for Ex and 10 nm for Em.

5.2.6 pH Equilibrium Titrations (Condition 2).

In this case, the PA_{63}-CMG2 complex was made using AF350-PA_{63} and AF488-or NEM-labeled CMG2 in a 1:2 ratio, in 20mM Tris pH 8.5, 1 mM $CaCl_2$ incubated at room temperature for 30 min. Protein complex was diluted to 300 nM of PA_{63} in CIS buffer system (50

mM Tris, 25 mM MES and 25 mM AcOH), supplemented with 0.2M NaCl and 0.1% n-dodecyl-β-d-maltopyranoside (DDM), and incubated for 10 min. 100µL aliquots were removed after the addition of 100 µL of pH 3 buffer (CIS buffer) to reduce the pH and samples were incubated overnight at 4°C. Samples were analyzed using a Cary-Eclipse spectrofluorometer at 20^{o}C and the 350 nm wavelength was used for excitation of donor fluorophore, AF350 (slits were set a 5 nm for Ex and 10 for Em.). Change in fluorescence intensity was calculated by subtracting expected from measured fluorescence.

5.2.7 pH Titrations (Condition 3).

The PA_{63}-CMG2 complex was made using AF350-PA_{63} and AF488-CMG2, 1:2 ratio in 20mM Tris pH 8.5, 1mM $CaCl_2$, incubated at room temperature for 30 min. Protein complex was diluted to 300 nM of PA_{63} in CIS buffer system (50 mM Tris, 25 mM MES and 25 mM AcOH) supplemented with 0.2M NaCl and 0.1% n-dodecyl-β-d-maltopyranoside (DDM), and incubated for 10 min. 100µL aliquots were removed after the addition of 100 µL of pH 3 buffer (CIS buffer) to reduce the pH and samples were incubated for short 10 min incubation and then analyzed by using a Cary-Eclipse spectrofluorometer at 20 ^{o}C and the 350 nm wavelength was used for excitation of donor fluorophore, AF350 (slits were set a 5 nm for Ex and 5 for Em.) Change in fluorescence intensity was calculated by subtracting expected from measured fluorescence.

5.2.8 Quantum Yield Calculations.

The relative quantum yields (QY) for AF350-PA_{63} at four different pHs (8, 7, 6 and 5) were calculated by using Quinine sulfate in 0.1N H_2SO_4, as a standard using the following equation:

$$\Phi_x = \Phi_{ST}\ (Grad_x/Grad_{ST})\ (\eta^2 x/\ \eta^2_{ST})$$

Where, X refers to the sample being measured and ST refers to Quinine sulfate. Φ is fluorescence QY, Grad refers to the gradient from the plot of integrated fluorescence intensity *vs* absorbance and η the refractive index of the solvent. Measurements were performed two times and an average of the QY was used in the FRET calculations.

5.2.9 Förster distance calculation between two fluorophores.

We also measured the distances between two fluorophores with respect to pH, if the receptor dissociates we will see increase in distance. The Förster distance (at which 50% energy transfer occurs) between AF350 PA_{63} and AF488 CMG2 was calculated from the degree of overlap between the AF350 PA_{63} emission spectrum and AF488CMG2 absorption spectrum (Figure 43) using

$$\mathbf{R_0^{6}{}_{(Å)} = (8.79 \times 10^{23})\ (\kappa^2 \eta^2 \Phi_x J)}$$

Where, the orientation factor, κ^2= 0.66 (2/3), assuming random orientation of the donor and acceptor, refractive index of the buffer was measured for each pH η = 1.33, quantum yield of AF350 PA (63)7 donor Φ and overlap integral *J* was calculated by using

$$\boldsymbol{J = \int F_D\ (\lambda)\ \varepsilon_A\ (\lambda)\ \lambda^4\ d\lambda}$$

Where, ε_A (λ) and F_D (λ) represent the molar extinction coefficient of the acceptor ($cm^{-1}M^{-1}$) and the normalized donor emission at wavelength l (cm), respectively. We used photochemcad software (http://www.photochemcad.com/pages/chemcad/chem-home.html) to calculate the overlap integral *J* and results are tabulated below (Table 8). We were not able to measure the

distance at low pH in case of WT PA_{63}, because of the protein aggregation which may be due to the structural change (pore formation) or WT PA_{63} is less stable at low pH.

5.3 Results and Discussion

Fluorescence is a highly sensitive technique that requires minimal concentrations of protein, and thus can mitigate the effects observed in some cases at higher concentrations such as aggregation. More importantly, FRET provides the potential for time-dependent changes in the association/dissociation to be observed. Initially, we anticipated that W346 located in domain II and E712C, located in domain IV, with the latter labeled with AF350 maleimide may provide a FRET pair. Secondly, AF350 PA and an AF488-CMG2 may constitute a second FRET pair. The first pair (W346-AF350) could possibly monitor the conformational change in PA to a pore, while the second would monitor the association/dissociation of the receptor.

WT and mutant PA proteins were expressed and purified as described earlier (86, 96) under reduced conditions using DTT and TCEP. All WT and mutant PA proteins yielded about 30 mg out of 5.0 L of media except W346F PA_{83} yielded only about 20 mg out of 5.0 L of media. WT and mutant CMG2 were also expressed and purified under reduced conditions as described in Appendix B.4.2. All proteins were above 96% pure. The proteins were then labeled with donor/acceptor fluorophores at the reactive cysteine to utilize in FRET experiments.

5.3.1 Monitoring the Association of CMG2 to PA_{63} by Fluorescence:

To examine the interaction between PA_{63} and CMG2, PA_{63} was labeled with AF350 (donor, AF350 PA_{63}) and R40C CMG2 labeled with AF488 (acceptor, AF488 CMG2).

Fluorescence spectra of AF350 PA_{63} bound with AF488 CMG2 (1:1) shows that FRET indeed occurs between PA_{63} and CMG2, quenching of donor fluorescence (Em 440nm) accompanied by an increase of acceptor emission (Em 520 nm) (Figure 38).

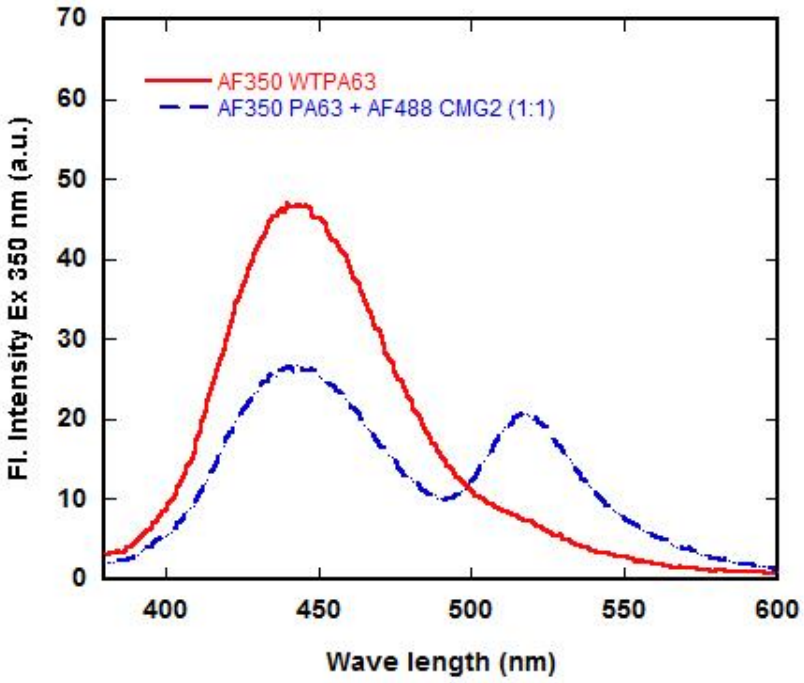

Figure 38. FRET emission spectra (Ex 350 nm) of AF350 PA_{63} solid line (50 nM) and a 1:1 complex of AF350 PA_{63} andAF488 CMG2 (dashed line). Spectra were acquired at 20°C in CIS buffer system supplemented with0.1mg/mL BSA, 1mM $CaCl_2$ and 1mM $MgCl_2$.

5.3.2 Equilibrium Binding Titration:

We monitored the binding of PA_{63} to CMG2 in a manner described by Wigelsworth and Rajapaksha *et. al.*(5, 61), by following the ratio of the 440 emission to the 520 emission upon excitation at 350 nm. PA_{63} proteins were diluted to 50 nM in 2 mL constant ionic strength (CIS) buffer and sub-stoichiometric quantities of CMG2 were added to increase the molar ratio of CMG2: PA from 0.1 to 20 (61). Our results shows that the stoichiometry is 1:7, AF 350 $(PA_{63})_7$ to AF488 CMG2 (Figure 39 A) which is consistent with previous studies (61). Increased FRET signal upon successive additions of acceptor (CMG2) (until all PA_{63} was bound to CMG2) indicates that all the binding sites in PA are saturated with CMG2 (Figure 39 A). Similar binding was observed in mutants D425A (Figure 39 B) and W346F (Figure 39 C).

A)

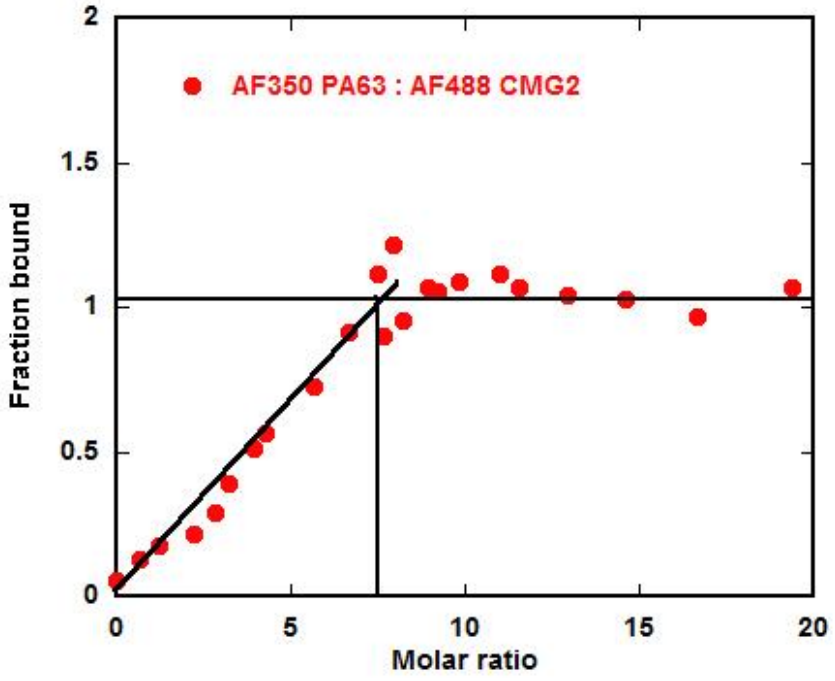

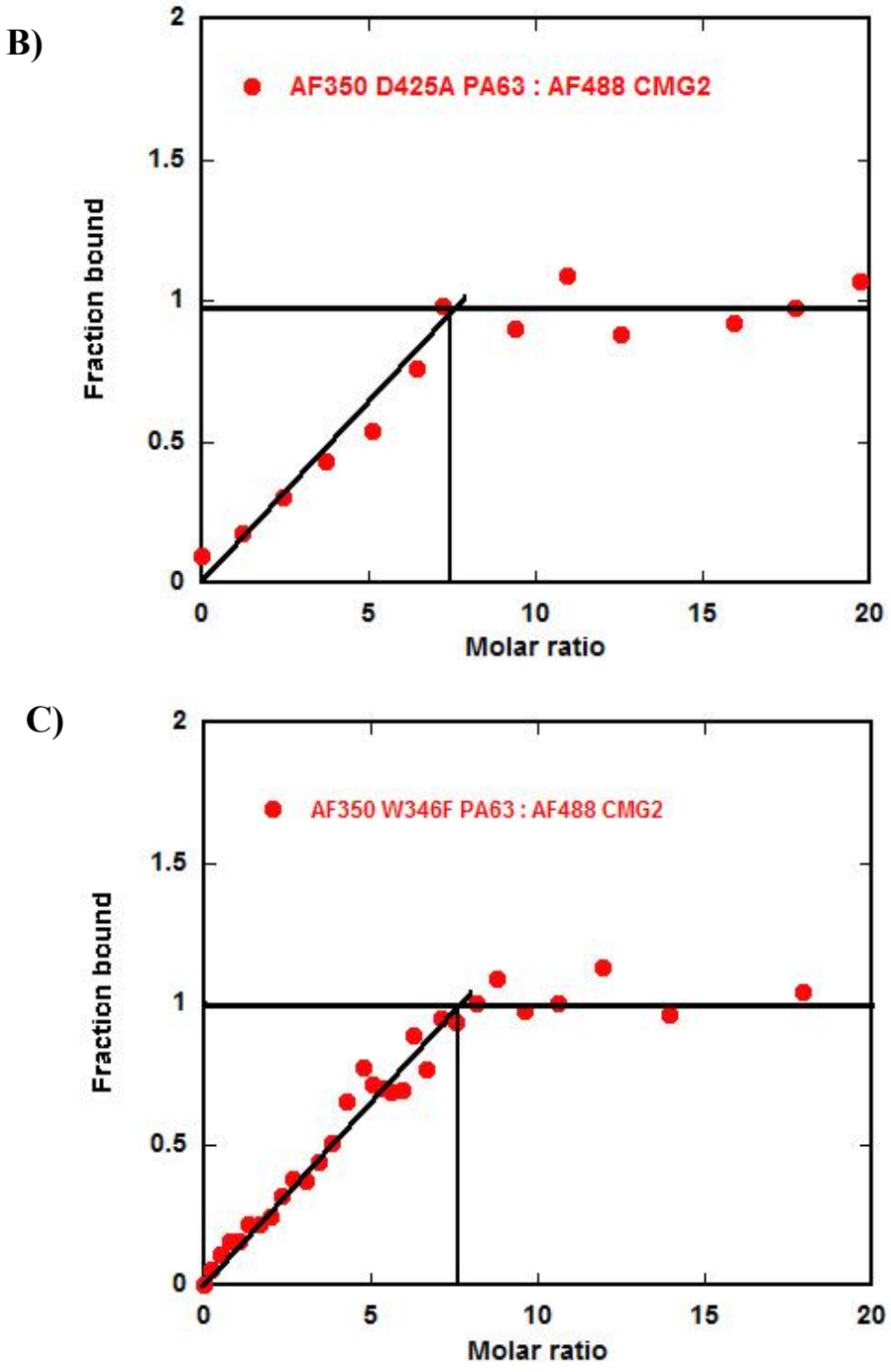

Figure 39. Equilibrium Binding Titration Assay. A) Fluorescence equilibrium binding titration of AF350 $(PA_{63})_7$ B) AF350 D425A $(PA_{63})_7$ and C) AF350 W346F $(PA_{63})_7$, molar ratio is defined by [CMG2] / $[(PA_{63})_7]$. Data were acquired on a Cary-Eclipse fluorescent instrument and the samples were maintained at 20^{o}C with a Peltier cooling system.

5.3.3 Size Exclusion Chromatography Analysis:

To confirm the size of the PA_{63} (heptameric prepore), D425A, W346F and and WT PA_{63} were applied (volume, concentration) to a Superdex-200, size exclusion column operating at 1 mL/min, and the elution monitored at 280 nm. Blue Dextran was used to measure the void volume. Figure 41, shows the elution profile of WT, D425A and W346F PA_{63} proteins. All proteins were eluted at same time period, confirming that they are the same size.

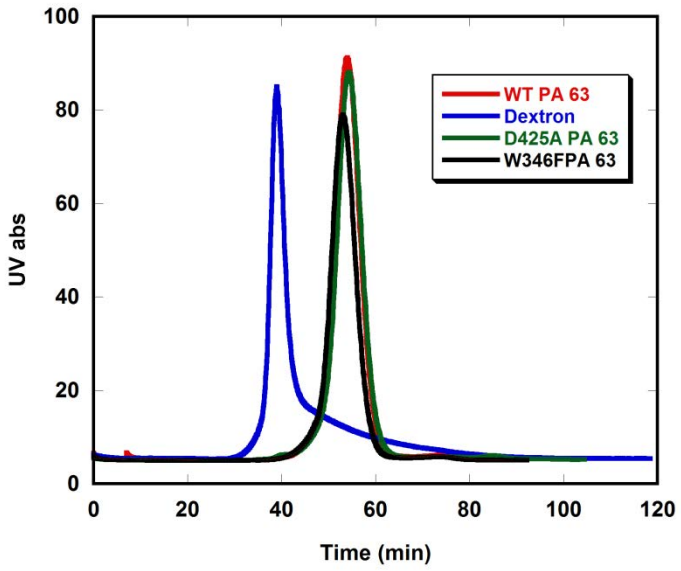

Figure 40. Gel filtration of WT PA_{63} (red), D425A PA_{63} (green) and W346F PA_{63} (black) on Superdex -200 Gel filtration. .

5.3.4 Equilibrium pH Titrations:

pH titration experiments were carried out in order to monitor the conformational change from the heptameric PA (pre-pore) to a pore at low pH (by monitoring the fluorescence at AF350), and also to monitor the receptor dissociation. AF350 PA_{63} was added to 5 fold excess of AF488 CMG2. PA_{63} in 20mM Tris pH 8.5, 0.4M NaCl, 1mM $CaCl_2$ and CMG2 in 20 mM Tris pH 8, 0.15 M NaCl) and incubated for 30 min at room temperature and then diluted with variable pH buffers (8.5 to 5) in CIS buffer, supplemented with 0.1 mg/mL BSA, 1 mM $MgCl_2$ and 1mM $CaCl_2$ to give a final concentration of 50 nM AF350PA_{63} and 250 nM of AF488 CMG2 to a final volume of 100µL. The samples were incubated overnight at 4°C and the fluorescence spectra were recorded the next day at 20°C. Buffer blanks were prepared in the same way as the samples (no protein) and subtracted from the original spectra.

Figure 41 A shows the pH titration of AF350 PA_{63} bound to AF488 CMG2 in a 1:5 ratio. As the pH is lowered, we observed drop in the fluorescence at pH ~5.5, which is consistent with the pH at which pore formation occurs (63). Previous studies by Rajapaksha (Ph.D. dissertation, 2009, Wichita State University) have shown that the AF350 emission at 440 nm is quenched, and that this quenching (drop in fluorescence intensity) is due to W346 located in domain II. Conversely, monitoring the emission at 520 nm shows a drop in the fluorescence intensity, which would be consistent with receptor dissociation, since the donor and acceptor are farther apart. (Figure 43 A). In order to determine if the drop in fluorescence is due to the formation of a pore, we have made the mutant D425A, which has been shown to be a dominant-negative mutant of PA that is incapable of forming a pore (Figure 43 B) (29, 124). D425A may prevent pore formation by the fact that the aspartic acid side-chain is larger than the alanine side chain, and

may occupy a hydrophobic cavity in a neighboring subunit in the $(PA_{63})_7$ heptamer, when the aspartic acid is in the protonated state(Figure 41 B)(1). In this case, lowering the pH of AF350

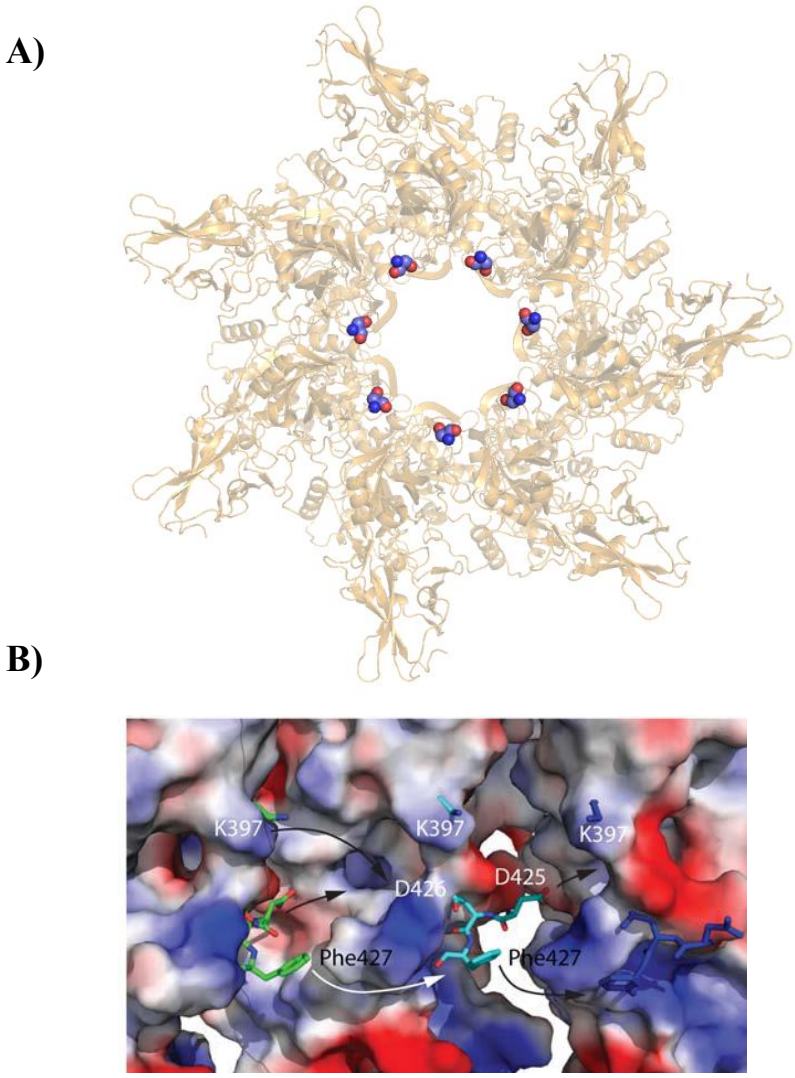

Figure 41. Crystal structure of PA_{63}. A) Cartoon model of PA_{63} crystal structure (PDB ID 1TZO) shown in golden brown and D425A in spheres and B) Vacuum electrostatic potential surface of a heptamer showing D425, K397 and F427 in sticks, hypothetical model indicating the potential of these residues to form a pore (1).

D425APA-AF488 CMG2 complex (1:5), and monitoring the fluorescence shows that the emission at 440 nm *increases*, while the emission at 520 nm decreases. Because the D425A mutant cannot undergo the conformational change to a pore, the quenching due to W346 is not observed. Instead, the observed increase in the emission at 440 nm would indicate that at low pH, the receptor, which also contributes to a drop in the fluorescence at 440 nm, dissociates. This is also observed in the emission at 520 nm, which shows a drop in the fluorescence, again consistent with receptor dissociation. (Figure 42 B and 43 B).

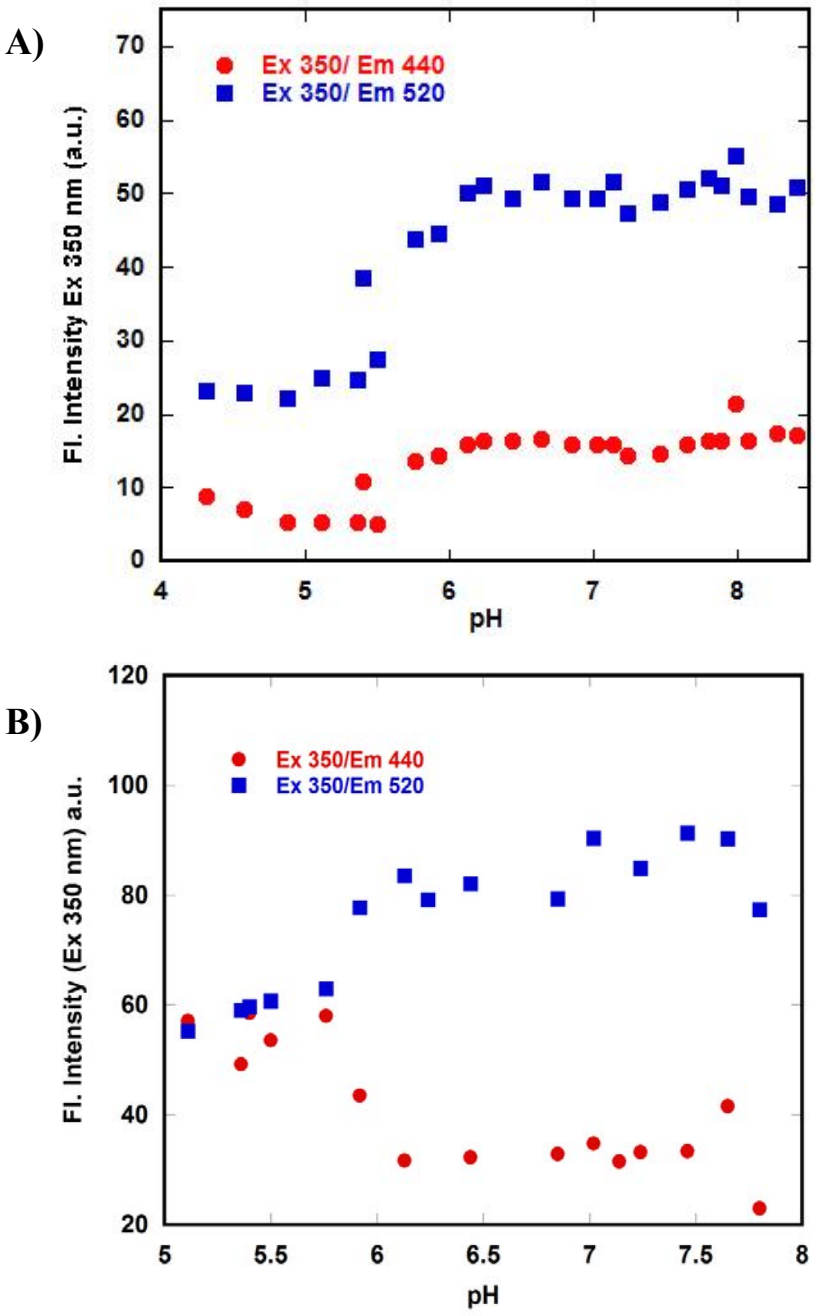

Figure 42. pH titration of A) AF350 PA_{63} and B) AF350 D425A PA_{63} with 5 fold excess of AF488 CMG2, fluorescence intensity is measured as a function of pH. All measurements were carried out at 20°C in CIS buffer system supplemented with 0.1mg/mL BSA, 1mM $CaCl_2$ and 1mM $MgCl_2$. Fluorescence emission spectra were collected for Ex350nm/ Em440nm and Ex350nm/ Em 520nm. The slits were set to 5nm for Ex and 10 for Em.

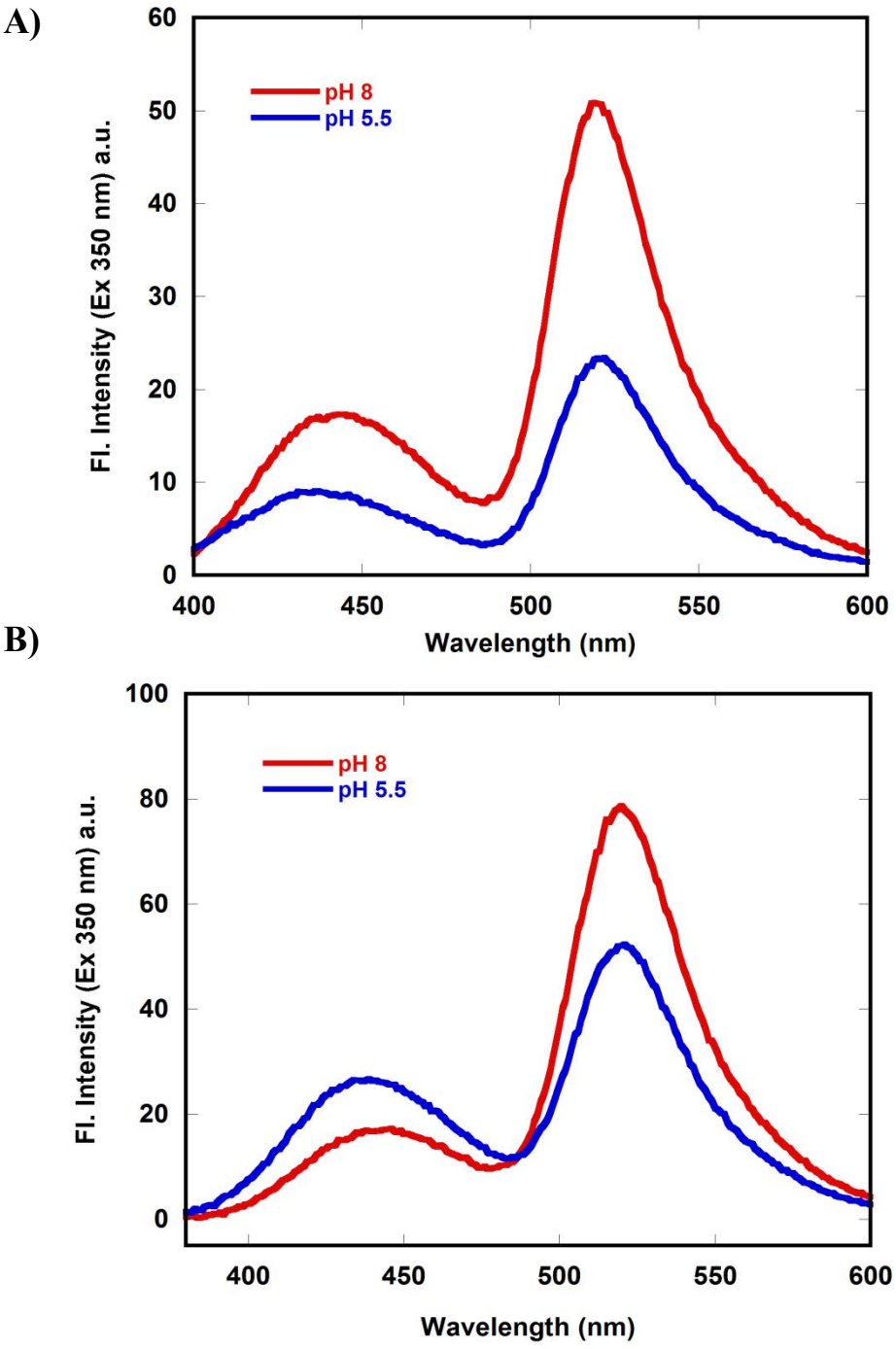

Figure 43. Fluorescence emission spectra (350 nm excitation) .A) AF350 PA_{63} with AF488 CMG2 (1:5) at pH 8 (red) and pH 5.5 (blue), B) AF350 D425A PA_{63} with AF488 CMG2 (1:5) at pH 8 (red) and pH 5.5 (blue). Spectra were acquired at 20^{o}C in CIS buffer system supplemented with 0.1 mg/mL BSA, 1mM $MgCl_2$ and 1mM $CaCl_2$. Data were acquired on Cary Eclipse fluorescent instrument

5.3.5 SDS-Resistant Pore Formation Assay.

Another independent study to measure the pore formation is the SDS-PAGE assay (63). Pore formation assay for WT and mutant PA_{63} proteins were carried out in the presence and absence of CMG2 as a function of pH (Figure 44 A). 2.5 μM PA_{63} was incubated with and without 5 μM CMG2 for 20 min at room temperature which is sufficient for binding PA to CMG2. Then the buffers with desired pH were added and incubated for 1 h to allow the pore formation event to occur. 10% SDS was then added to get a final concentration of 1.25% and was further incubated for 20 min at room temperature. The samples were then loaded on to a 4-20% gradient SDS-PAGE gel and were run for 3.5 h at a constant 200 V in the cold room. SDS-PAGE shows that, in presence of receptor CMG2, the pH requirement for the conversion of PA_{63} prepore to a SDS-resistant pore form only occurred at pH ~6 or below in presence of receptor and pH ~7 or below in the absence of receptor. No pore formation was observed in case of D425A PA_{63} (Figure 44 B). Our results matched with earlier studies (63) and our pH titration studies.

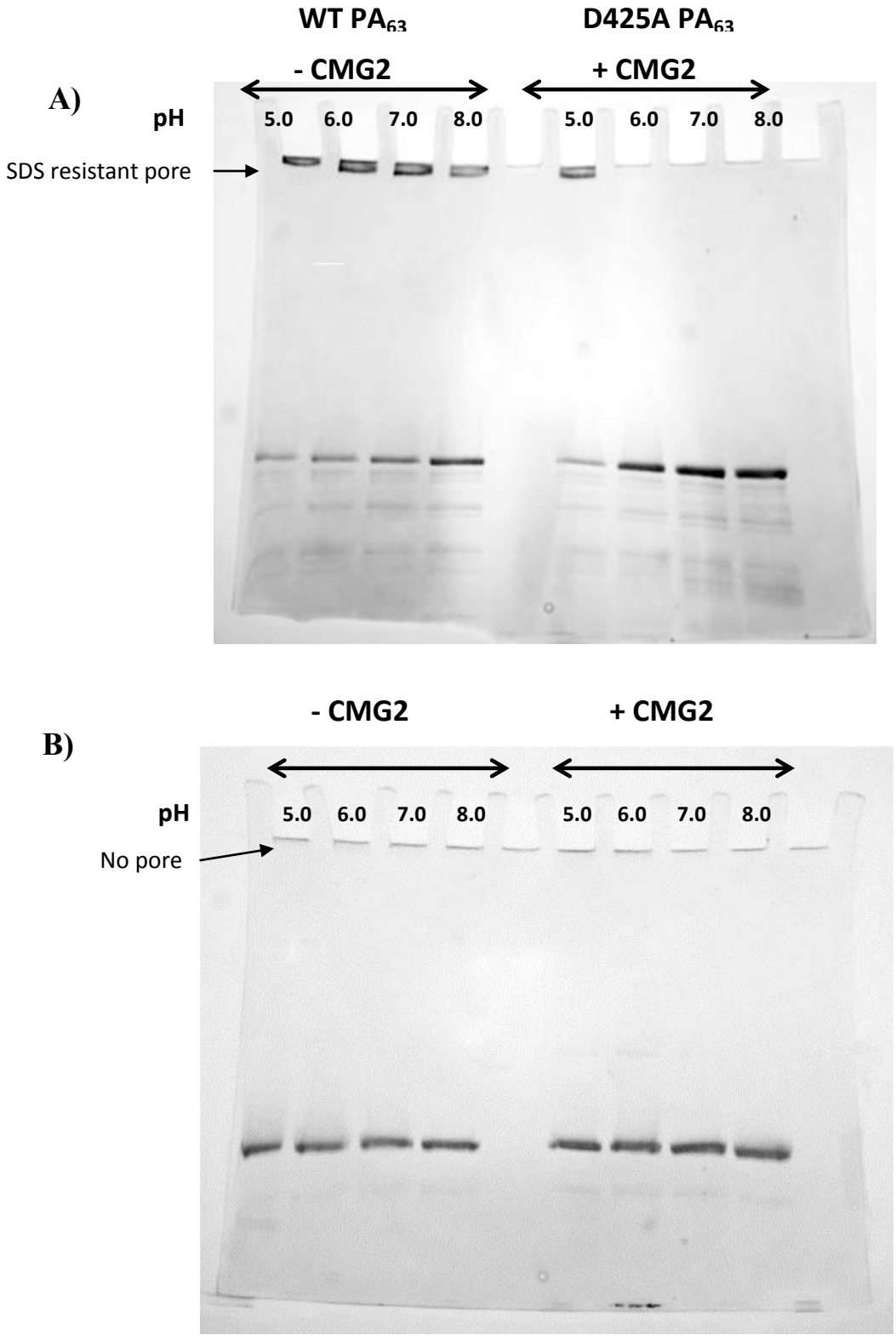

Figure 44. pH dependent conversion of prepore to pore in the presence and absence of CMG2. A) WT PA_{63} and B) D425A PA_{63}

5.3.6 Quantum Yield of AF350 PA_{63}

The quantum yield (Φ) of AF350PA_{63}, D425A AF350PA_{63} and AF350 PA_{83} were measured as described in Materials and Methods. Protein concentrations were varied from 0.002 to 0.01 and fluorescence emission spectra were recorded by exciting AF350 at 350 nm (Figure 45 A). Integrated fluorescence emission values *vs.* UV absorbance are plotted to obtain a straight line (Figure 45 B). Quantum yield of each protein was measured at different pH s with Quinine sulfate as the standard and the values are listed in Table-7.

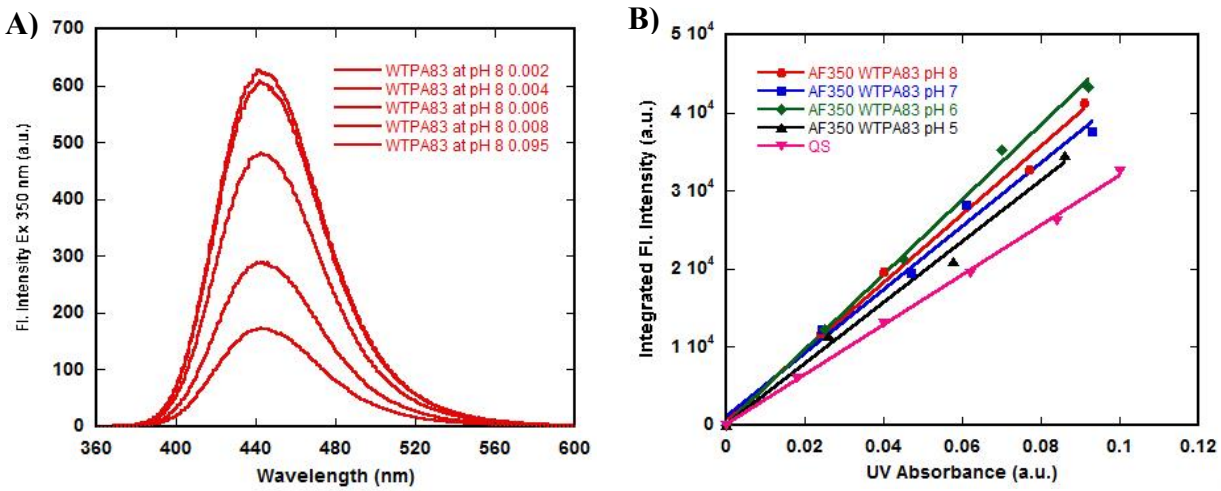

Figure- 45. Determination of Quantum Yield of WT PA_{83} protein. Quinine sulfate (QS) was used as the standard. A) Fluorescence emission spectra of different concentrations of AF350 PA_{83}; (B) the plot of integrated fluorescence intensity *vs* UV absorbance. All data was acquired on a Cary- Eclipse spectrofluorometer at 20^{o}C. Proteins were kept in CIS buffer system pH8 and QS was dissolved in water. The slits were set to 5nm.

At pH 8 and pH 7 all three proteins has similar quantum yields around ~0.76 however at lower pH (6 and 5) Φ of PA_{63} dropped to 0.57 and 0.43, almost a 40% decrease in the fluorescence of the PA_{83} at pH 5. Φ for PA_{63} was ~40% lower than its monomer and D425A PA_{63}; these results are similar to the quantum yield of WT PA without the fluorophore, AF350. These values indicate that the loss of fluorescence of AF350 in PA is dominated by residue W346 in domain II (Rajapaksha, Ph.D.-dissertation, 2009, WSU).

Table 7

		D425A PA(63)7	**WT PA_{83}**	**WT PA_{63}**
Quantum Yield (Φ)	pH 8	0.627	0.770	0.765
	pH 7	0.752	0.754	0.765
	pH 6	0.75	0.819	0.575
	pH 5	0.647	0.692	0.429

Table 8

	pH	D425A PA_{63}	WT PA_{83}	WT PA_{63}
Overlap Integral **(J)**	pH 8	7.48×10^{-14}	8.2×10^{-14}	8.19×10^{-14}
	pH 7	8.035×10^{-14}	8.16×10^{-14}	8.194×10^{-14}
	pH 6	7.96×10^{-14}	8.54×10^{-14}	8.53×10^{-14}
	pH 5	7.43×10^{-14}	7.54×10^{-14}	6.95×10^{-14}
Foster distance **(R_o) Å**	pH 8	45.29	47.49	47.44
	pH 7	46.83	47.31	47.46
	pH 6	46.72	48.25	45.56
	pH 5	45.085	45.95	41.94
Distance between two dye **(r) Å**	pH 8	48.99	48.9	49
	pH 7	46.39	51.49	44.97
	pH 6	43.41	45.95	43.78
	pH 5	44.32	45.29	33.92

5.3.7 pH titration with D50A CMG2.

In parallel experiments we carried out studies to determine the influence of pH on the fluorescence of PA and CMG2 in the absence of receptor binding. D50A CMG2 has been shown to abrogate the binding to PA by disrupting the metal coordination (119). To verify lack of binding, we performed an equilibrium binding experiment with D50A AF488 CMG2 which showed no binding to AF350 PA_{63} (Figure 46 A). In the pH titration experiment of AF350 PA_{63}-D50A AF488 CMG2 complex, we expected to see the quenching of fluorescence Em 440 nm at pH ~7 (pore formation in the absence of receptor) and little or no change in fluorescence Em 520 nm indicating that mutant CMG2 is not binding to PA and does not change its pH requisite for pore formation.

Although our results showed no change in fluorescence of the AF488 (Em520), which is expected from the lack of binding, we noticed a shallow drop in fluorescence at Em440, at pH values that were different than that found in WT PA alone (Rajapaksha, Ph.D.-dissertation, 2009, WSU). In those experiments, the pH of a solution containing 250 nM AF-350PA was adjusted by the slow addition of pH 3 buffer (20 mM Tris/BisTris/NaCacodylate, 0.2M NaCl). We recapitulated these experiments, comparing our buffer system (CIS) to that of the previous buffer system, and obtained similar results (Figure 47). The pH transition is steep and occurs at pH values consistent with previous studies. To better mimic a pore environment, we also carried out these studies in the presence of the detergent n-Dodecyl β-D-Maltopyranoside (DDM) at 0.1% (the critical micelle concentration is 0.01% or 0.16 mM). DDM has been shown in independent experiment to not influence the structure of the pre-pore. If the experiment above is carried out in the presence and absence of 0.1 mg/mL BSA, two different types of transitions are observed (Figure 48 A and B). These data would suggest that BSA may be influencing the pH transition

to a pore, and may explain the rather shallow transition observed in the AF-350 PA experiment in the presence of the D50A mutant (Figure 46). In this case the pH transition occurs at lower pH values, suggesting that BSA may stabilize the pre-pore structure. Therefore, in the following series of experiments, data were accumulated using a buffer containing CIS with 0.2 M NaCl and 0.1% DDM.

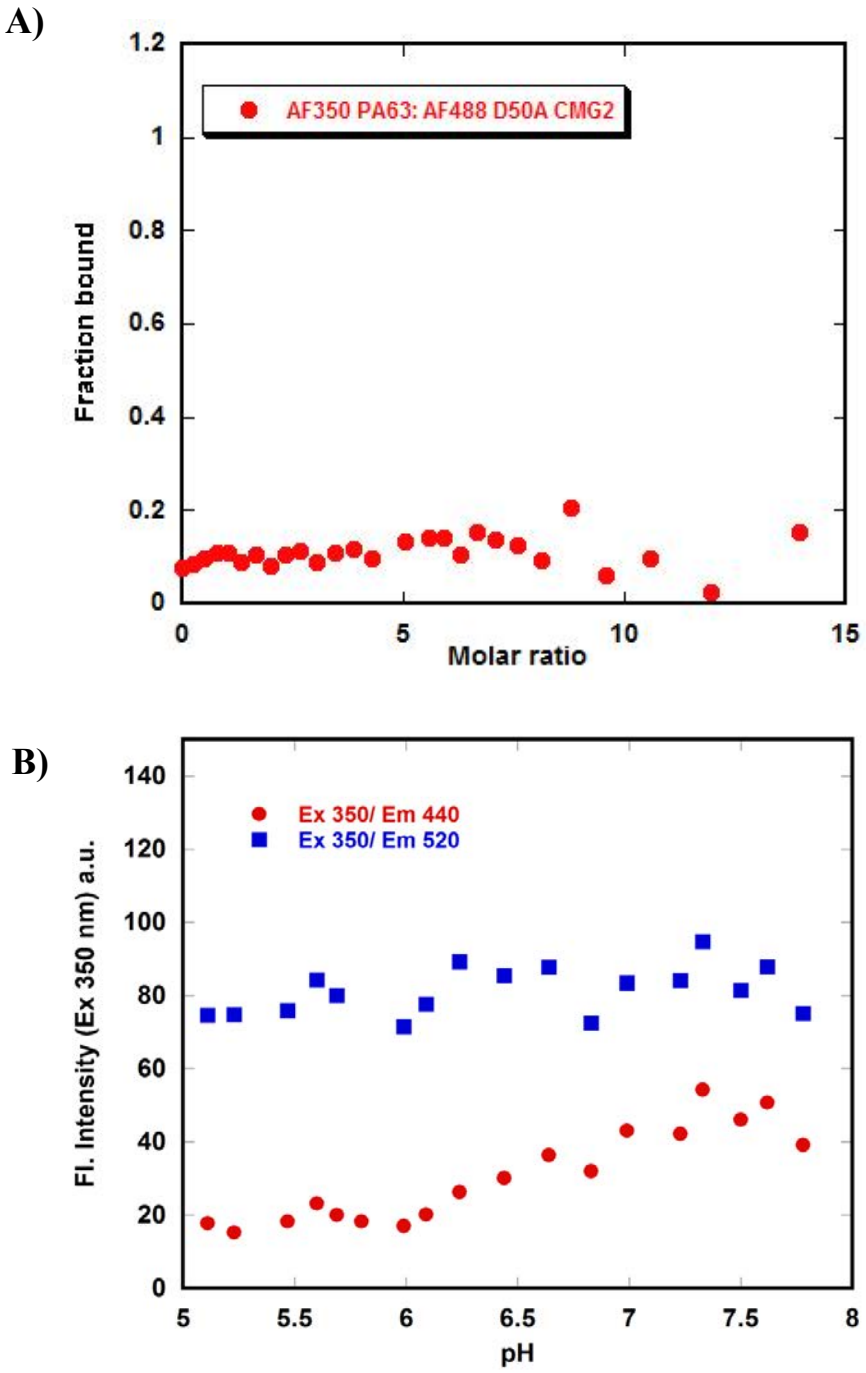

Figure 46. Equilibrium pH and Binding Titration. A) Fluorescence equilibrium binding titration of AF350 PA_{63} with AF488 D50A CMG2, molar ratio is defined by [CMG2] / [PA]. B) pH titration experiment for AF350 PA_{63} 5 fold excess of AF488 D50A CMG2, fluorescence intensity was measured as a function of pH. Data were acquired on a Cary-Eclipse fluorescent instrument and the samples were maintained at 20^{o}C with a Peltier cooling system.

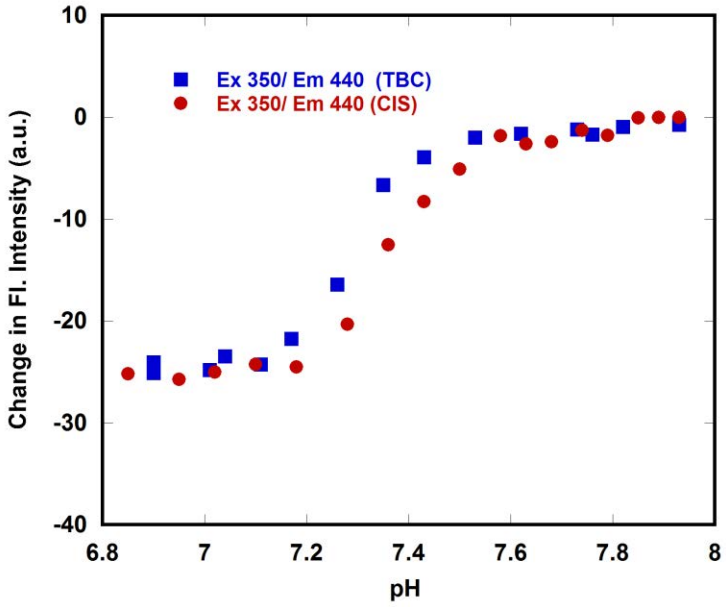

Figure 47. pH titration of AF350 PA_{63} alone without BSA in presence of 0.1% DDM, with CIS buffer system (red) and TBC buffer (blue) under non-equilibrium conditions; change in fluorescence intensity (measured-expected) was measured as a function of pH. Data were acquired on a Cary-Eclipse fluorescent instrument and the samples were maintained at 20^{o}C with a Peltier cooling system.

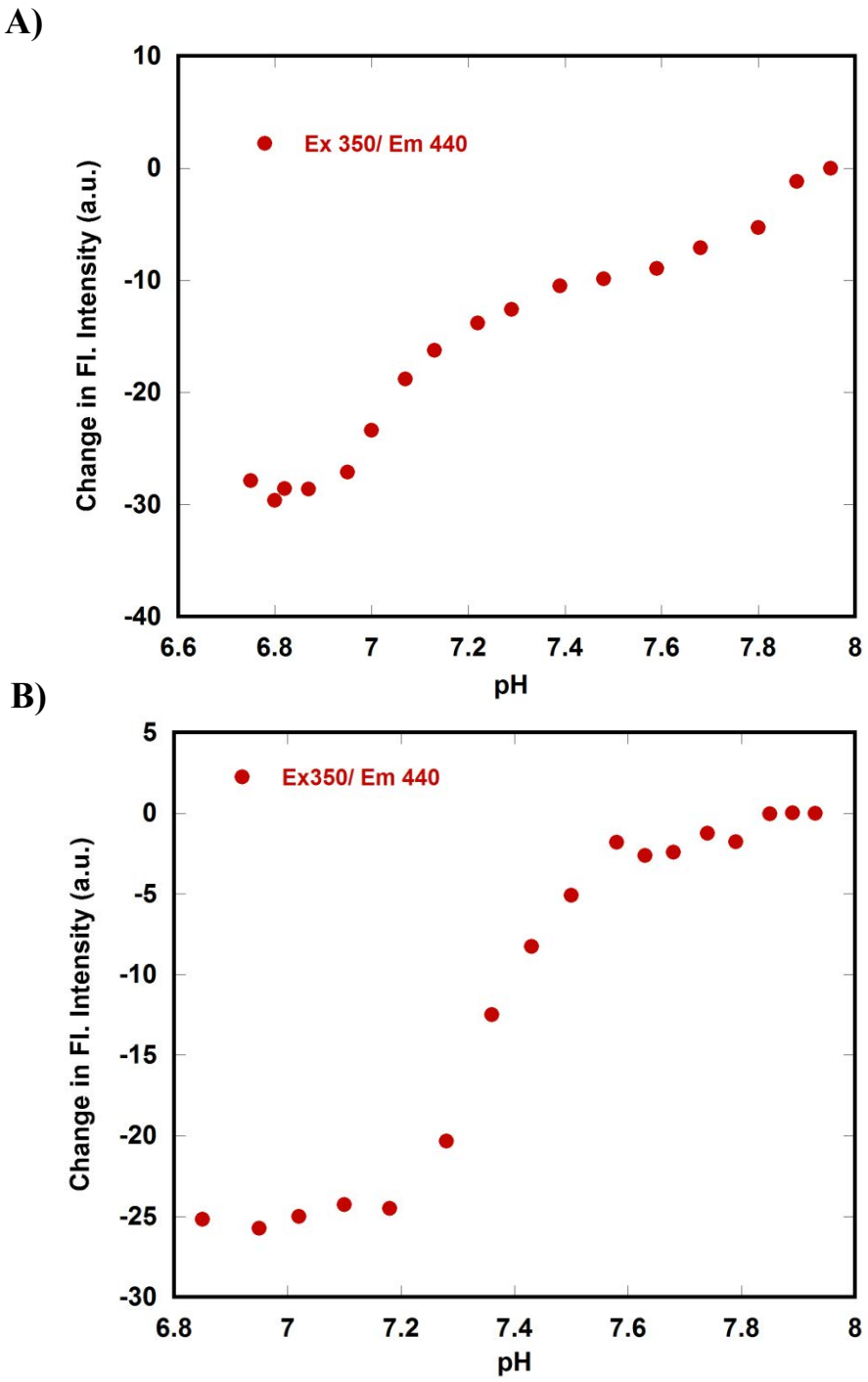

Figure 48. pH titration of AF350 PA_{63} alone in presence of 0.1% DDM (condition 3). A) pH titration of AF350 PA_{63} in the presence of 0.1 mg/mL BSA; B) pH titration of AF350 PA_{63} in absence of 0.1 mg/mL BSA. Change in fluorescence intensity (measured-expected) was measured as a function of pH. Data were acquired on a Cary-Eclipse fluorescent instrument and the samples were maintained at 20^{o}C with a Peltier cooling system.

We then recapitulated the experiment with the D50A mutant, which showed a rather shallow transition of PA, using the above buffer system. Under these new conditions, results show no change in fluorescence at Em 520, as was observed previously, but now we observe a drop in fluorescence at Em 440 (Figure 49 A) and it matched well with PA_{63} alone titrations under the same conditions. In these experiments with CMG2, we also changed the concentration of CMG2 to a 1:2 ratio, versus a 1:5, to in part conserve on protein, and secondly to not overwhelm the fluorescence upon excitation at 350 nm, as the AF488 can also be excited at this wavelength. The binding constant is ~300 pM, well below the concentrations used in our studies (100 nM).

Our previous studies had shown that for the AF350 PA_{63} bound to AF488 CMG2, as the pH was lowered, we observed a drop in both the emission at 440 and emission at 520 upon excitation of AF350 (350 nm). Using the above conditions, we carried a similar experiment, monitoring continually the fluorescence of the PA-CMG2 complex as the pH was lowered. The incubation time from addition of low pH buffer (pH 3.0) to measurement was ~10 minutes. Under these conditions, however, we observed no change in fluorescence (Figure 50). This was quite surprising, and we hypothesized that the lack of a drop may be due to a potential slow equilibration. It is known that the receptor is slow to dissociate, with a rate constant of ~4 x 10-5 s-1, and if receptor dissociation is required for pore formation, a 10 min incubation would not be sufficient to allow for full dissociation. In these studies, 100 µL aliquots are removed and discarded, and a 100 mL aliquot of low pH buffer is added to slowly lower the pH. The assumption is made that the fluorescence is directly proportional to the concentration, which is valid since the absorbance of the fluorescent solution is less than 0.01 and should not be subject

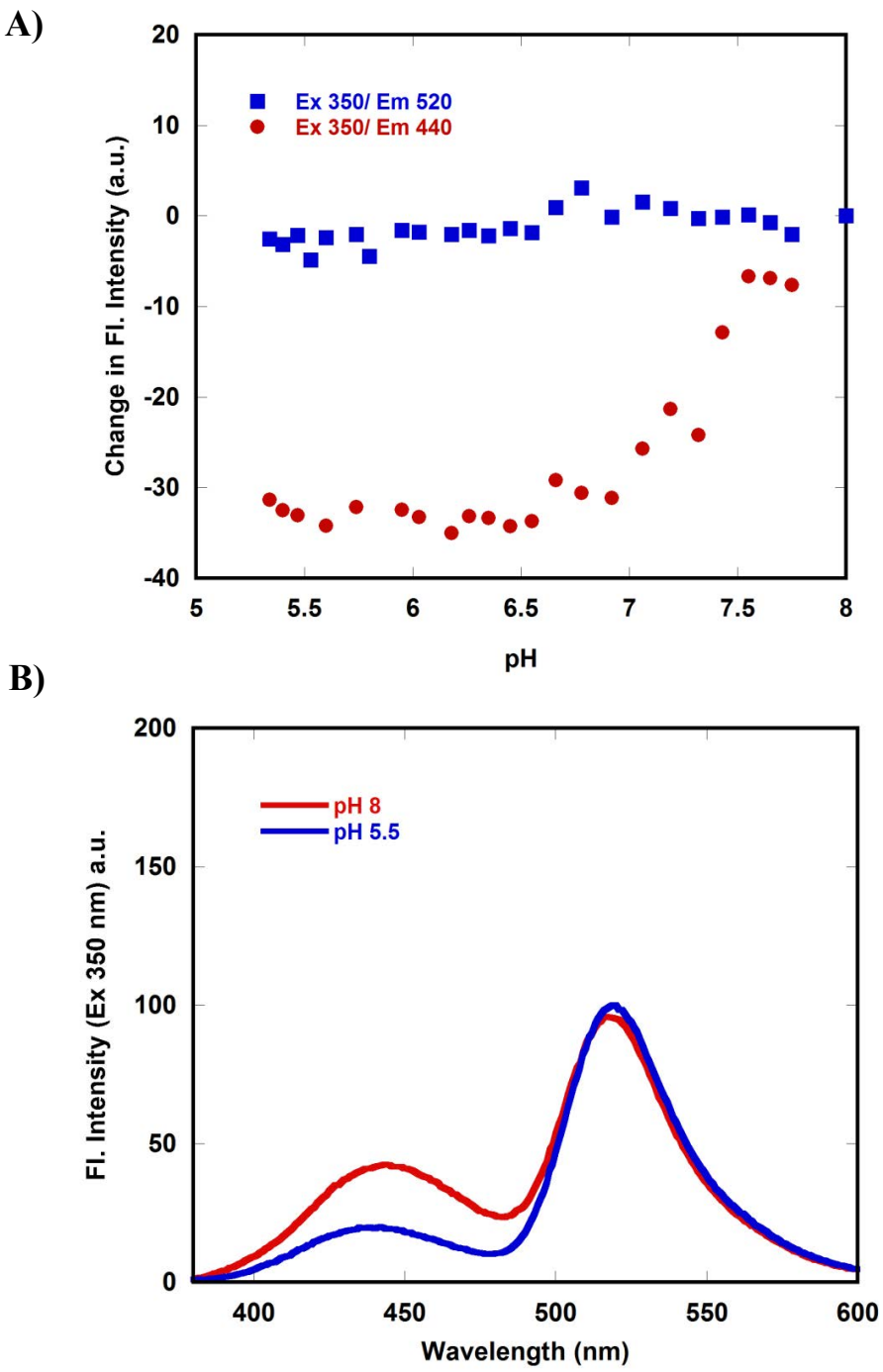

Figure 49. Equilibrium pH titration in presence of 0.1 % DDM. A) Fluorescence equilibrium pH titration of AF350 PA_{63} with AF488 D50A CMG2, in absence of BSA B) Fluorescence emission spectra of PA_{63}-D50A CMG2 at pH 8 and pH 5.5. Data were acquired on a Cary-Eclipse fluorescent instrument and the samples were maintained at 20°C with a Peltier cooling system.

to inner filter effects. Thus the fluorescence that is reported contains a correction factor that accounts for the concentration change (see Materials and Methods). We decided to do the above experiment, but rather than discard the 100 µL aliquots, these were saved and incubated overnight at room temperature, and the fluorescence recorded. We note that the cuvette used in these experiments gave slightly more distorted values of fluorescence as a function of pH, but the transitions are fairly clear.

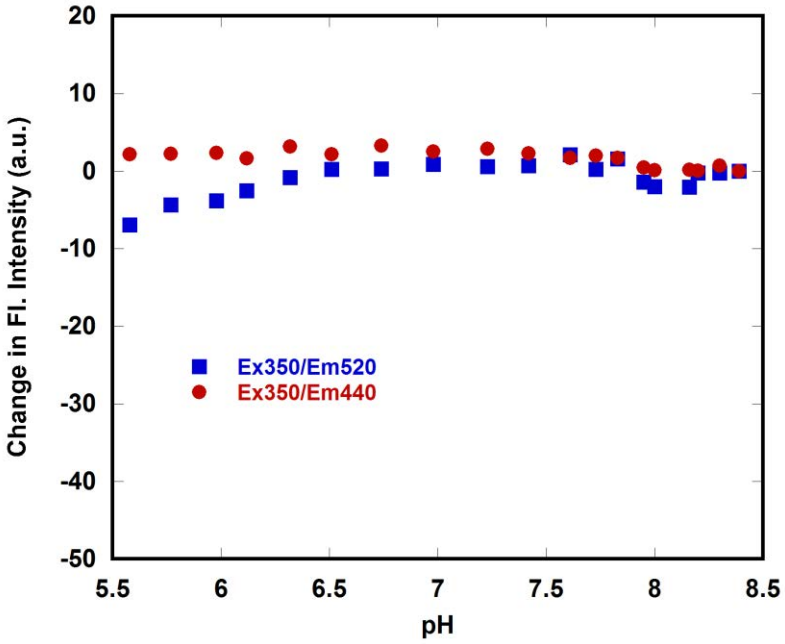

Figure 50. Equilibrium pH titration of AF350 PA_{63}-AF488 CMG2 in the presence of 0.1 % DDM under condition 3. Data were acquired on a Cary-Eclipse fluorescent instrument and the samples were maintained at 20°C with a Peltier cooling system.

Figure 51 shows the pH titration of AF350 PA and AF488 CMG2 (A) and (B) the same pH titration with NEM-labeled CMG2. The former experiment recapitulates the data we observed with the WT PA in CIS buffer, with 0.1 mg/mL BSA, but importantly shows a transition to a pore. Therefore, there is a strong kinetic effect on pore formation that is dependent on the receptor. If experiments on PA alone with an overnight incubation, we observe the same transition that is observed with a 10 minute incubation.

These data would suggest that a rate determining step is the dissociation of the receptor. In previous experiments, the D425A mutant was used to follow pore formation. We carried a similar set of experiments under the above conditions, incubating the D425A with AF488 CMG2 overnight, and measuring the fluorescence (Figure 52). Now, in these experiments, we observed the exact same transition as the WT protein, which was completely unexpected. We initially hypothesized that the wrong mutant had been made accidentally. To check this we measured the ability to form a pore using the SDS-PAGE assay (Figure 53). If the samples are incubated in low pH buffer for 1 h, no SDS resistant heptamer are observed. However, if the samples are incubated overnight, we do not observe the high molecular aggregates indicative of pore formation, but the lack of monomeric species is evidence that pore formation has occurred (Figure 53 B).

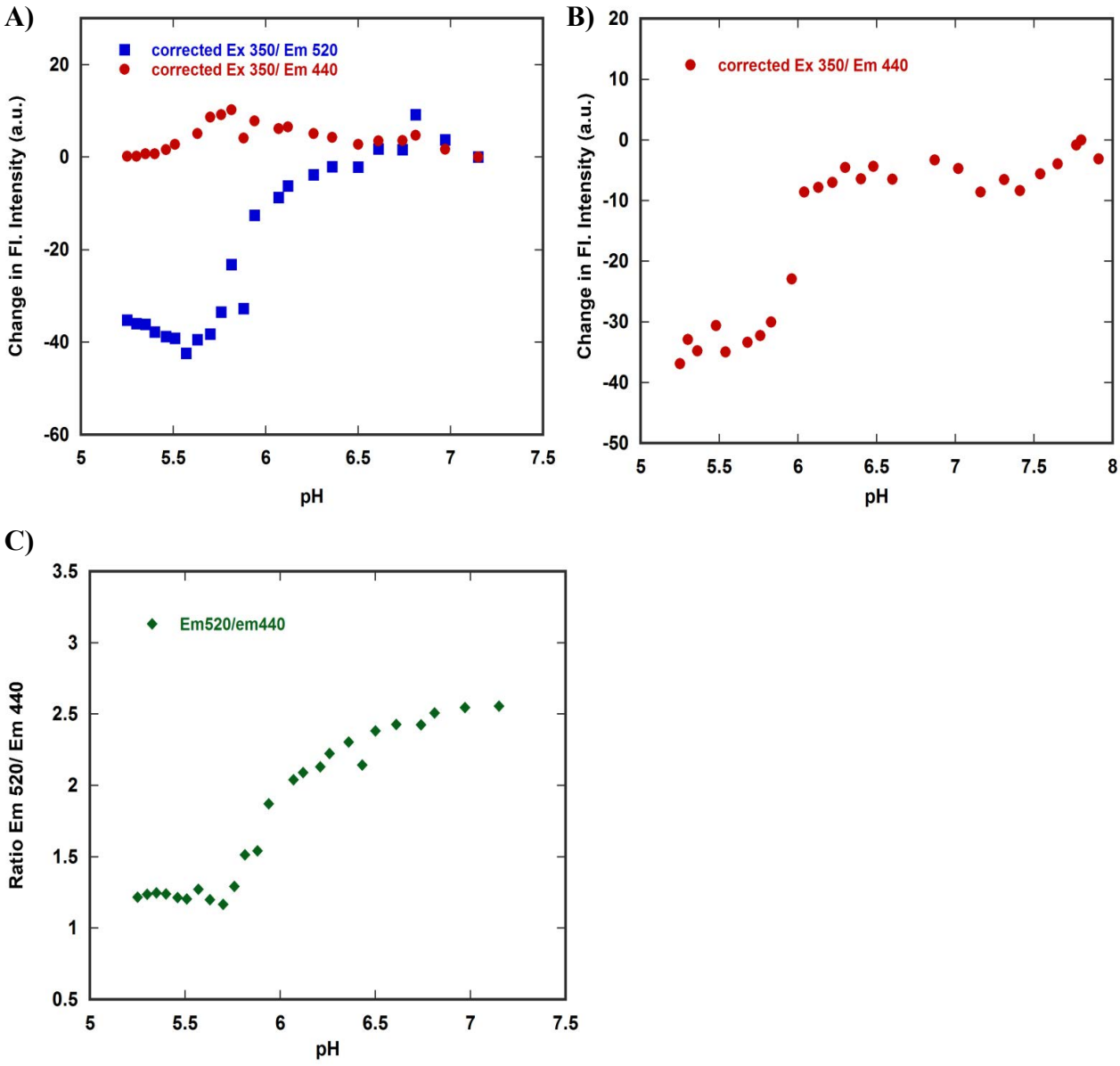

Figure 51. Equilibrium pH titration of AF350 PA_{63} in presence of 0.1 % DDM at 20°C. A) Fluorescence equilibrium pH titration of AF350 PA_{63} with AF488 CMG2. B) Fluorescence equilibrium pH titration of AF350 PA_{63} with NEM-CMG2; C) Plot of the ratio of Em520/Em440 from figure 52 A. Data were acquired on a Cary-Eclipse fluorescent instrument and the samples were maintained at 20°C with a Peltier cooling system.

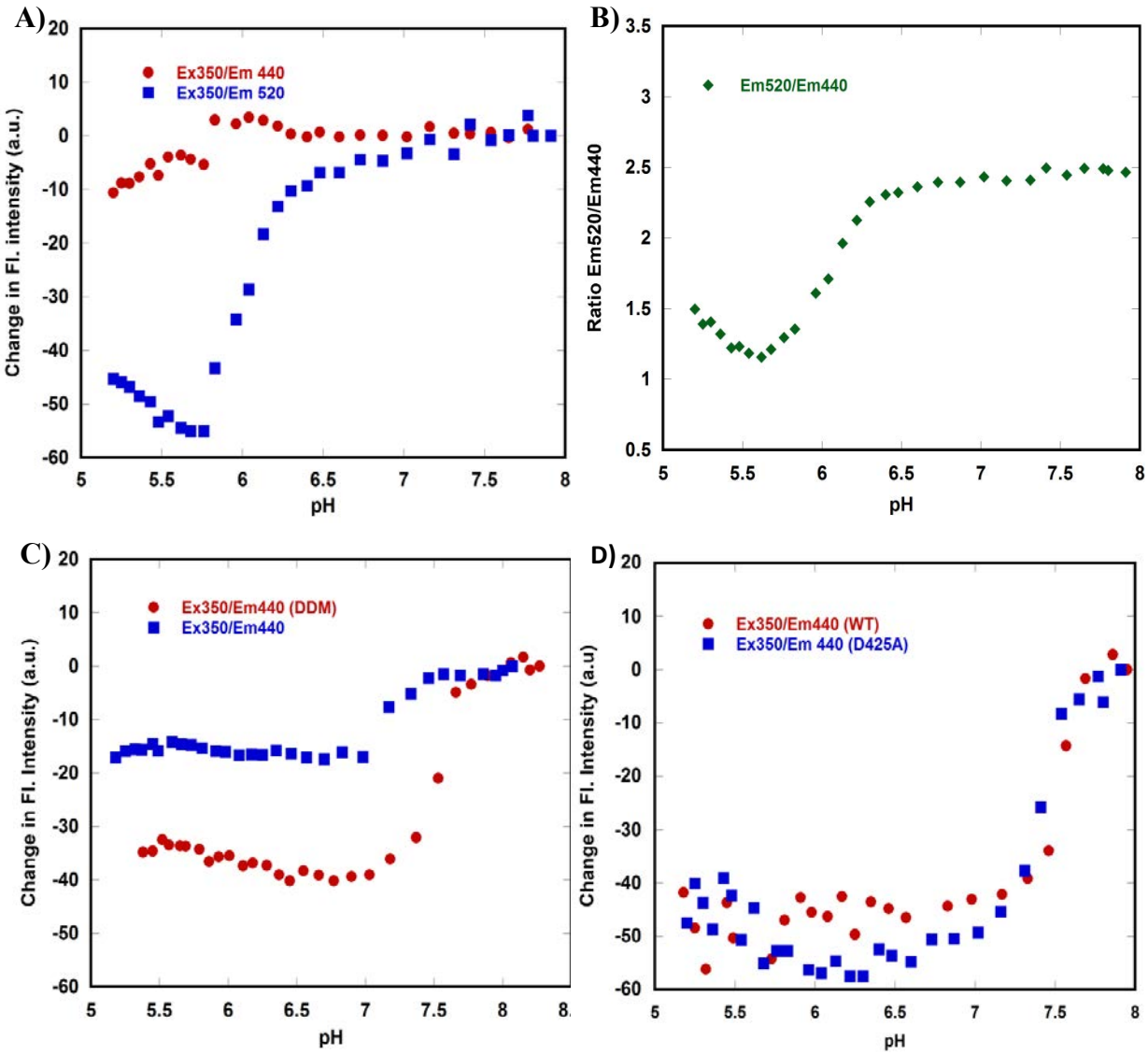

Figure 52. Equilibrium pH Titration of AF350 D425A PA_{63} in presence of 0.1% DDM. A) Fluorescence equilibrium pH titration of AF350 D425A PA_{63} with AF488 CMG2. B) Plot of the ratio of Em520/Em440 from Figure 53 A. C) Fluorescence equilibrium pH titration of AF350 D425A PA_{63} alone in presence of DDM (red) and in absence (blue) and D) Fluorescence equilibrium pH titration of AF350 D425A PA_{63} alone (blue) and WT PA_{63} (red). Change in fluorescence intensity was calculated by subtracting the expected fluorescence from measured. Data were acquired on a Cary-Eclipse fluorescence instrument and the samples were maintained at 20^{o}C with a Peltier cooling system.

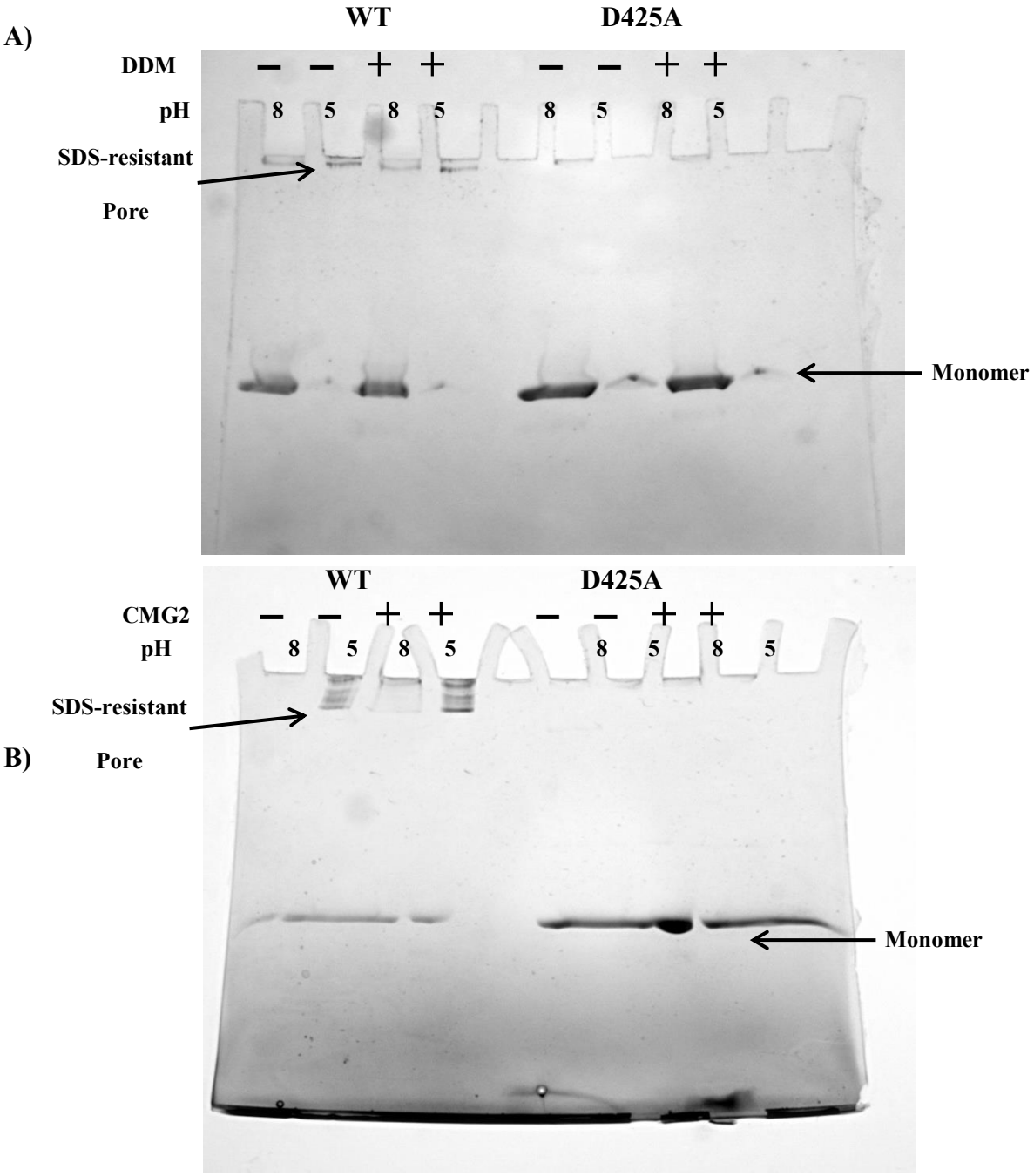

Figure 53. SDS-Pore formation assay. A) Pore formation assay of WT PA_{63} alone (1-4 lanes) and D425A PA_{63} alone (6-9 lanes) in presence and absence of DDM. B) Pore formation assay of WT PA_{63} (1-4 lanes) and D425A PA_{63} (6-9 lanes) in presence and absence of CMG2 (without DDM).

We had shown under the conditions previously used (CIS, 0.1 mg/mL BSA, 1mM $CaCl_2$, 1 mM $MgCl_2$ – condition 1), that the D425A mutant did not undergo pore formation, but receptor release was observed (Figure 42 B). We reasoned that the detergent DDM may be influencing the formation of a pore, as had been observed in previous experiments using the detergent Fos-14 (Figure 63 B and D, inset). Therefore, we carried out identical experiments as above, but in the absence of detergent. In this experiment, we can again recapitulate the data acquired under condition 1, and indeed the data indicate that at low pH, the receptor dissociates, as observed by the decrease in the emission at 520 nm, and the increase in fluorescence at 440 nm.

These data would suggest that the addition of detergent influences the formation of the pore, under these conditions with the D425A mutant (alone). We therefore incubated the D425A mutant with the detergent DDM overnight, and the next day followed the transition to a pore. The data in figure 52 D shows that both the WT and the D425A mutant undergo the exact same transitions to a pore state, indicating that detergent facilitates the formation of a pore state.

These data suggested that, under these new conditions (condition 2 – CIS, 0.2 M NaCl, 0.1% DDM) that pore formation is influenced by detergent. If detergent is removed, we observe a small transition that occurs at lower pH values, suggesting that detergent may be destabilizing the prepore to changes in pH. Likewise, in experiments carried out with AF488 CMG2, we observe an increase in the fluorescence at 440, and a drop in the emission at 520, consistent with our previous findings using condition 1, and further supporting the view that at low pH the receptor dissociates. Further, the data indicate that even in the case of the D425A mutant, pore formation, if given a long enough incubation periods, can occur to a limited extent. Previously we had hypothesized that the region around D425 was the initiation site for pore formation. If we take the data accumulated on the D425A mutant, a model for pore formation becomes

apparent. In the presence of detergent, pore formation occurs at pH values identical to the WT. It is known that the domain II β_3-β_4 loop is sensitive to pH, and likely is important for maintenance of receptor binding. The dissociation of CMG2, but lack of pore formation in the absence of detergent would suggest that this region becomes more dynamic and that this causes receptor release – but in the case of D425A, pore formation, if it occurs is small. This is reflected in the amplitude of the difference in the ratio of 520/440 emission (Figure 54). This is consistent with recent NMR studies suggesting that the domain II β_3-β loop becomes dynamic at low pH, but prior to the formation of a pore. Addition of detergent, because it destabilizes the structure of the prepore, receptor dissociation and pore formation become concomitant processes.

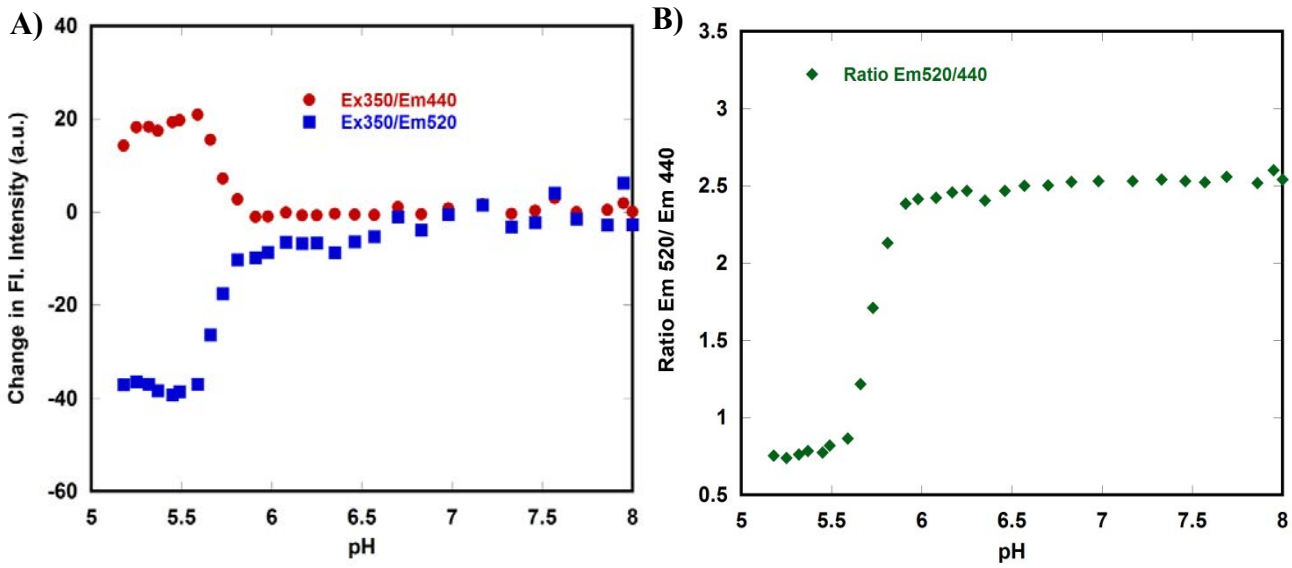

Figure 54. Equilibrium pH Titration of AF350 D425A PA_{63}. A) Fluorescence equilibrium pH titration of AF350 D425A PA_{63} with AF488 CMG2. B) Plot of the ratio of Em520/Em440 from figure 55 A. Change in Fluorescence intensity was calculated by subtracting the expected fluorescence from measured. Data were acquired on a Cary-Eclipse fluorescent instrument and the samples were maintained at 20^{o}C with a Peltier cooling system.

In the case of D425A, addition of detergent overcomes an energetic barrier to pore formation. How this occurs is not known. We speculate that the detergent may occupy the groove that is normally occupied by the domain II β_2-β_3 strands, which may facilitate pore formation.

5.3.8 Binding Kinetics of D425A PA_{63} and CMG2

To monitor the binding kinetics of D425A PA_{63}, a stopped-flow FRET method was utilized. The binding of D425A PA_{63} to CMG2 was determined by exciting donor fluorophore AF350 which is attached to PA at 350 nm and the emission of the donor was measured at 516 nm using a 475 nm cutoff filter. The experiments were carried out by 1 to 1 jump, under pseudo

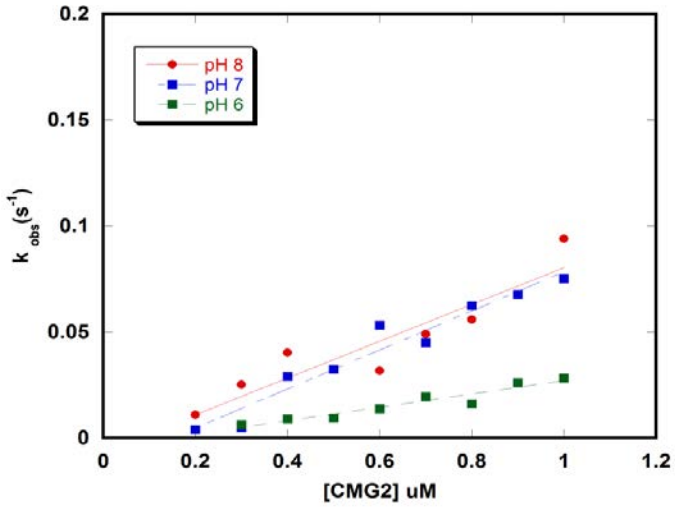

Figure- 55. Stopped flow Binding Kinetics as a Function of CMG2 Concentration. Binding rate constants were calculated using the slope of the linear fits using pseudo first order conditions where the [CMG2] was kept at a minimum 5 fold excess, using the relationship k_{obs} =ka[A0]+kd. All kinetic experiments were carried out at 20°C in CIS buffer system containing 50 mM Tris/ 25 mM MES/ 25 mM AcOH with 0.1mg/ mL BSA and 2 mM MgCl2 on an Applied Photophysics SX-18MV Stopped flow instrument.

First order reaction conditions where the concentration of CMG2 was kept at a minimum of 5 fold or higher than PA_{63}. The resulting FRET signal was monitored for 200 seconds and the kinetic traces were plotted against the concentration of CMG2.

The association rate of D425A PA was 0.132 $M^{-1}s^{-1}$ at pH 8. When the pH dropped, a gradual decrease in the association rates was observed from 0.14 and 0.0477 at pH 7 and pH 6 respectively (Figure 55). The trend we observed for D425A PA could also explain that at low pH the binding interaction between PA and CMG2 weakens, leading to receptor dissociation.

5.3.9 Is the Decrease in Fluorescence Emission due to Trp 346 Quenching the Fluorescence of AF350?

Previous studies under condition 1 and studies by Rajapaksha (Rajapaksha, Ph.D.-dissertation, 2009, WSU) suggested that the W346 was the cause of the emission drop at 440 nm (Ex 350). We recapitulated these experiments under condition 2, incubating 100 µL samples overnight at 4°C, and measuring fluorescence at 4°C. We acquired the data at 4°C because of the lack of stability and the data are shown in Figure 56 A, in the presence of AF488 CMG2, and B in the presence of NEM CMG2. In either case, there is little change in the emission at 440 nm, but in Figure 56 A, we observe a significant drop in the EM 520, suggesting receptor dissociation. This is consistent with the hypothesis that W346 quenches the fluorescence of the AF350 dye. The drop in fluorescence may be due to either a collisional or static quenching mechanism. Indendent lifetime experiments carried out in the laboratory of Carey Johnson (University of Kansas) show that the lifetime of the WT and W346F at pH 8 or pH 5 is unchanged, suggesting that the quenching observed is due to the formation of a dark complex (Figure 57).

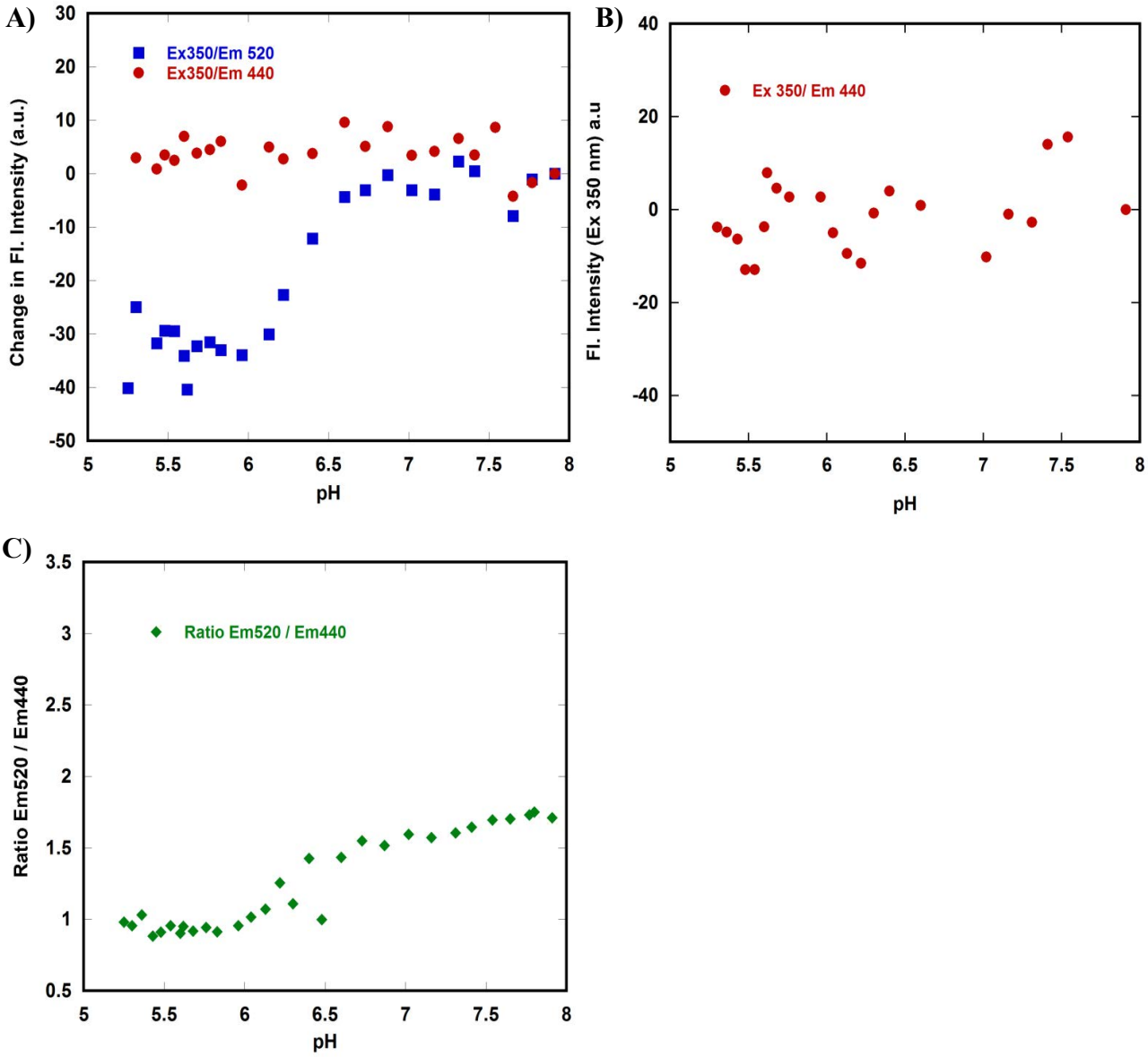

Figure 56. Equilibrium pH Titration of AF350 W346F PA_{63} in presence of 0.1 % DDM at 4°C. A) Fluorescence equilibrium pH titration of AF350 W346F PA_{63} with AF488 CMG2. B) Fluorescence equilibrium pH titration of AF350 W346F PA_{63} with NEM- CMG2. And C) Plot of the ratio of Em520/Em440 from Figure 57 A. Data were acquired on a Cary-Eclipse fluorescent instrument and the samples were maintained at 20°C with a Peltier cooling system.

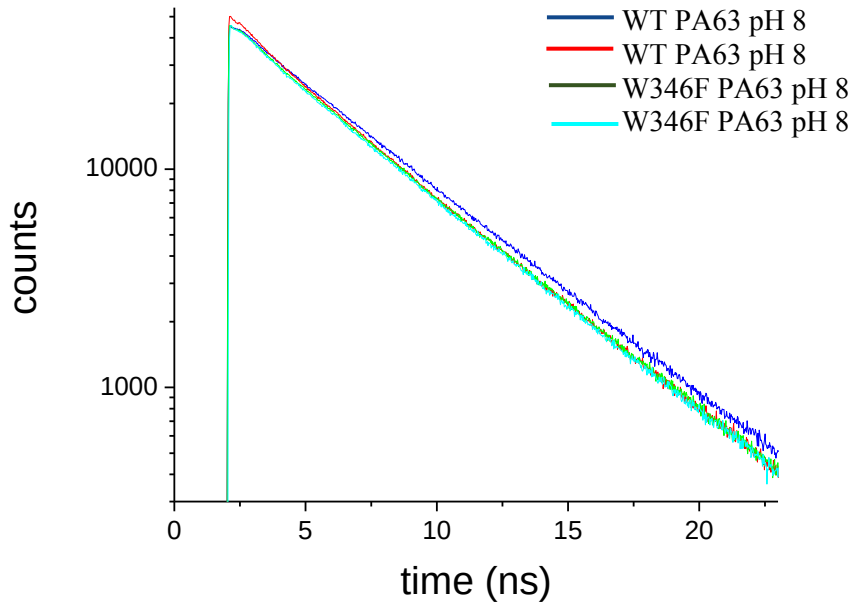

Figure 57. Observed fluorescence lifetime of AF350 labeled PA_{63} (pH 8 in blue and pH 5 in red) and W346F PA_{63} (pH 8 in green and pH 5 in cyan).

To verify that the quenching is independent of the dye, and to provide a measure of the distance between the tryptophan and the fluorophore, we labeled E712C PA with monobromobiamine (mBBr, Ex 385 and Em 480 nm) (Figure 58 A), mBBr can be quenched by tryptophan but only if the two dyes are ≤ 15 Å away from one another (125). Figure 58 shows the influence of pH on the fluorescence of mBBr in the presence of CMG2. In this case, we again observed a decrease in the fluorescence emission of mBBr, suggesting that the distances between E712C and W346 become close during the formation of the pore (126).

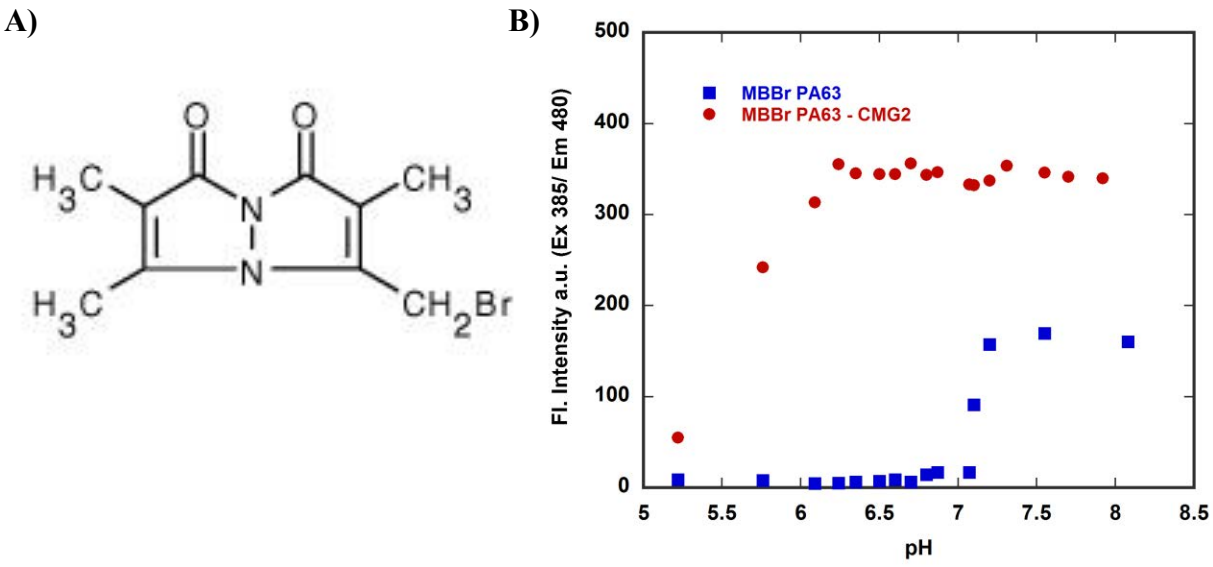

Figure 58. A) Structure of mBBr. B) Fluorescence equilibrium pH titration of mBBr PA_{63} in presence of CMG2 (red), in absence of CMG2 (blue). Data were acquired on a Cary-Eclipse fluorescent instrument and the samples were maintained at 20°C with a Peltier cooling system.

5.3.10 Monitoring the Pore Formation using Tryptophan Fluorescence

Since, Trp346 in domain II is the only one closer (~20 Å) to the fluorescence dye AF350 in domain IV, Trp346 quenching of AF350 fluorescence during the structural change result in less energy transfer to AF488. As an independent way to monitor the pore formation, we are using tryptophan fluorescence in presence of CMG2. vWA domain -CMG2 has only one tryptophan, which may possibly interfere in fluorescence studies. In order to eliminate the tryptophan contribution, we chose to label CMG2 with 4-fluoro tryptophan, which has been shown to eliminate the fluorescence contribution of tryptophan (111, 112).

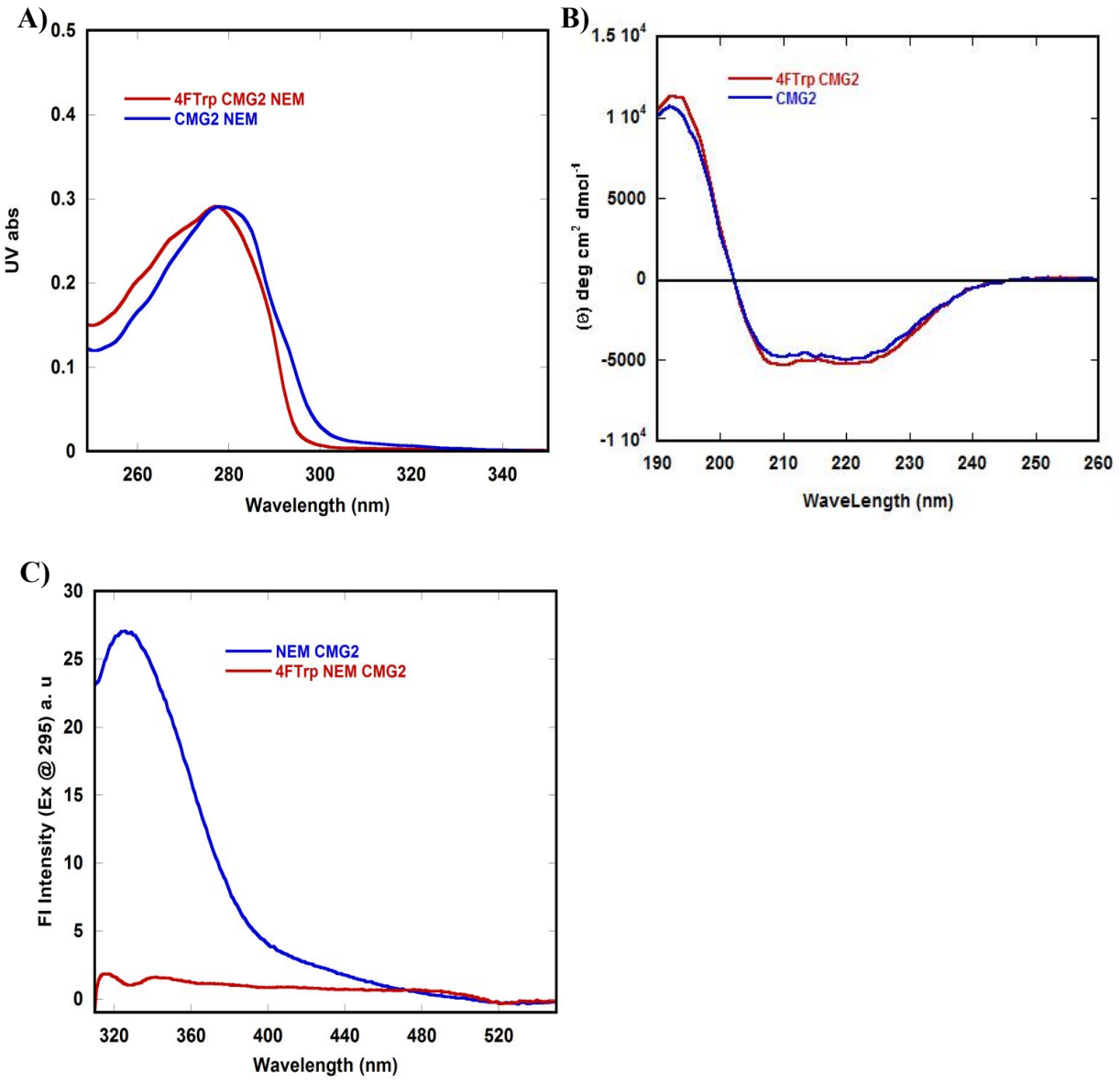

Figure-59. Spectral Analysis of 4-FTrp labeled CMG2. A) UV-Vis spectrum of 4-FTrp CMG2 (red) and WT CMG2 (blue), B) CD spectrum of 4-FTrp CMG2 (red) and WT CMG2 (blue), and C) Fluorescence emission spectrum of 4-FTrp CMG2 (red) and WT CMG2 (blue), excitation at 295 nm, Ex and Em slits were set to 5.

Fluorine is smaller and only slightly larger than hydrogen, and we anticipated that this change would not affect the structure of CMG2. Absorption and emission spectrum of 4-FTrp CMG2, shows that the majority of the contribution of fluorescence of CMG2 was eliminated (Figure 59 A and C.). Even CD analysis shows similar structure (Figure 59 B). The degree of labeling was >90% as determined by mass spectrometry and both proteins AF488 CMG2 and AF488 4-FTrp CMG2 exhibit similar binding profiles to AF350 PA_{63}, suggesting that we have not dramatically influenced the binding affinity. We used 4-Trp CMG2 in all experiments where we excited the tryptophan at 295 nm.

Trp346 in domain II is the only one closer (~20 Å) to the fluorescence dye AF350 in domain IV; Trp346 could quench AF350 fluorescence during the structural change results less energy transfer to AF488. To check the fluorescence quenching we used W346F mutant as a control and conducted binding and pH titration experiments. W346F mutant binds to 4-FTrp-CMG2 with same stoichiometry (1:7) as WT PA_{63} (Figure 60 A and B) but in pH titration experiment, no drop in fluorescence was observed (Figure 61 B.) which reveals that W346 was the quencher for AF350, similar results was observed at 350 nm excitation (Figure 58 A.).

pH titration and fluorescence emission data shows that tryptophan at 346 in domain II comes closer to domain IV (AF350) and therefore causes quenching at pH ~5.5 in presence of receptor (Figure 61 A), which we also confirmed with W346 PA_{63} where we were not able to see any quenching (Figure 61 B). Again, we observe the same drop in fluorescence in case of mBBr labeled protein, below pH 7.4 in absence of CMG2 and at pH ~5.5 in presence of CMG2, indicating that the fluorescence of both chromophores are quenched in a distance dependent manner (Figure 62). This observation is only possible if the two domains get close together. These experiments confirm that the distance between domain II and domain IV gets shorter than

10 Å during pore formation. By labeling the proteins with two different fluorescent probes, we also show that the results we see are probe independent

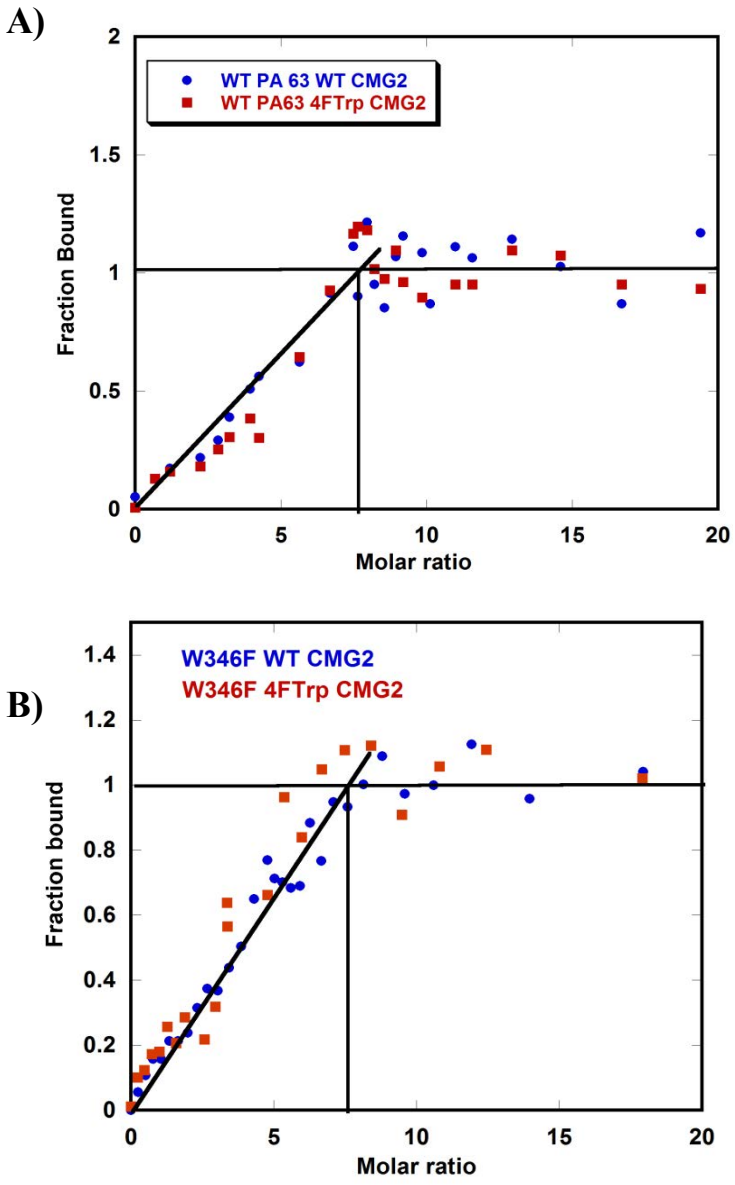

Figure 60. Equilibrium Binding Titration. A) Fluorescence equilibrium binding titration of AF350 PA_{63} B) AF350 W346F PA_{63}, molar ratio is defined by [CMG2] / [PA]. Data were acquired on a Cary-Eclipse fluorescent instrument and the samples were maintained at 20°C with a Peltier cooling system.

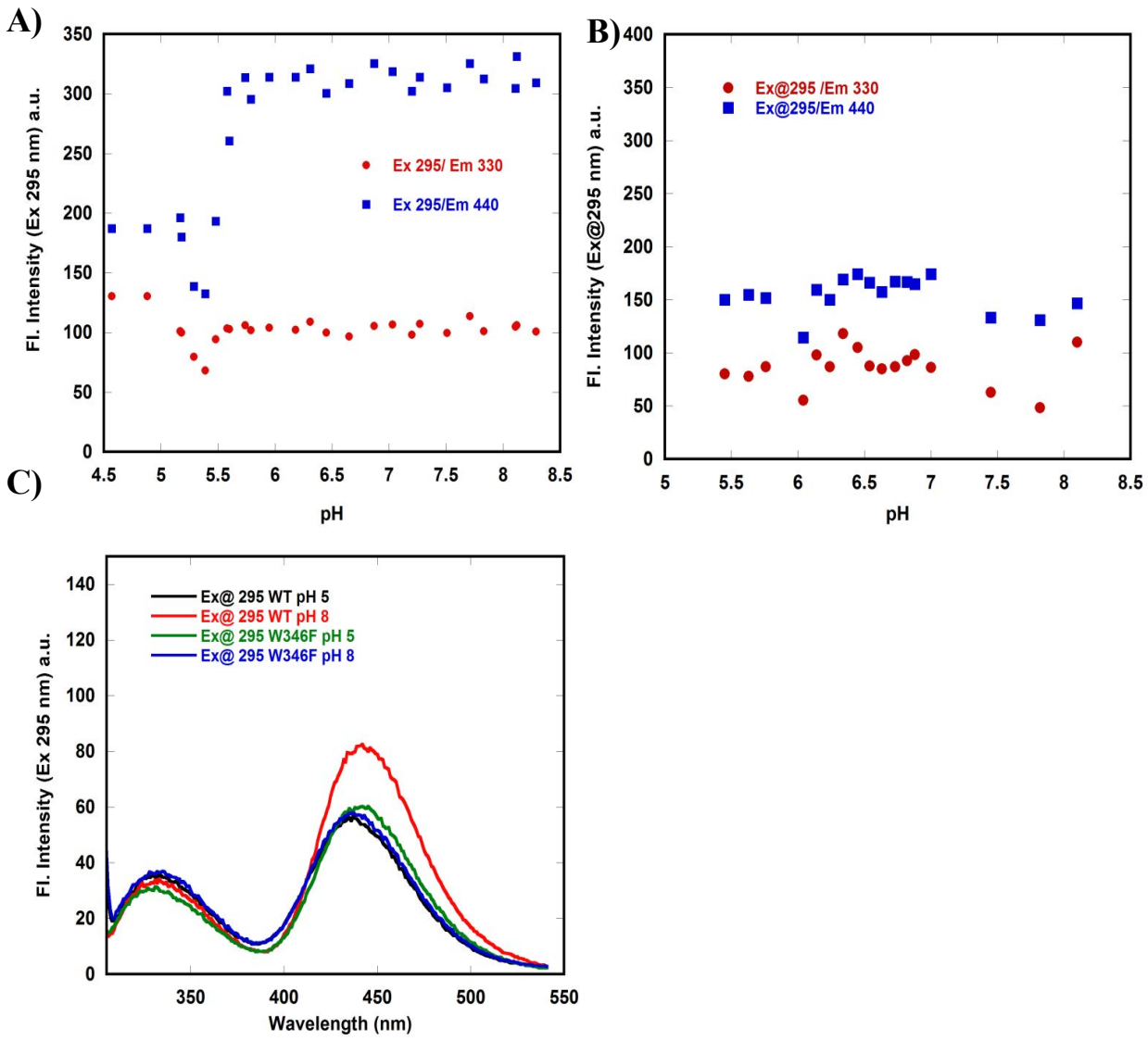

Figure 61. Equilibrium pH Titration. A) Fluorescence equilibrium pH titration of AF350 PA_{63} in presence of 4-FTrp-NEM-CMG2 B) Fluorescence equilibrium pH titration of AF350 W346F PA_{63} in presence4-FTrp- CMG2; C) Fluorescence emission spectra of AF350 PA_{63} and AF350 W346F PA_{63} bound to 4-FTrp CMG2.Data were acquired on a Cary-Eclipse fluorescent instrument and the samples were maintained at 20^{o}C with a Peltier cooling system.

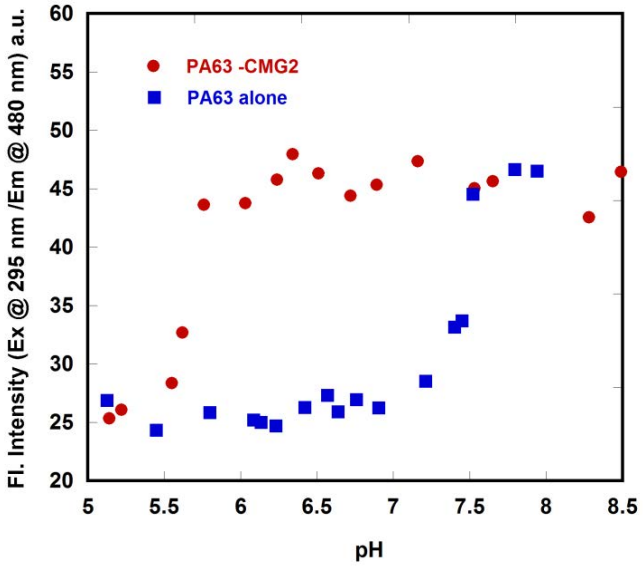

Figure 62. Equilibrium pH Titration. A) Fluorescence equilibrium pH titration of mBBr PA_{63} in presence of 4-FTrp-NEM-CMG2. Data were acquired on a Cary-Eclipse fluorescent instrument and the samples were maintained at 20^{o}C with a Peltier cooling system.

5.3.11 Determination of Rate Associated with Pore Formation and Receptor Dissociation.

To determine the kinetics of the structural transition of PA_{63} at low pH stopped flow pH jump experiments were carried out at 20°C from an initial pH 8 to a final pH 5.5. PA_{63} proteins labeled with AF 350 were incubated at pH 8 and 5.5 for 30 min at 20°C and the data was collected by rapid mixing of protein at pH 8 with buffer pH 8 to establish the upper margin which represents the maximum fluorescence before structural transition. Then the protein at pH 5.5 was mixed rapidly with buffer pH 5.5 and the lower margin which represents the minimum fluorescence after structural transition was established. Next the protein at pH 8 was rapidly mixed with buffer pH 4 (in 1:5 ratio) so as to achieve a final pH of 5.5 in the reaction mixture and the drop in fluorescence was measured using a cutoff filter for 200 sec to obtain a kinetic

trace as in Figure 63 (A and B). A similar set of experiments were carried out at excitation of 350 nm and the results are summarized in Figure 63 C and D.

The rate of pore formation of AF350 PA_{63} bound to CMG2 was determined in the presence and absence of detergent, Fos-14. Our results show that the rate of receptor dissociation (0.11 s^{-1}) and rate of the conformational change (0.14 s^{-1}) to a pore occur at similar rates. However, in the presence of the detergent FOS14, the rate of the conformational change to a pore (0.42 s^{-1}) is ~6-fold faster than the rate of dissociation (0.06 s^{-1}), suggesting that receptor release occurs subsequent to the conformational change to a pore. The release of the receptor in all cases was incomplete, indicating that a significant fraction of receptor remains bound upon pore formation, even in the presence of detergent. Our results support a model in which pore formation is triggered by pH dependent conformational changes which is more rapid than the rate of receptor dissociation.

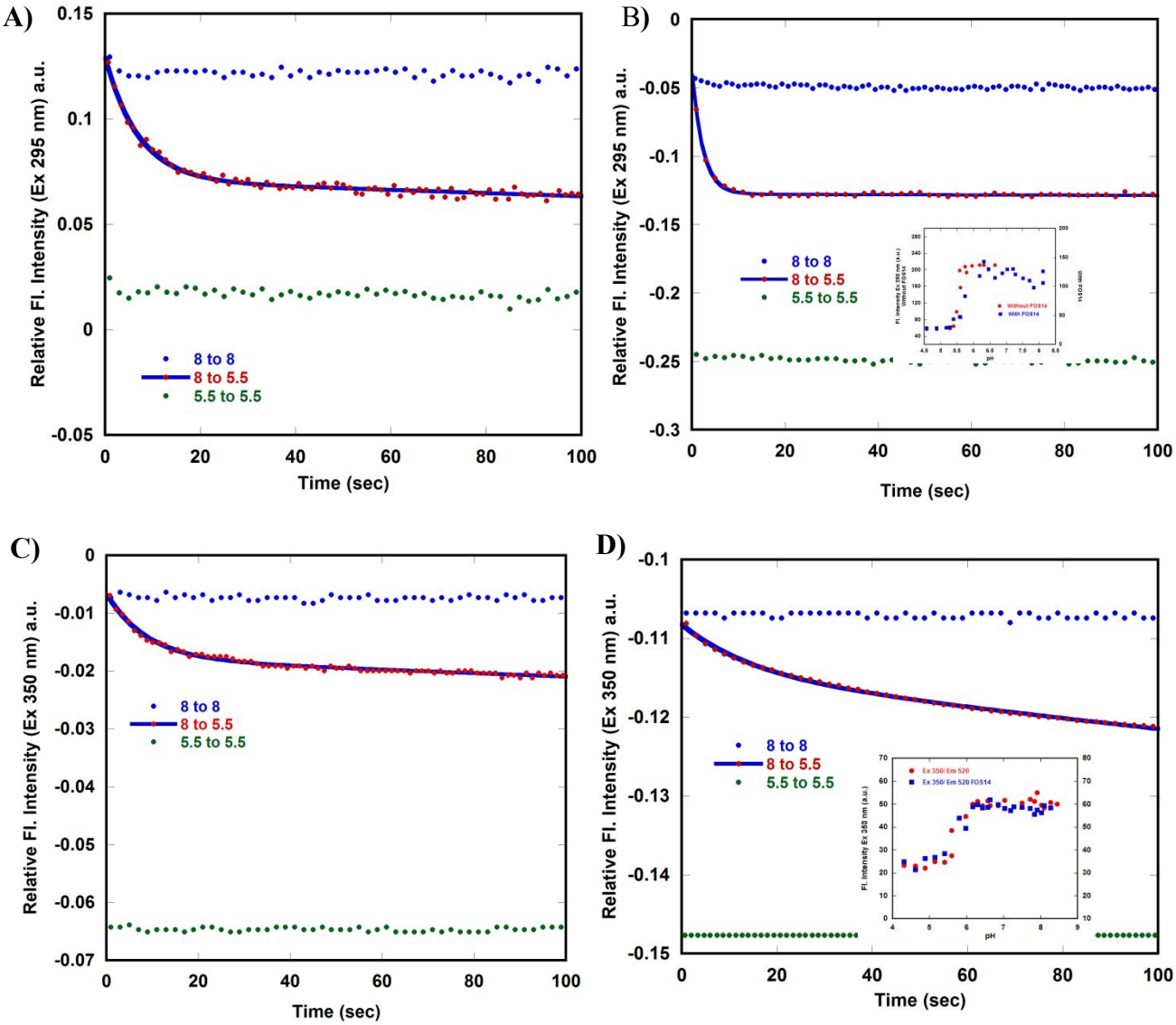

Figure 63. Fluorescence traces obtained for pH jump experiments. Monitoring kinetics for conformational change during the conversion of pre-pore to pore by exciting tryptophan in E712C A) AF350 PA_{63} bound to (4FTry) labeled NEM CMG2 (Ex 295 nm), B) Kinetics in the presence of 5mM FOS-14. C) Monitoring FRET based kinetics of receptor dissociation, AF350 $PA(63)_7$ bound to AF488 CMG2 (Ex 350 nm),1:5 ratio, at 20° C. D) Kinetics in presence of 5mM FOS14 detergent (Inset, pH titration with and without Fos 14). All measurements were carried out at 20°C in CIS buffer system supplemented with 0.1 mg/mL BSA, 1 mM $MgCl_2$ and 1 mM $CaCl_2$ on an Applied Photophysics SX-18MV Stopped flow instrument.

5.4 Conclusions

In this study, we established a FRET pair, AF350 PA_{63} and receptor AF488 CMG2. Our results showed that the fluorescence of both AF350 and AF488 were quenched at below pH 6 (63). However, when W346 is mutated to phenylalanine, we do not observe any change in the fluorescence emission at Em 440 nm but the fluorescence is decreased at Em 520 nm, suggesting receptor dissociation (loss of FRET). We also labeled the PA with monobromobiamine (mBBr), if tryptophan and mBBr are at a distance less than 18 Å, quenching of mBBr fluorescence should be reported (125). We observed the similar trend in fluorescence quenching at acidic pH. Our results are in agreement stating a large conformational change in PA in which domain IV and domain II come close together upon pore formation.

We used D425A mutant PA, to study the influence of receptor, during the pore formation. pH titration studies show that the drop in fluorescence of AF488, Em 520 along with increase in fluorescence at Em440 nm, were due to the receptor dissociation. Since receptor binds to domain II and domain IV of PA, receptor dissociation will increase the distance between donor and acceptor which results in loss of FRET signal, which was observed in D425A PA_{63} accompanied with high amplitude change in the ratio of Em520/Em440 when compared to WT and W346F PA_{63}. Binding kinetics showed that the decrease in rate of binding by lowering the pH is in agreement with receptor dissociation.

One discovery during this work was that D425A PA_{63} undergoes a structural change in the presence of detergent at the same pH ~5.5 on an overnight equilibration which was not observed in the absence of detergent. We also confirmed this by SDS-PAGE assay, clearly

showing that there might be a kinetic step which induces pore formation, but the structural evidence is still unclear.

Even in case of mBBr labeled PA we observed the same quenching (drop in mBBr fluorescence) as the pH falls below pH 7.5 and in the presence of CMG2, fluorescence drops below pH 6 indicating that the fluorescence is quenched in a distance dependent manner suggesting that the quenching mechanism is irrespective of the dye. Similar results were also observed in case of tryptophan excitation at 295 nm, made possible by eliminating the tryptophan fluorescence (in CMG2) on successful labeling with 4-F-tryptophan.

With all these evidences we propose that during the pore formation, domain II and domain IV come closer together, which is irrespective of receptor dissociation, concluded by D425A. Our kinetics data states that the rate of pore formation was six times faster than the rate of receptor dissociation which may be due to the sensitivity of β3-β4 loop in domain II to pH. In both the cases we did not observe the complete dissociation or complete pore formation, also indicates that there might be a kinetic step involved, which can achieved by longer incubation.

REFERENCES

REFERENCES

1. Bann JG (2012) Anthrax toxin protective antigen--insights into molecular switching from prepore to pore. *Protein Sci.* 21(1):1-12.

2. Spencer RC (2003) Bacillus anthracis. *J. Clin. Pathol.* 56(3):182-187.

3. Beierlein JM & Anderson AC (2011) New developments in vaccines, inhibitors of anthrax toxins, and antibiotic therapeutics for Bacillus anthracis. *Curr. Med. Chem.* 18(33):5083-5094.

4. Driks A (2009) The Bacillus anthracis spore. *Molecular aspects of medicine* 30(6):368-373.

5. Rajapaksha M, *et al.* (2012) pH effects on binding between the anthrax protective antigen and the host cellular receptor CMG2. *Protein Sci.* 21(10):1467-1480.

6. Levy H, *et al.* (2012) Differential contribution of Bacillus anthracis toxins to pathogenicity in two animal models. *Infect. Immun.* 80(8):2623-2631.

7. Turnbull PC (2002) Introduction: anthrax history, disease and ecology. *Curr. Top. Microbiol. Immunol.* 271:1-19.

8. Meselson M, *et al.* (1994) The Sverdlovsk anthrax outbreak of 1979. *Science* 266(5188):1202-1208.

9. Dixon TC, Fadl AA, Koehler TM, Swanson JA, & Hanna PC (2000) Early Bacillus anthracis-macrophage interactions: intracellular survival survival and escape. *Cell. Microbiol.* 2(6):453-463.

10. Beyer W & Turnbull PC (2009) Anthrax in animals. *Molecular aspects of medicine* 30(6):481-489.

11. Mobley JA (1995) Biological warfare in the twentieth century: lessons from the past, challenges for the future. *Mil. Med.* 160(11):547-553.

12. Christopher GW, Cieslak TJ, Pavlin JA, & Eitzen EM, Jr. (1997) Biological warfare. A historical perspective. *JAMA : the journal of the American Medical Association* 278(5):412-417.

13. Manchee RJ, Broster MG, Anderson IS, Henstridge RM, & Melling J (1983) Decontamination of Bacillus anthracis on Gruinard Island? *Nature* 303(5914):239-240.

14. Abramova FA, Grinberg LM, Yampolskaya OV, & Walker DH (1993) Pathology of inhalational anthrax in 42 cases from the Sverdlovsk outbreak of 1979. *Proceedings of the National Academy of Sciences of the United States of America* 90(6):2291-2294.

15. Christopher GW, Agan MB, Cieslak TJ, & Olson PE (2005) History of U.S. military contributions to the study of bacterial zoonoses. *Mil. Med.* 170(4 Suppl):39-48.

16. Centers for Disease C & Prevention (2002) Suspected cutaneous anthrax in a laboratory worker--Texas, 2002. *MMWR. Morbidity and mortality weekly report* 51(13):279-281.

17. Friedlander AM (1986) Macrophages are sensitive to anthrax lethal toxin through an acid-dependent process. *J. Biol. Chem.* 261(16):7123-7126.

18. Sternbach G (2003) The history of anthrax. *J. Emerg. Med.* 24(4):463-467.

19. Green BD, Battisti L, Koehler TM, Thorne CB, & Ivins BE (1985) Demonstration of a capsule plasmid in Bacillus anthracis. *Infect. Immun.* 49(2):291-297.

20. Kintzer AF*, et al.* (2009) The protective antigen component of anthrax toxin forms functional octameric complexes. *J. Mol. Biol.* 392(3):614-629.

21. Petosa C, Collier RJ, Klimpel KR, Leppla SH, & Liddington RC (1997) Crystal structure of the anthrax toxin protective antigen. *Nature* 385(6619):833-838.

22. Gao-Sheridan S, Zhang S, & Collier RJ (2003) Exchange characteristics of calcium ions bound to anthrax protective antigen. *Biochem. Biophys. Res. Commun.* 300(1):61-64.

23. Mogridge J, Mourez M, & Collier RJ (2001) Involvement of domain 3 in oligomerization by the protective antigen moiety of anthrax toxin. *J. Bacteriol.* 183(6):2111-2116.

24. Koehler TM & Collier RJ (1991) Anthrax toxin protective antigen: low-pH-induced hydrophobicity and channel formation in liposomes. *Mol. Microbiol.* 5(6):1501-1506.

25. Blaustein RO, Koehler TM, Collier RJ, & Finkelstein A (1989) Anthrax toxin: channel-forming activity of protective antigen in planar phospholipid bilayers. *Proceedings of the National Academy of Sciences of the United States of America* 86(7):2209-2213.

26. Benson EL, Huynh PD, Finkelstein A, & Collier RJ (1998) Identification of residues lining the anthrax protective antigen channel. *Biochemistry* 37(11):3941-3948.

27. Nassi S, Collier RJ, & Finkelstein A (2002) PA63 channel of anthrax toxin: an extended beta-barrel. *Biochemistry* 41(5):1445-1450.

28. Song L*, et al.* (1996) Structure of staphylococcal alpha-hemolysin, a heptameric transmembrane pore. *Science* 274(5294):1859-1866.

29. Sellman BR, Nassi S, & Collier RJ (2001) Point mutations in anthrax protective antigen that block translocation. *J. Biol. Chem.* 276(11):8371-8376.

30. Mourez M, *et al.* (2003) Mapping dominant-negative mutations of anthrax protective antigen by scanning mutagenesis. *Proceedings of the National Academy of Sciences of the United States of America* 100(24):13803-13808.

31. Mogridge J, Cunningham K, Lacy DB, Mourez M, & Collier RJ (2002) The lethal and edema factors of anthrax toxin bind only to oligomeric forms of the protective antigen. *Proceedings of the National Academy of Sciences of the United States of America* 99(10):7045-7048.

32. Varughese M, Teixeira AV, Liu S, & Leppla SH (1999) Identification of a receptor-binding region within domain 4 of the protective antigen component of anthrax toxin. *Infect. Immun.* 67(4):1860-1865.

33. Scobie HM, Rainey GJ, Bradley KA, & Young JA (2003) Human capillary morphogenesis protein 2 functions as an anthrax toxin receptor. *Proceedings of the National Academy of Sciences of the United States of America* 100(9):5170-5174.

34. Lacy DB, *et al.* (2005) A model of anthrax toxin lethal factor bound to protective antigen. *Proceedings of the National Academy of Sciences of the United States of America* 102(45):16409-16414.

35. Ribot WJ, *et al.* (2006) Anthrax lethal toxin impairs innate immune functions of alveolar macrophages and facilitates Bacillus anthracis survival. *Infect. Immun.* 74(9):5029-5034.

36. Tournier JN, *et al.* (2005) Anthrax edema toxin cooperates with lethal toxin to impair cytokine secretion during infection of dendritic cells. *J. Immunol.* 174(8):4934-4941.

37. During RL, *et al.* (2007) Anthrax lethal toxin paralyzes actin-based motility by blocking Hsp27 phosphorylation. *EMBO J.* 26(9):2240-2250.

38. During RL, *et al.* (2005) Anthrax lethal toxin paralyzes neutrophil actin-based motility. *J. Infect. Dis.* 192(5):837-845.

39. Paccani SR, *et al.* (2005) Anthrax toxins suppress T lymphocyte activation by disrupting antigen receptor signaling. *J. Exp. Med.* 201(3):325-331.

40. Fang H, Cordoba-Rodriguez R, Lankford CS, & Frucht DM (2005) Anthrax lethal toxin blocks MAPK kinase-dependent IL-2 production in CD4+ T cells. *J. Immunol.* 174(8):4966-4971.

41. Comer JE, Chopra AK, Peterson JW, & Konig R (2005) Direct inhibition of T-lymphocyte activation by anthrax toxins in vivo. *Infect. Immun.* 73(12):8275-8281.

42. Fang H, Xu L, Chen TY, Cyr JM, & Frucht DM (2006) Anthrax lethal toxin has direct and potent inhibitory effects on B cell proliferation and immunoglobulin production. *J. Immunol.* 176(10):6155-6161.

43. Shen Y, Zhukovskaya NL, Guo Q, Florian J, & Tang WJ (2005) Calcium-independent calmodulin binding and two-metal-ion catalytic mechanism of anthrax edema factor. *EMBO J.* 24(5):929-941.

44. Kumar P, Ahuja N, & Bhatnagar R (2001) Purification of anthrax edema factor from Escherichia coli and identification of residues required for binding to anthrax protective antigen. *Infect. Immun.* 69(10):6532-6536.

45. Ahuja N, Kumar P, & Bhatnagar R (2004) The adenylate cyclase toxins. *Crit. Rev. Microbiol.* 30(3):187-196.

46. Maldonado-Arocho FJ, Fulcher JA, Lee B, & Bradley KA (2006) Anthrax oedema toxin induces anthrax toxin receptor expression in monocyte-derived cells. *Mol. Microbiol.* 61(2):324-337.

47. Drum CL, Shen Y, Rice PA, Bohm A, & Tang WJ (2001) Crystallization and preliminary X-ray study of the edema factor exotoxin adenylyl cyclase domain from Bacillus anthracis in the presence of its activator, calmodulin. *Acta crystallographica. Section D, Biological crystallography* 57(Pt 12):1881-1884.

48. Bradley KA, Mogridge J, Mourez M, Collier RJ, & Young JA (2001) Identification of the cellular receptor for anthrax toxin. *Nature* 414(6860):225-229.

49. Bell SE*, et al.* (2001) Differential gene expression during capillary morphogenesis in 3D collagen matrices: regulated expression of genes involved in basement membrane matrix assembly, cell cycle progression, cellular differentiation and G-protein signaling. *J. Cell Sci.* 114(Pt 15):2755-2773.

50. Dowling O*, et al.* (2003) Mutations in capillary morphogenesis gene-2 result in the allelic disorders juvenile hyaline fibromatosis and infantile systemic hyalinosis. *Am. J. Hum. Genet.* 73(4):957-966.

51. Hanks S*, et al.* (2003) Mutations in the gene encoding capillary morphogenesis protein 2 cause juvenile hyaline fibromatosis and infantile systemic hyalinosis. *Am. J. Hum. Genet.* 73(4):791-800.

52. Whittaker CA & Hynes RO (2002) Distribution and evolution of von Willebrand/integrin A domains: widely dispersed domains with roles in cell adhesion and elsewhere. *Molecular biology of the cell* 13(10):3369-3387.

53. Lee JO, Rieu P, Arnaout MA, & Liddington R (1995) Crystal structure of the A domain from the alpha subunit of integrin CR3 (CD11b/CD18). *Cell* 80(4):631-638.

54. Shimaoka M, Takagi J, & Springer TA (2002) Conformational regulation of integrin structure and function. *Annu. Rev. Biophys. Biomol. Struct.* 31:485-516.

55. Lacy DB, Wigelsworth DJ, Scobie HM, Young JA, & Collier RJ (2004) Crystal structure of the von Willebrand factor A domain of human capillary morphogenesis protein 2: an anthrax toxin receptor. *Proceedings of the National Academy of Sciences of the United States of America* 101(17):6367-6372.

56. Hotchkiss KA, *et al.* (2005) TEM8 expression stimulates endothelial cell adhesion and migration by regulating cell-matrix interactions on collagen. *Exp. Cell Res.* 305(1):133-144.

57. Nanda A, *et al.* (2004) TEM8 interacts with the cleaved C5 domain of collagen alpha 3(VI). *Cancer Res.* 64(3):817-820.

58. Fu S, *et al.* (2010) The structure of tumor endothelial marker 8 (TEM8) extracellular domain and implications for its receptor function for recognizing anthrax toxin. *PloS one* 5(6):e11203.

59. Fish DC, Mahlandt BG, Dobbs JP, & Lincoln RE (1968) Purification and properties of in vitro-produced anthrax toxin components. *J. Bacteriol.* 95(3):907-918.

60. St Croix B, *et al.* (2000) Genes expressed in human tumor endothelium. *Science* 289(5482):1197-1202.

61. Wigelsworth DJ, *et al.* (2004) Binding stoichiometry and kinetics of the interaction of a human anthrax toxin receptor, CMG2, with protective antigen. *J. Biol. Chem.* 279(22):23349-23356.

62. Scobie HM & Young JA (2005) Interactions between anthrax toxin receptors and protective antigen. *Curr. Opin. Microbiol.* 8(1):106-112.

63. Lacy DB, Wigelsworth DJ, Melnyk RA, Harrison SC, & Collier RJ (2004) Structure of heptameric protective antigen bound to an anthrax toxin receptor: a role for receptor in pH-dependent pore formation. *Proceedings of the National Academy of Sciences of the United States of America* 101(36):13147-13151.

64. Rainey GJ, *et al.* (2005) Receptor-specific requirements for anthrax toxin delivery into cells. *Proceedings of the National Academy of Sciences of the United States of America* 102(37):13278-13283.

65. Young JA & Collier RJ (2007) Anthrax toxin: receptor binding, internalization, pore formation, and translocation. *Annu. Rev. Biochem.* 76:243-265.

66. Santelli E, Bankston LA, Leppla SH, & Liddington RC (2004) Crystal structure of a complex between anthrax toxin and its host cell receptor. *Nature* 430(7002):905-908.

67. Pellizzari R, Guidi-Rontani C, Vitale G, Mock M, & Montecucco C (2000) Lethal factor of Bacillus anthracis cleaves the N-terminus of MAPKKs: analysis of the intracellular consequences in macrophages. *Int. J. Med. Microbiol.* 290(4-5):421-427.

68. Lehmann M, Noack D, Wood M, Perego M, & Knaus UG (2009) Lung epithelial injury by B. anthracis lethal toxin is caused by MKK-dependent loss of cytoskeletal integrity. *PloS one* 4(3):e4755.

69. Scobie HM*, et al.* (2006) Anthrax toxin receptor 2-dependent lethal toxin killing in vivo. *PLoS Pathog* 2(10):e111.

70. Williams AS, Lovell S, Anbanandam A, El-Chami R, & Bann JG (2009) Domain 4 of the anthrax protective antigen maintains structure and binding to the host receptor CMG2 at low pH. *Protein Sci.* 18(11):2277-2286.

71. Chitlaru T, Altboum Z, Reuveny S, & Shafferman A (2011) Progress and novel strategies in vaccine development and treatment of anthrax. *Immunol. Rev.* 239(1):221-236.

72. Klimpel KR, Molloy SS, Thomas G, & Leppla SH (1992) Anthrax toxin protective antigen is activated by a cell surface protease with the sequence specificity and catalytic properties of furin. *Proceedings of the National Academy of Sciences of the United States of America* 89(21):10277-10281.

73. Gordon VM, Klimpel KR, Arora N, Henderson MA, & Leppla SH (1995) Proteolytic activation of bacterial toxins by eukaryotic cells is performed by furin and by additional cellular proteases. *Infect. Immun.* 63(1):82-87.

74. Beauregard KE, Collier RJ, & Swanson JA (2000) Proteolytic activation of receptor-bound anthrax protective antigen on macrophages promotes its internalization. *Cell. Microbiol.* 2(3):251-258.

75. Christensen KA, Krantz BA, Melnyk RA, & Collier RJ (2005) Interaction of the 20 kDa and 63 kDa fragments of anthrax protective antigen: kinetics and thermodynamics. *Biochemistry* 44(3):1047-1053.

76. Abrami L, Liu S, Cosson P, Leppla SH, & van der Goot FG (2003) Anthrax toxin triggers endocytosis of its receptor via a lipid raft-mediated clathrin-dependent process. *J. Cell Biol.* 160(3):321-328.

77. Abrami L, Leppla SH, & van der Goot FG (2006) Receptor palmitoylation and ubiquitination regulate anthrax toxin endocytosis. *J. Cell Biol.* 172(2):309-320.

78. Abrami L, Bischofberger M, Kunz B, Groux R, & van der Goot FG (2010) Endocytosis of the anthrax toxin is mediated by clathrin, actin and unconventional adaptors. *PLoS Pathog* 6(3):e1000792.

79. Kochi SK, Martin I, Schiavo G, Mock M, & Cabiaux V (1994) The effects of pH on the interaction of anthrax toxin lethal and edema factors with phospholipid vesicles. *Biochemistry* 33(9):2604-2609.

80. Wei W, Lu Q, Chaudry GJ, Leppla SH, & Cohen SN (2006) The LDL receptor-related protein LRP6 mediates internalization and lethality of anthrax toxin. *Cell* 124(6):1141-1154.

81. Ryan PL & Young JA (2008) Evidence against a human cell-specific role for LRP6 in anthrax toxin entry. *PloS one* 3(3):e1817.

82. Liddington R, Pannifer A, Hanna P, Leppla S, & Collier RJ (1999) Crystallographic studies of the anthrax lethal toxin. *J. Appl. Microbiol.* 87(2):282.

83. Krantz BA, Finkelstein A, & Collier RJ (2006) Protein translocation through the anthrax toxin transmembrane pore is driven by a proton gradient. *J. Mol. Biol.* 355(5):968-979.

84. Krantz BA, *et al.* (2005) A phenylalanine clamp catalyzes protein translocation through the anthrax toxin pore. *Science* 309(5735):777-781.

85. Miller CJ, Elliott JL, & Collier RJ (1999) Anthrax protective antigen: prepore-to-pore conversion. *Biochemistry* 38(32):10432-10441.

86. Wimalasena DS, *et al.* (2007) Effect of 2-fluorohistidine labeling of the anthrax protective antigen on stability, pore formation, and translocation. *Biochemistry* 46(51):14928-14936.

87. Krantz BA, Trivedi AD, Cunningham K, Christensen KA, & Collier RJ (2004) Acid-induced unfolding of the amino-terminal domains of the lethal and edema factors of anthrax toxin. *J. Mol. Biol.* 344(3):739-756.

88. Vernier G, *et al.* (2009) Solubilization and characterization of the anthrax toxin pore in detergent micelles. *Protein Sci.* 18(9):1882-1895.

89. Katayama H, *et al.* (2008) GroEL as a molecular scaffold for structural analysis of the anthrax toxin pore. *Nat. Struct. Mol. Biol.* 15(7):754-760.

90. Katayama H, *et al.* (2010) Three-dimensional structure of the anthrax toxin pore inserted into lipid nanodiscs and lipid vesicles. *Proceedings of the National Academy of Sciences of the United States of America* 107(8):3453-3457.

91. Sun J, Lang AE, Aktories K, & Collier RJ (2008) Phenylalanine-427 of anthrax protective antigen functions in both pore formation and protein translocation. *Proceedings of the National Academy of Sciences of the United States of America* 105(11):4346-4351.

92. Milne JC, Furlong D, Hanna PC, Wall JS, & Collier RJ (1994) Anthrax protective antigen forms oligomers during intoxication of mammalian cells. *J. Biol. Chem.* 269(32):20607-20612.

93. Gordon VM, Leppla SH, & Hewlett EL (1988) Inhibitors of receptor-mediated endocytosis block the entry of Bacillus anthracis adenylate cyclase toxin but not that of Bordetella pertussis adenylate cyclase toxin. *Infect. Immun.* 56(5):1066-1069.

94. Nguyen TL (2004) Three-dimensional model of the pore form of anthrax protective antigen. Structure and biological implications. *J. Biomol. Struct. Dyn.* 22(3):253-265.

95. Wimalasena DS, *et al.* (2010) Evidence that histidine protonation of receptor-bound anthrax protective antigen is a trigger for pore formation. *Biochemistry* 49(33):6973-6983.

96. Rajapaksha M, *et al.* (2009) Monitoring anthrax toxin receptor dissociation from the protective antigen by NMR. *Protein Sci.* 18(1):17-23.

97. Pilpa RM, Bayrhuber M, Marlett JM, Riek R, & Young JA (2011) A receptor-based switch that regulates anthrax toxin pore formation. *PLoS Pathog* 7(12):e1002354.

98. Gao M & Schulten K (2006) Onset of anthrax toxin pore formation. *Biophys. J.* 90(9):3267-3279.

99. Collier RJ & Young JA (2003) Anthrax toxin. *Annu. Rev. Cell. Dev. Biol.* 19:45-70.

100. Wesche J, Elliott JL, Falnes PO, Olsnes S, & Collier RJ (1998) Characterization of membrane translocation by anthrax protective antigen. *Biochemistry* 37(45):15737-15746.

101. Wynia-Smith SL, Brown MJ, Chirichella G, Kemalyan G, & Krantz BA (2012) Electrostatic ratchet in the protective antigen channel promotes anthrax toxin translocation. *J. Biol. Chem.* 287(52):43753-43764.

102. Feld GK, *et al.* (2010) Structural basis for the unfolding of anthrax lethal factor by protective antigen oligomers. *Nat. Struct. Mol. Biol.* 17(11):1383-1390.

103. Ezzell JW, Jr. & Abshire TG (1992) Serum protease cleavage of Bacillus anthracis protective antigen. *Journal of general microbiology* 138(3):543-549.

104. Arora N & Leppla SH (1993) Residues 1-254 of anthrax toxin lethal factor are sufficient to cause cellular uptake of fused polypeptides. *J. Biol. Chem.* 268(5):3334-3341.

105. Chen B, Cao H, Yan P, Mayer MU, & Squier TC (2007) Identification of an orthogonal peptide binding motif for biarsenical multiuse affinity probes. *Bioconjug Chem* 18(4):1259-1265.

106. Cao H, *et al.* (2007) A red cy3-based biarsenical fluorescent probe targeted to a complementary binding peptide. *J. Am. Chem. Soc.* 129(28):8672-8673.

107. Kapanidis AN, Ebright YW, & Ebright RH (2001) Site-specific incorporation of fluorescent probes into protein: hexahistidine-tag-mediated fluorescent labeling with (Ni(2+):nitrilotriacetic Acid (n)-fluorochrome conjugates. *J. Am. Chem. Soc.* 123(48):12123-12125.

108. Gaietta G, *et al.* (2002) Multicolor and electron microscopic imaging of connexin trafficking. *Science* 296(5567):503-507.

109. Klein DC, *et al.* (1976) 2-Fluoro-L-histidine, an inhibitor of enzyme induction. *Mol. Pharmacol.* 12(5):720-730.

110. Thomas CA, Talaty ER, & Bann JG (2009) 3S-fluoroproline as a probe to monitor proline isomerization during protein folding by 19F-NMR. *Chemical communications* (23):3366-3368.

111. Hott JL & Borkman RF (1989) The non-fluorescence of 4-fluorotryptophan. *Biochem. J.* 264(1):297-299.

112. Bronskill PM & Wong JT (1988) Suppression of fluorescence of tryptophan residues in proteins by replacement with 4-fluorotryptophan. *Biochem. J.* 249(1):305-308.

113. Kirsch JF (1973) Mechanism of enzyme action. *Annu. Rev. Biochem.* 42:205-234.

114. Frieden C, Hoeltzli SD, & Bann JG (2004) The preparation of 19F-labeled proteins for NMR studies. *Methods Enzymol.* 380:400-415.

115. Bann JG, Pinkner J, Hultgren SJ, & Frieden C (2002) Real-time and equilibrium (19)F-NMR studies reveal the role of domain-domain interactions in the folding of the chaperone PapD. *Proceedings of the National Academy of Sciences of the United States of America* 99(2):709-714.

116. Eichler JF, Cramer JC, Kirk KL, & Bann JG (2005) Biosynthetic incorporation of fluorohistidine into proteins in E. coli: a new probe of macromolecular structure. *ChemBioChem* 6(12):2170-2173.

117. Hu L, *et al.* (2012) Comparison of the structural stability and dynamic properties of recombinant anthrax protective antigen and its 2-fluorohistidine-labeled analogue. *J. Pharm. Sci.* 101(11):4118-4128.

118. Martchenko M, Jeong SY, & Cohen SN (2010) Heterodimeric integrin complexes containing beta1-integrin promote internalization and lethality of anthrax toxin. *Proceedings of the National Academy of Sciences of the United States of America* 107(35):15583-15588.

119. Bradley KA, *et al.* (2003) Binding of anthrax toxin to its receptor is similar to alpha integrin-ligand interactions. *J. Biol. Chem.* 278(49):49342-49347.

120. Scobie HM, *et al.* (2005) A soluble receptor decoy protects rats against anthrax lethal toxin challenge. *J. Infect. Dis.* 192(6):1047-1051.

121. Scobie HM, *et al.* (2007) Anthrax toxin receptor 2 determinants that dictate the pH threshold of toxin pore formation. *PloS one* 2(3):e329.

122. Patterson GH, Piston DW, & Barisas BG (2000) Forster distances between green fluorescent protein pairs. *Anal. Biochem.* 284(2):438-440.

123. Panchuk-Voloshina N, *et al.* (1999) Alexa dyes, a series of new fluorescent dyes that yield exceptionally bright, photostable conjugates. *The journal of histochemistry and cytochemistry : official journal of the Histochemistry Society* 47(9):1179-1188.

124. Janowiak BE, Finkelstein A, & Collier RJ (2009) An approach to characterizing single-subunit mutations in multimeric prepores and pores of anthrax protective antigen. *Protein Sci.* 18(2):348-358.

125. Mansoor SE & Farrens DL (2004) High-throughput protein structural analysis using site-directed fluorescence labeling and the bimane derivative (2-pyridyl)dithiobimane. *Biochemistry* 43(29):9426-9438.

126. Minks C, Huber R, Moroder L, & Budisa N (1999) Atomic mutations at the single tryptophan residue of human recombinant annexin V: effects on structure, stability, and activity. *Biochemistry* 38(33):10649-10659.

APPENDIXES

APPENDIX A

PROCEDURES IN MOLECULAR BIOLOGY

A.1 Competent cell preparation

An isolated single colony of a desired bacterial strain was inoculated in to 5 mL of LB taken in a Falcon culture tube, was allowed to incubate at 37°C overnight equipped with continuous shaking. Cells were diluted 1:100 in 100 ml LB and were grown up to an OD 600 of 0.4-0.7. Cells were centrifuged at 3800 rpm at 4°C, resuspended the cell pellet in 10 mL of ice cold and sterile 0.1M CaCl2. The cells were left on ice for a period of 30 minutes, second centrifugation was done after 30 minutes at 4°C, resuspended the cells in 2 mL ice cold 0.1 M CaCl2. Storing the cells as bacterial stock involves the re suspension of the cell pellet in 500 µl of 85% CaCl2/15% glycerol (v/v), prepared 100 mL aliquots in to sterile Eppendorf tubes, quick freeze in liquid N2 and stored at -80°Cfor future use.

A.2 Transformation into XL-10 Gold and UTH 780 cells

Frozen cell aliquots stored at -80°C were thawed on ice for about 5-10 min. About 400 µl of ice cold sterile 0.1M CaCl2 was added to the cells. The cells were separated in to 100 mL aliquots in to pre chilled falcon culture tubes. Plasmids of concentration 50 ng were added to the tubes. No plasmid DNA was added to the control and tubes were allowed to stay on ice for about 30 min. Heat shock the cells for 45 seconds at 42°C by holding the tubes in a water bath and then placed on ice bucket for 2 min followed by the addition of 250 µl of LB to each tube. Incubated the tubes for 1 h at 37°C with continuous shaking and then 200 µl aliquots were plated on the plates with required antibiotic and incubated at 37°C overnight in an inverted position.

APPENDIX A (continued)

A.3 Plasmid construction

A.3.1 PA_{83}

UTH 780- Histidine auxotroph was obtained from *E.Coli* genetic stock at Yale University (New Heaven Ct). The protective antigen gene in pET22b(+) which is under T7 promoter was moved to the plasmid PQE80 (Qiagen) by removing the EcoR1 site in the protective antigen gene using the Quick-change mutagenesis kit (Stratagene) with primers (5_-GCAGGATTTAGTAATTCG**AAC**TCAAGTACGGTCGC-3_ and 5_-GCGACCGTACTTGAGTTCGAATTACTAAATCCTGC-3_ (Sigma Genosys) that directed a silent change from G*AAT*TC (*AAT = Asn*) to G*AAC*TC (*AAC = Asn*). PCR was then used to clone the full-length PA_{83} gene (including the phoA signal sequence from pET22b (+)) as an EcoR1/KpnI fragment into pQE80 (forward primer, 5_ CCCGAATTCATTAAAGAGGAGAAATTAACTATGAAATACCTGCTGCCGAC C-3_; reverse primer, 5_ GGGGGTACCTCAGCTAATTATCCTATCTCATAG-3_).

A.3.2 GST- CMG2

PGEX4T-1 (Amersham Biosciences) places a thrombin cleavable site glutathione s-transferase in the aninoterminus of the expressed protein using Bam H1 and 3 Not 1 restriction sites, was cloned with a DNA sequence of 35-225 residues of CMG2 VWA domain. Transformation of these plasmids in to E.Coli strains of either UTH780 Histidine auxotroph or BL21. Truncated version of CMG2 often called as R40C CMG2 ranging from residues 38-218

was generated using Bam H1 and Not 1sites through PCR. Labeling of CMG2 with AF488 requires the presence of a cysteine residue in the more exposed aninoterminus region of CMG2. This was achieved by the mutation of R40 to cysteine. Successive site directed mutations carried out to mutate C17; a buried cysteine to alanine resulted in the elimination of a natural disulfide bond in CMG2.

A.3.3 Site directed mutagenesis of PA_{83}/CMG2

Oligonucleotide primers obtained from SIGMA Genosys and Quick change site directed mutagenesis kit from Stratagene, La Jolla CA were used in the mutations of H211Q, H253Q, H263Q, H299Q, H304310Q, H336Q/F, H597Q, H616Q, H299QH336F, E712C, W346F, and E712CW346F in PA. Key mutation in PA, D425A was made using the primers, forward 5' CGCCAATCGCATTAAATGCACAAGCGGATTTCAGTTCTACTCC 3'and reverse 5' GGAGTAGAACTGAAATCCGCTTGTGCATTTAATGCGATTGGCG 3'. R40 mutation in CMG2 resulted in attaining a solvent exposed cysteine in the protein. E712 mutation to cysteine leads to the formation of a single cysteine residue in domain IV. Oligo nucleotide primers for the mutation D50A in CMG2 were obtained from SIGMA Genosys. Forward and reverse primers were of the sequences 5'CTACTTCGTCCTGGCCAAGTCTGGGAGTG 3' and 5'CACTCCCCAGACTTGGCCAGGACGAAGTAG 3'. PNACL (Protein and Nucleic Acid Chemistry Laboratory) at Washington University St. Louis, MO verified all the sequences obtained after mutagenesis.

APPENDIX B

PROTEIN EXPRESSION AND PURIFICATION

B.1 Growth of Bacterial cultures

A single colony from a freshly streaked plate is used to grow bacterial cultures. 5 mL of LB media having 5 µl of required antibiotic (100mg/ mL) was inoculated with single isolated colony and is incubated at 37°Cwith continuous stirring for about 6-8 hours. The growth was continued by inoculating 1:1000 dilution of the 5 mL culture to a 100 mL culture added with 100 µl of desired antibiotic and incubating it at 37°Covernight. Later growth of cells was still enhanced by inoculating the 100 mL cultures in to 600 mL cultures and protein expression was induced using IPTG (Isopropyl β-D-1-thio galactopyranoside).

Regular protein expressions of PA/CMG2/D4 were carried out in 600 mL cultures of ECPM1 media accompanied with desired antibiotic and CaCl2/MgCl2 solution. This involved the growth of cells at 32°Cfor PA, 37°Cfor CMG2 and up to an OD600 of 3.0. Protein expression in the cultures was then induced by adding 1mM IPTG and incubating at 26°C for PA or at 37°C for CMG2 and D4 with continuous shaking until the OD600 was doubled. The cells were then centrifuged in a swinging bucket rotor (3000g) centrifuge for 10 min at 4°C. PA proteins were immediately subjected to periplasm isolation whereas CMG2 and D4 cells were frozen at -20°C for further purification.

B.2 PA Labeling with 2-F-Histidine

Reformed or altered version of ECPM1 media is used to grow UTH780 cells with calculated amounts of amino acids and glucose instead of yeast extract, glycerol and NZ amine.

APPENDIX B (continued)

For PA the cells were grown in Fern Bach shaker flasks. Cells were grown up to an OD600 of 3. 0.9% NaCl solution was used to wash the cells prior to the suspension in the same media containing 2-F histidine instead of Histidine. Cells were incubated at a reduced temperature of 26°Cfor PA, and then were induced with 1mM IPTG followed by incubation with continuous shaking until the OD600 is doubled. Doubling of OD600 was followed by harvesting the cells by spinning them in a swinging rotor bucket centrifuge (3000g) for 10 min at 4°C. PA proteins were immediately preceded to periplasmic isolation.

B.3 CMG2 Labeling with 4-F-Tryptophan

Reformed or altered version of ECPM1 media is used to grow DL41 cells with calculated amounts of amino acids and glucose instead of yeast extract, glycerol and NZ amines. CMG-2 cells were grown in Fern Bach shaker flasks. Cells were grown up to an OD600 of 2. 0.9% NaCl solution was used to wash the cells prior to the suspension in the same media containing 4-F tryptophan instead of Tryptophan. Cells were incubated at a reduced temperature of 32°C, and then were induced with 1mM IPTG followed by incubation with continuous shaking until the OD600 is doubled. Doubling of OD600 was followed by harvesting the cells by spinning them in a swinging rotor bucket centrifuge (3000g) for 10 min at 4°C. Cells were frozen at -20°C.

APPENDIX B (continued)

B.4 Protein purification

B.4.1 PA_{83} Isolation and purification

Cells were spun in centrifuge equipped with swinging rotor bucket (3000g) for 10 min at 4°C, supernatant was discarded and the cell pellet was resuspended in buffer 1 made out of 20:20 solution (20 mM Tris HCl, pH 8.0 and 20% sucrose solution), with 1mM EDTA. The pellet was allowed to stir gently for 15 min at room temperature followed by centrifugation (8000g) at 4°C for 15 min. The supernatant was discarded; cell pellet was resuspended in ice cold 5mM MgSO4 solution and is stirred for 15 min at 4°C. Next 20 mL of 1 M Tris HCl pH-8.0 was added to the solution to attain 20mM final concentration. DTT was added to 1mM final concentration if an additional cysteine residue was added by mutagenesis. Cells were centrifuged (8000g) at 4°Cfor 15min. The supernatant is called the isolated periplasm was retained and filtered through a Millipore 200 μm under suction and was loaded on to a Hi-Trap Q anion exchange column (GE Health care). The column was equilibrated with 50 mL of 20 mM Tris HCl pH-8.0 (buffer A), 50 mL of 20 mM Tris HCl pH-8.0 added with 1M NaCl (buffer B) followed by buffer A again at 4°C. A salt gradient of 30 % buffer B was used to elute the protein in an Akta Prime LC system.

Protein elution started at 15% buffer B these fractions were characterized by SDS-PAGE analysis. Fractions containing PA protein were pooled and concentrated to 2 mL using a 10 kDa Amicon Ultra-15 cutoff centrifugal filter (Millipore), applied to a Sephadex-200 gel filtration column (GE Healthcare) which purifies the protein based of the molecular size. 20 mM Tris HCl

pH 8.0/150 mM NaCl is used to equilibrate the column at 4°C. A most noticeable peak at 65-80 minutes elution time was observed which corresponds to PA_{83}. An electrophoretically pure protein of molecular weight 83 kDa was obtained which was concentrated and aliquated and stored at -20°C.

A slight modification to this general protocol was made for the purification of cysteine mutants. Buffers used for the purification were supplemented with 1mM final concentration of Dithiothreitol (DTT) making 20 mM Tris HCl pH-8.0/1 mM DTT as buffer A and 20 mM Tris HCl pH-8.0/1M NaCl/1 mM DTT as buffer B. DTT is known to prevent the oxidation of cysteine residues in protein. The mutant protein was purified by Q anion exchange chromatography using buffer A, B. When purified with Superdex-200 Gel filtration column the protein is buffered using 20 mM Tris HCl/150 mM NaCl/1 mM DTT. Protein concentrations were obtained by using Beer-Lamberts Law using calculated extinction coefficient of 80220 M^{-1} cm^{-1} for PA_{83}. Fractions were concentrated and were frozen at -20°C.

B.4.2 Isolation and Purification of CMG2

Frozen cells of CMG2 from -20°Cfreezer were thawed on ice for about 1 hour followed by resuspension of the cell pellet in 30 mL of Phosphate Buffered Saline (PBS), pH-7.4 (30 mL of PBS approximately for 2.5 liters of media). Resuspended cell pellet was stirred at 4°C for 15 min. cells were lysed using sonicator (Branson) for about 5 min. The cells were then centrifuged at 15000g for 45 min at 4°C. A second centrifugation was done to the supernatant that was

transferred into fresh tubes to ensure easy filtration. The supernatant was then filtered through a Millipore 200μm filter under vacuum and was loaded on to Glutathione-Sepharose (Hi-Trap GST) HP column (GE Health care) with the required flow rate. Prior equilibration of GST columns was necessary. Two column volumes of 6 M guanidine hydrochloride is used for washing the columns which is followed by washing with 5 column volumes of PBS buffer. Reduced glutathione was made up to 10mM final concentration in 20 mM Tris pH-8.0 and is passed through the column for washing. Final washing was done using 5 column volumes of PBS.

Thrombin (80 Units/mL) was used for the elution of protein by cleaving the CMG2 and the Glutathione tag attached. A 500 μL of PBS was used to dissolve thrombin. 400 μL of this was diluted with 4.6 mL of PBS to make it up to a final volume of 5 mL. The column was injected with this 5 mL diluted thrombin and is incubated at room temperature for 16 h.

A pre equilibrated benzamidine column was connected to the GST column and was eluted with PBS to attain pure CMG2 as the GST tag was trapped by benzamidine column. The CMG2 fractions were pooled, concentrated and the protein was stored at -20°C.

An additional purification by size exclusion chromatography was attempted for E712C. As indicated by SDS-PAGE analysis CMG2 was obtained electrophoretically pure making this method of purification effective and common to all types of CMG2 purifications including ^{13}C CMG2, ^{13}C 2F-His CMG2, R40C CMG2 and WTCMG2. A calculated extinction coefficient of

12950 M^{-1} cm^{-1} for CMG2 was used in the calculation of protein concentration by the Beer-Lambert Law

A slight modification for R40C CMG2 made was after elution; the protein was concentrated and added with 10 fold excess of TCEP prior to the storage at 4°C. TCEP is known to protect the free thiol group.

B.4.3 Formation of pre-pore; Trypsin cleavage

A heptameric structure often referred to as Pre-pore $(PA63)_7$ – a functional unit of anthrax toxin was obtained in vitro by Trypsin (Trypzean, Sigma-Aldrich) cleavage. The ratio of the concentrations was 1µg of trypsin to 1 mg of PA_{83}. The prescribed concentration of trypsin was added to PA_{83} and is incubated at room temperature for 30 min. Further action of trypsin was inhibited by adding 10 fold excess of soybean trypsin inhibitor and allowed to stand at room temperature for 15 min. Trypsin charged PA was then loaded on to a Hi-Trap Q column which was pre-equilibrated with 20 mM Tris pH-8.5/1 mM $CaCl_2$ as buffer A and 20 mM Tris pH-8.5/1M NaCl/1 mM $CaCl_2$ as buffer B. Heptamer was eluted using a gradient of 50% buffer B over 120 mL volume.

Final purification involves Sephadex-200 gel filtration chromatography (GE Health care) equilibrated with 20 mM Tris-HCl/400 mM NaCl/1mM CaCl2 pH 8.5 eluting the most prominent peak. Fractions were collected and concentrated based on the UV-absorption. Approximately 3 mg of $(PA_{63})_7$ was obtained when 5 mg of PA_{83} was digested. Variations in the yields of protein were observed for 2-FHis labeled PA_{63} and WT. Reduced yield was observed in

case of labeled proteins compared to WT. Some mutations greatly affected the yield of the heptamer showing significant alterations to the structure or the function of the protein.

B.4.4 Determination of protein concentrations

Isolated pure protein was used for the calculation of concentration of the protein using UV-Visible spectrum based on the following Beer-Lamberts law $A = \varepsilon * c * l$

Where A= Absorbance of protein at 280 nm, ε= Molar extinction co efficient of protein

l= path length of the cuvette used for measurement

From the above relationship the concentration is calculated using the formula

$c = A / \varepsilon$ i.e., absorbance at 280 nm/Molar extinction coefficient

Path length of the cuvette used was always 1 cm. Molar extinction co efficient for all the proteins were pre-defined. Using the above relation and calculated values of extinction coefficients protein concentrations are calculated.

B.4.5 Expression and purification of LF_N

Fused lethal factor (N-terminal domain, LFn) with glutathione S-transferase (GST) was expressed in E. Coli strain BL21 DE3 and purified by affinity chromatography on a GST column followed by anion-exchange and size-exclusion chromatography. Yield more than 90% was observed.

APPENDIX C

BACTERIAL E.coli GROWTH MEDIA FOR PROTEIN EXPRESSION

C.1 LB media (Luria-Bertani medium)

20 g of LB (Fischer) were dissolved in 1 liter Millipore water and is allowed to stir at room temperature until LB is completely dissolved in water. Medium was distributed in to 200 mL portions and was autoclaved for 30-45 min. It can be stored at room temperature for several months if handled without contamination.

C.2 ECPM1 media

Table 9

	Ingredient	1.0L	5.0L
1	K_2HPO_4	4 g	20 g
2	KH_2PO_4	1 g	5 g
3	NH_4Cl	1 g	5 g
4	K_2SO_4	2.4 g	12 g
5	Trace element solution	10 mL	50 mL
6	Casamino acids	20 g	100 g
7	Yeast extract	3 g	15 g
8	Glycerol	40g	200g

APPENDIX C (continued)

Calculated quantities of the ingredients were added to Millipore water and was adjusted to the required volume either (either 1.0L or 5.0L). A precipitate will be formed while addition but goes in to the solution with continuous stirring. The media was then autoclaved for 30-45 minutes and let to cool. 2.0 mL (if 1.0 L media was prepared) and 10 mL (if 5.0 L media was prepared) of 1 M $MgCl_2 \cdot 6H_2O$ (VWR# MK595804)/0.45 M $CaCl_2 \cdot 2H_2O$ SIGMA# C-7902 (sterilized by autoclaving) was added prior to usage. Once media prepared can be stored for 10 days at 4°C.

C.3 Trace element solution

5 g EDTA (Mallinckrodt 5958- VWR# MK595804)

0.5 g $FeCl_3 \cdot 6H_2O$ (SIGMA# F-1513)

0.5 g $FeCl_3 \cdot 6H_2O$ (SIGMA# F-1513)

0.01 g $CuCl_2 \cdot 2H_2O$ (SIGMA# 307 483-100G)

0.01 g Co $(NO_3)_2 \cdot 6H_2O$ NOTE: Oxidizer Shelf (SIGMA# C-2769)

0.01 g $(NH_4)_6Mo_7O_{24} \cdot 4H_2O$ (SIGMA# A-7302)

EDTA was first dissolved in 700 mL water. Each element is dissolved separately to the EDTA solution. 10 N HCl was added to bring all the ingredients in to the solution. Made it up to 1 L and the pH is adjusted to 7.0 using concentrated NaOH. Autoclaved and stored in dark at 4°C.

APPENDIX C (continued)

C.4 Minimal media

Medium was prepared in two parts. Ingredients 1 to 26 constitution part A (800 mL for 1.0 L and 4.5 L for 5.0 L of medium) were mixed in Millipore water and autoclaved for 30-45 min. and allowed to cool down to room temperature. Ingredients 27 to 33 (part B) (200 mL for 1.0 L and 500 mL for 5.0 L of medium) were mixed separately and dissolved completely adjusted to the final volume and sterifiltered. Prior to growth the two parts were mixed and were distributed to appropriate volumes in the flasks, incubated at required temperatures. Histidine was added to get a final concentration of 0.2 g/l which is used for first part of labeling. 2-FHistidine was added up to a final concentration of 0.2 g/l and was used for second part of labeling after washing with 0.9% NaCl. Tryptophan and 4-Ftryptophan were used instead of Histidine and 2-FHistdine when labeling a tryptophan residue.

Table 10

	Ingredient	Molecular weight	Conc.	1.0L	5.0L
1	Alanine	89.100	5.612	0.5	2.5
2	Arginine	210.70	2.296	0.5	2.5
3	Aspartic acid	133.10	3.005	0.4	2.0
4	Cysteine	240.30	0.208	0.05	0.25

Table 10 (continued)

	Ingredient	Molecular weight	Conc.	1.0L	5.0L
5	Glutamine	146.10	2.738	0.4	2.0
6	Glutamic acid	147.10	4.419	0.65	3.25
7	Glycine	75.070	7.326	0.55	2.75
8	Isoleucine	131.20	1.753	0.23	1.15
9	Leucine	131.20	1.753	0.23	1.15
10	Lysine Hydrochloride	146.20	2.873	0.42	2.1
11	Methionine	149.20	1.676	0.25	1.25
12	Phenyl alanine	165.20	0.800	0.13	0.65
13	Proline	115.10	0.869	0.10	0.5
14	Serine	105.10	19.981	2.1	10.5
15	Threonine	119.10	1.931	0.23	1.15
16	Tyrosine	181.20	0.938	0.17	0.85
17	Valine	117.10	1.964	0.23	1.15
18	Adenine	135.10	3.701	0.5	2.5
19	Guanosine	283.20	2.295	0.65	3.25

Table 10 (continued)

	Ingredient	Molecular weight	Conc.	1.0L	5.0L
20	Thymine	126.10	1.586	0.2	1.0
21	Uracil	112.10	4.460	0.5	2.5
22	Cytosine	111.10	1.800	0.2	1.0
23	NH_4Cl	53.490	9.348	1.0	5.0
24	K_2HPO_4	174.20	60.276	4.0	20
25	KH_2PO_4	136.09		1.0	5
26	K_2SO_4	174.26		2.4	12
27	Glucose	180.20		5.0	25
28	Trace element solution			10 mL	50 mL
29	1M $MgCl_2$/0.45M $CaCl_2$ solution			2 mL	10 mL
30	Thiamine	337.30	0.148	0.05	0.25
31	Niacin	123.10	0.406	0.05	0.25
32	Biotin	244.30	0.004	0.001	0.005
33	Tryptophan	204.20	0.245	0.05	0.25
34	4-FTryptophan	222.22	0.200	0.045	0.22

Table 10 (continued)

	Ingredient	Molecular weight	Conc.	1.0L	5.0L
35	Histidine	165.00	0.200	0.03	0.155
36	2-FHistidine	173.00		0.035	0.175

APPENDIX D

PREPARATION OF BUFFERS AND REAGENT

D.1 1M Tris stock solution

Dissolve 121.1g of Tris (base) in 800 ml of MQ water and adjust the pH to 8 by adding 6cN HCl. The final volume was then adjusted to 1liter. The buffer was sterile filtered through a 0.22um Millipore filter and stored at room temperature.

D.2 20 mM Tris-HCl pH 8

A 20 mL of 1M stock solution of Tris pH 8 was diluted into 1 liter of Milli-Q water, sterile filtered using a 0.22 um filter and stored at 4°C.

D.3 20mM Tris-HCl, 1M NaCl pH8

A 20 mL of 1M stock solution of Tris pH 8 was diluted into 900 mL of Milli-Q water and 58.4 g of NaCl added and mixed well. Then the volume was adjusted to 1liter. The buffer was passed through a 0.22 um filter and stored at 4°C.

D.4 20mM Tris-HCl, 0.15M NaCl pH8

A 20 mL of 1M stock solution of Tris pH8 was diluted into 900 mL of Milli-Q water and 8.8 g of NaCl was added and mixed well. Then the volume was adjusted to 1liter. The buffer was passed through a 0.22 um filter and stored at 4°C.

D-5 20 mM Tris-HCl, 1mM $CaCl_2$ pH 8.5

A stock solution of 1M Tris/HCl pH 8.5 was made as described previously. 20 mL of the stock was diluted to 900 mL of Milli-Q water and 147mg of $CaCl_2$ was added and mixed well. The final volume was adjusted to 1 liter sterile filter and stored at 4°C.

D.6 PBS pH7.4

Dissolve 8 g of NaCl, 0.2g KCl, 1.44 g Na_2HPO_4, 0.24 g KH_2PO_4 in 800 mL of Milli-Q water and the final pH was adjusted to 7.4 by adding 6 N HCl. The final volume was then adjusted to 1 liter. The buffer was then sterilized filtered into in 800 mL of Milli-Q water and adjust the pH to 8 by adding 6 N HCl. The final volume is then adjusted to 1liter. The buffer was sterile filtered through a 0.22 um Millipore filter and stored at 4°C.

D.7 Universal buffer systems

These buffer systems were used to achieve buffering capacity over a wide range of pHs.

D.7.1 Tris/Bis-Tris/ Cacodylate

6.06 g of Tris (base), 10.46 g of Bis-Tris and 7.5 mL of 1 M stock solution of Cacodylate were mixed and final volume was adjusted to 50 mL using a volumetric flask. Then the stock buffer solution was divided into two 25 mL portions. pH of one portion was adjusted to pH 8 and the other to pH 5 and the final volumes were adjusted to 50 mL using a volumetric flask so that the molarity of each solution was 0.5 M.

50 mL each of 20mM Tris/Bis-Tris/ Cacodylate pH 8 and 5 were then prepared by mixing 2mL of stock solution with 48 mL of MQ water.

To prepare other pHs of this buffer such as pH 7.5, 7, 6.5 and 6, a titration curve was described below (Table-11). The linear equation is used to calculate the volumes of pH 8 and pH 5 buffers need to be mixed, to obtain the desired pH.

Table-11 volumes added from pH8 and 5 buffers and the pH measured for each sample.

Vol. pH 8/ul	Vol. pH 5/ul	Actual pH
0	1000	5.0
100	900	5.54
200	800	5.82
300	700	6.09
400	600	6.29
500	500	6.52
600	400	6.75
700	300	6.99

Table 11 (continued)

Vol. pH 8/ul	Vol. pH 5/ul	Actual pH
800	200	7.3
900	1000	7.63
1000	0	8

APPENDIX D (continued)

Other universal buffer systems such as Bis-Tris / HEPES / Cacodylate /citrate (BHCC). Bis-Tris / HEPES / Cacodylate (BHC), Tris / MES / HEPES / HOAc, were made according to a similar procedure described for Tris / Bis-Tris / Cacodylate**.**

D.7.2 Constant ionic strength (CIS) buffer

This buffer consists of Tris / MES / HOAc in the ratio of 0.1 M / 0.05 M / 0.05 M. 1 M stock solutions of each buffer were combined to get the desired molarity in a total of 50 mL. The pH was adjusted to 8 and 5 and final volumes were adjusted using 50 mL volumetric flasks. The buffers were sterile filtered and stored at 4°C.

APPENDIX-E

GEL ELECTROPHORESIS TECHNIQUES

E.1 SDS-PAGE (for protein studies).

SDS-PAGE stands for Sodium dodecyl sulfate (SDS) polyacrylamide gel electrophoresis (PAGE) and is a method used to separate proteins according to their size. SDS/PAGE was carried out using the Bio-Rad Mini-protein II electrophoresis cell. Since different proteins with similar molecular weights may migrate differently due to their differences in secondary, tertiary or quaternary structure, SDS, an anionic detergent, is used in SDS-PAGE to reduce proteins to their primary (linearized) structure and coat them with uniform negative charges. Procedures for SDS-PAGE generally involve 1) making a gel and assembling the gel apparatus, 2) mixing protein samples with sample buffer containing SDS and heating the mixture at high temperature, 3) loading samples and running the electrophoresis and 4) fixing and staining the separated proteins.

E.2 Buffers and stock solutions used

1.5M Tris-HCl pH8

18.15 g Tris base was dissolved in 100 mL of DI water. pH was adjusted to 8.8 with 6 N HCl.

0.5M Tris-HCl pH 6.8

6g Tris base was dissolved in 100 mL of DI water and pH was adjusted to 6.8 with 6 N HCl.

10% SDS

1.01g of SDS in 10 mL of DI water and was stored at room temperature

5X running buffer pH 8.3

9 g of Tris base

43.2 g Glycine

3.0 g SDS in 600 mL of DI water

E.3 SDS reducing sample loading buffer

4 mL DI water

1.0 mL 0.5M Tris-HCl pH 6.8

0.8 mL Glycerol

1.6mL 10% SDS

400 mg Dithiothreitol

4 mg Bromophenol blue

Mix all components. This can either be stored at room temperature or can be stored at -20^{o}C and can be used over again.

E.4 Preparation of SDS-PAGE gels.

Acrylamide/ Bis (37.5:1 mixture) stock solutions were purchased from Bio-Rad. Resolving and stacking gels were made as follows.

Table 12

Ingredients	15% resolving	4% stacking
1. 40% acrylamide/Bis	3.75 mL	1mL
2. 0.5M Tris-HCl/pH 6.8	-	2.5 mL
3. 1.5M Tris-HCl pH 8.8	2.5 mL	-
4. 10% SDS	100ul	100ul
5. DI water	3.6 mL	6.4 mL
6. TEMED	10ul	10ul
7. 10% ammonium per sulfate (APS)	50ul	50ul

Total volume of resolving gel is ~10 mL

Appropriate amounts of solutions 1, 2 and 3 were added into a round bottom flask and degassed for 5 minutes. Then 4 were added and degassed for another 5 minutes. Then 5 and 6 were added and mixed well. The gel was poured as described according to the manufacture's protocol and water saturated butanol was carefully added on top of the mixture and was allowed to polymerize for 20-30 minutes. The stacking gel was made following the same procedure. After the gel was polymerized, butanol was removed completely and the stacking gel was poured on top of it the comb was inserted and kept for 15-20 minutes to get polymerized.

E.5 Sample preparation.

All samples were made in the loading buffer and then placed in a water bath for 5 minutes at 95^{o}C. 15-20 ul of each sample was loaded to the gel noting the respective lanes. A molecular weight marker in the desired range was used to determine the molecular weight of the protein. Gels were run for 45 minutes at a constant voltage of 200V. The gels were then developed using Simply Blue Safe-stain (Invitrogen) according to manufacturer's protocol.

E.6 Native gel electrophoresis

Native gel electrophoresis is run in the absence of SDS. While in SDS-PAGE the mobility of proteins depends primarily on their molecular weight, in native PAGE the mobility depends on both the protein's charge and its hydrodynamic size. Since the protein retains its folded conformation in native gel, its mobility on the gel will vary with the conformation (higher mobility for more compact conformations, lower for larger structures like oligomers).

E.7 Agarose gel electrophoresis (for DNA studies)

Ultrapure Agarose powder (0.4 g) was mixed with 50 mL of SYBR Safe DNA gel stain in 0.5X TBE (Invitrogen) and was heated in a microwave oven until completely melted. The safe stain DNS gel stains which allows us to visualize DNA after electrophoresis. This is a substitute for ethidium bromide which is a neurotoxin. After cooling the solution to about 60^{o}C, the solution is poured into a casting tray containing a sample comb and allowed to solidify at room temperature

for about 20 min. After the gel has solidified, the comb is removed and is inserted horizontally into the electrophoresis chamber and was covered with 1X TBE buffer.

Samples containing DNA (10 uL) mixed with loading buffer (2 uL) were then pipetted into the sample wells. The lid and power leads were placed on the apparatus, and a current was applied. Bubbles were observed if the current was flowing through and DNA migrated towards the positive electrode. After the DNA migrated sufficiently the bands were observed under UV light.